Received: 14 May 2024 | Revised: 19 July 2024 | Accepted: 23 July 2024

DOI: 10.1002/jmor.21757

RESEARCH ARTICLE

JOURNAL OF morphology WILEY

Male genitalia, hierarchical homology, and the anatomy of the bullet ant (*Paraponera clavata*; Hymenoptera, Formicidae)

Brendon E. Boudinot[1] | **Thomas van de Kamp**[2,3] | **Patricia Peters**[1] | **Katja Knöllinger**[1,4]

[1]Department of Terrestrial Zoology, Entomology II, Senckenberg Research Institute and Natural History Museum, Frankfurt am Main, Germany

[2]Institute for Photon Science and Synchrotron Radiation (IPS), Karlsruhe Institute of Technology (KIT), Karlsruhe, Germany

[3]Laboratory for Applications of Synchrotron Radiation (LAS), Karlsruhe Institute of Technology (KIT), Karlsruhe, Germany

[4]Zurich University of the Arts, Zurich, Switzerland

Correspondence
Brendon E. Boudinot, Department of Terrestrial Zoology, Entomology II, Senckenberg Research Institute and Natural History Museum, Frankfurt am Main 60325, Germany.
Email: boudinotb@gmail.com and brendon.boudinot@senckenberg.de

Funding information
Senckenberg Ocean Species Alliance

Abstract

The male genitalia of insects are among the most variable, complex, and informative character systems for evolutionary analysis and taxonomic purposes. Because of these general properties, many generations of systematists have struggled to develop a theory of homology and alignment of parts. This struggle continues to the present day, where fundamentally different models and nomenclatures for the male genitalia of Hymenoptera, for example, are applied. Here, we take a multimodal approach to digitalize and comprehensively document the genital skeletomuscular anatomy of the bullet ant (*Paraponera clavata*; Hymenoptera: Formicidae), including hand dissection, synchrotron radiation microcomputed tomography, microphotography, scanning electron microscopy, confocal laser scanning microscopy, and 3D-printing. Through this work, we generate several new concepts for the structure and form of the male genitalia of Hymenoptera, such as for the endophallic sclerite (=fibula ducti), which we were able to evaluate in detail for the first time for any species. Based on this phenomic anatomical study and comparison with other Holometabola and Hexapoda, we reconsider the homologies of insect genitalia more broadly, and propose a series of clarifications in support of the penis-gonopod theory of male genital identity. Specifically, we use the male genitalia of *Paraponera* and insects more broadly as an empirical case for hierarchical homology by applying and refining the 5-category classification of serial homologs from DiFrisco et al. (2023) (DLW23) to all of our formalized concepts. Through this, we find that: (1) geometry is a critical attribute to account for in ontology, especially as all individually identifiable attributes are positionally indexed hence can be recognized as homomorphic; (2) the definition of "structure" proposed by DLW23 is difficult to apply, and likely heterogeneous; and (3) formative elements, or spatially defined foldings or in- or evaginations of the epidermis and cuticle, are an important yet overlooked class of homomorphs. We propose a morphogenetic model for male and female insect genitalia, and a model analogous to gene-tree species-tree mappings for the hierarchical homology of male genitalia specifically. For all of the structures evaluated in the present

study, we provide 3D-printable models – with and without musculature, and in various states of digital dissection – to facilitate the development of a tactile understanding. Our treatment of the male genitalia of *P. clavata* serves as a basic template for future phenomic studies of male insect genitalia, which will be substantially improved with the development of automation and collections-based data processing pipelines, that is, collectomics. The Hymenoptera Anatomy Ontology will be a critical resource to include in this effort, and in best practice concepts should be linked.

KEYWORDS

digital anatomy, evolutionary morphology, homomorphy, internal genitalia, paramorphy, serial homology

1 | INTRODUCTION

The origins of the sexes are rooted in the evolutionary derivation of gametes and the fundamental asymmetry between eggs and sperm, in terms of size and developmental pathway. The primary differences in the sexes of the ocean-dwelling ancestors of the six-legged arthropods was in the fates of their internal genitalia, which develop from the mesodermal cell layer and are embedded in the ectodermal oviduct or ejaculatory duct (Snodgrass, 1935). The ancestral external genitalia of insects were coopted abdominal appendages; in other words, they are gonopods, or genital legs. Most of the wingless or apterygote orders of Hexapoda had genital appendages from one segment, as exemplified by the simple genital papillae of Collembola and Diplura (e.g., Tuxen, 1970a, 1970b), and the complex and medially fused copulatory appendage of Protura (e.g., François & Dallai, 1989). The insects, in contrast, derived a bi-segmental complex of external genitalia, with the female ovipositor comprising the appendages of abdominal segments VIII and IX, and the male genitalia of abdominal segments IX and X (Boudinot, 2018). Whereas the female genitalia retained this identity for hundreds of millions of years across nearly all orders of insects (e.g., Mickoleit, 1973), the medially fused penis of males became developmentally integrated with the gonopods of segment IX. The tenth-segmental identity of the penis is retained and indicated by muscles Cb-8 and Cb-9 of the penis in Archaeognatha (see tab. 1 and fig. 1A4 of Boudinot, 2018; also Bitsch, 1973, 1974a, 1974b; Birket-Smith, 1974; Klass & Matushkina, 2018), as this muscle connects the penis to the tenth abdominal tergum, and as the internal rami of arthropod legs (gonapophyses) do not have muscles that are from extrinsic body segments (e.g., Hessler & Yager, 1998).

Because of the developmental integration of the ninth- and tenth-segmental gonopods in the ancestor of the insects, we are confronted with a basic conflict for observation and interpretation: In the lifetime of an individual male insect, the penis and ninth-segmental gonopods can arise from the same anlage and outgrowth of the body wall (Qadri, 1940; Snodgrass, 1935), while at the same time, the penis and these gonopods are derived from ancestral appendages of two succeeding segments. The developmental–historical dichotomy of perspective is exacerbated by the decoupling of adult and juvenile structures in insects with complete metamorphosis, which has led to extreme confusion and conflict for the systems of male genital nomenclature and homology inference. This is exemplified by the alternative systems and theories of origin that have been proposed for the Hymenoptera: The phallic-periphallic model of Snodgrass (Snodgrass, 1935, see fig. 299 therein; Snodgrass, 1941) as modified by Mikó et al. (2013) and Dal Pos et al. (2023); the penis-gonopod model of Boudinot (2018) and its modification by Griebenow et al. (2023); and the homology neutral system of Boulangé (1924) as modified by Schulmeister (2001, 2003). These works further draw on a body of observation and thought, including Crampton (1920), Peck (1937a,b), Smith (1970, 1972) for Hymenoptera broadly, and Kempf (1956), Birket-Smith (1981), Ogata (1991), and Boudinot (2013) for Formicidae, the focal group of our anatomical case study.

In an effort to reduce this confusion and to evaluate these systems, we revisit the male genitalia of ants by undertaking a detailed multimodal anatomy of *Paraponera clavata* (Fabricius, 1775), the iconic bullet ant (Figure 1). The genus *Paraponera* comprises two Neotropical species, one extant and one extinct. The extant species, *P. clavata*, is large bodied (>2 cm), distributed from Honduras into the Amazon basin, and famed for its extremely potent sting, which is maximally rated on the Schmidt pain index and "induce[s] immediate, excruciating pain and numbness … as well as trembling in the form of a totally uncontrollable urge to shake the affected part" (Schmidt et al., 1983). The extinct species, †*P. dieteri* Baroni Urbani, 1994, is from Miocene-age Dominican amber and appears to have been an island dwarf, although it was among the largest ants of the Hispaniolan fauna (Fiorentino et al., 2023). These two species are the sole representatives of the subfamily Paraponerinae, which is morphologically isolated (e.g., Bolton, 2003; Richter et al., 2023), having diverged from its closest relatives perhaps in the Early Cretaceous (e.g., Romiguier et al., 2022).

Paraponera clavata are arboreal, omnivorous ants and have been the focus of numerous behavioral and ecological studies (e.g., Breed & Bennett, 1985; Breed & Harrison, 1988; Harrison & Breed, 1987; Peeters, 2017; reviewed in Janzen & Carroll, 1983 and Longino & Hanson, 1995), and their venom chemistry has been of particular interest (e.g., Aili et al., 2020; Johnson et al., 2017; Piek et al., 1991; Schmidt et al., 1983). Due in part to their size and cultural importance,

FIGURE 1 Lateral habitus of a male *Paraponera clavata* (SMFHYM0000119). Scale bar = 2 mm. **Abbreviations: ce** = cercus; **G** = gonopod, **S9** = sternum IX.

Paraponera has also represented an attractive reference for morphological study, with treatments of worker allometry (Breed, 2002), character evolution (Baroni Urbani et al., 1992; Keller, 2011; Kugler, 1991; Richter et al., 2023), various elements of the head (Andrade et al., 2019; Whiting et al., 1989; Richter, Schoeters, et al., 2021), the queen and male mesosoma (Boudinot, 2015; Tulloch, 1929, 1935), the basitarsal gland (Billen et al., 2021), the metapleural gland (Martins et al., 2022), the digestive tract (Caetano et al., 1986), metasomal glands (Hölldobler & Haskins, 1976), larval form (Wheeler & Wheeler, 1952), and especially the sting (Daly, 1955; Hermann, 1967; Hermann & Blum, 1966; Hermann et al., 1984; Kugler, 1991). These studies have relied on hand dissections, histology, photomicrography, and scanning electron microscopy (SEM). Here, we provide the first treatment of the male genitalia as well as first application of microcomputed tomography (μ-CT) and confocal laser scanning microscopy (CLSM) for the species. Our study is conducted in the emerging framework of phenomics, which relies heavily on μ-CT for the digitization of phenotypes, the documentation of fine external and internal anatomy, and the analysis of evolutionary and developmental patterns. Ants have received special interest in this regard, having been the subject of phenomic study for the head (e.g., workers: Richter et al., 2019, 2020, 2022; Richter, Garcia, et al., 2021; Richter et al., 2021; males: Boudinot et al., 2021), the mesosoma (workers: Aibekova et al., 2022), the abdomen (workers: Lieberman et al., 2022), and recently, the male genitalia (Griebenow et al., 2023).

Our present study has three focal objectives. The broadest objective is to empirically evaluate the five-category system of hierarchical homology proposed by DiFrisco, Love, and Wagner (DLW) (2023) by applying this system to a complete set of anatomical entities, exemplified by *P. clavata*. Hierarchical homology, in brief, recognizes serial homology as key evidence for the existence of genetic-developmental character identity mechanisms (DiFrisco et al., 2020). These mechanisms (or modules) can experience duplication and individuation in their evolutionary history, resulting in both the origin of apparent novelty and a hierarchical-phylogenetic relationship among similar, iterated body parts. The second, broad objective, is to reconsider the terminologies and homologies of male genitalia for Hymenoptera in the context of the Holometabola and the Hexapoda more widely. The primary evidence we rely on for this morphological reevaluation of male genitalia is derived from patterns of skeletomusculature, as muscle identity is biologically meaningful (see Section 4 for an overview). The narrower objective is to digitize, document, and depict the structural fact – that is, anatomy – of one species (*P. clavata*) is as much detail as currently possible given the technologies available. This narrower objective is conducted as an exercise in the use of these methods, as a means of anchoring our considerations in a readily observable format, and to develop a template for future phenomic study of insect genitalia, especially via character discovery.

We conducted our anatomical sampling using a multimodal approach, including: (1) hand dissection to understand physical attachments; (2) microphotography to capture information about sclerotization; (3) SEM to observe fine structural detail; (4) μ-CT to provide three-dimensional reconstructions of genital structure; (5) CLSM to visualize local variation in material properties; and (6) 3D printing, which allowed us to visually comprehend the structures at a

more intuitive scale, and to develop a tactile knowledge of sclerite form. Through our work, we aim to: (I) establish the groundwork for large-scale specimen digitization and analysis through the empirical application of ontology and hierarchical homology; (II) contribute further comparative data toward a comprehensive phylogenetic analysis of male genital evolution across the Formicidae, Hymenoptera, and Hexapoda more broadly; (III) generate new anatomical concepts for male genitalia using μ-CT data; (IV) evaluate the alternative systems of genital skeletomuscular nomenclature, as introduced above; and (V) provide 3D-printing-ready models of *Paraponera* as a standard, albeit derived reference for future work on the male genitalia. We also provide our design of a 3D-printable 2-axis specimen manipulator to ease future studies.

2 | MATERIALS AND METHODS

2.1 | Specimens

All specimens of *P. clavata* (Fabricius, 1775) used in the present study were collected during the ALAS survey of La Selva, Costa Rica. The specimens were preserved in 95% ethanol and transferred from the Longino collection (JTLC) to the Boudinot collection (BEBC) and subsequently deposited in the Senckenberg Naturmuseum Frankfurt Hymenoptera collection (SMFH). Each specimen was provided a unique specimen identifier with a QR code in the series SMFHYM0000###.

2.2 | Imaging

We imaged multiple specimens of male *P. clavata* using four different techniques: Microphotography (Section 2.2.1), SEM (Section 2.2.2), CLSM (Section 2.2.3), and X-ray scanning (Section 2.2.4). The methods for each technique are explained below.

2.2.1 | Microphotography

To capture information about setation, color, and degree of sclerotization, we relied on microphotography.

For the whole-body habitus, we chose and prepared one specimen (SMFHYM0000119) to represent *P. clavata*. The specimen was imaged in lateral view using a GIGAmacro Magnify 2 Robotic Imaging System (Four Chambers Studio LLC) with a mounted Canon EOS Rebel T6i camera carrying a Canon MPE 65 mm 1× objective, and lighting provided by a Canon MT26-EX Dual Flash. We took about 180 individual images and used Zerene Stacker (Zerene Systems) for stacking and Autopano Giga (Kolor) for stitching. The pin was positioned in a ball of Patafix (UHU GmbH & Co KG) mounted in a custom 3D-printed 2-axis specimen manipulator. This manipulator was designed during the present study using Cinema 4D 2024.2.0 (Maxon Computer GmbH) and printed using a Bambu Lab X-1 Carbon 3D printer with PLA-CF (carbon fiber) filament. The model is available for download and printing at Zenodo (https://doi.org/10.5281/zenodo.13208662); if printed, used, and/or modified, please cite the present study.

For the genital images another specimen of *Paraponera* (SMFHYM000227) was transferred from long-term 95% ethanol storage and dissected by hand under the same grade ethanol using size 5 forceps and a Leica M205C stereomicroscope with 10× oculars and a 1.0× Planopo objective. Lighting for this was provided by a Schott KL 1600 dual-head gooseneck LED lamp. For microphotography, the genital capsule and ninth sternum were fixed in each view using Blu-Tack (Bostik) also under 95% ethanol. Positioning was performed under a Wild Heerbrugg (Switzerland) M5 dissecting microscope with 10× objectives, a 1.0× objective, and an LED ring light. The genital images were captured using a mirrorless Nikon Z7 camera mounted on a motorized Kaiser RSD rig (Kaiser Fototechnik GmbH) and controlled using an MJKZZ Macro Rail (MJKZZ Europa), with the controller mounted on a Velbon CX Mini tripod (Hakuba Photo Industry Co., Ltd.). The camera was mounted with an Aurogon (LAOWA) 10× lens and illumination was provided by an OGGLAB vertical LED lighting system with a 3-channel dimmer and 5-channel switch (MJKZZ). Zerene Stacker was used for both stacking and stitching.

For the interordinal comparison figures in the discussion, stacked and stitched photomicrographs of *Machilis aurantiacus* (Schoett, 1897) (Archaeognatha: Machilidae), *Agulla* sp. (Raphidioptera: Raphidiidae), *Tipula californica* (Doane, 1908) (Diptera: Tipulidae), *Boreus reductus* (Carpenter, 1933) (Mecoptera: Boreidae), *Xyela* sp. (Hymenoptera: Xyelidae), and *Cimbex rubidus* (Cresson, 1880) (Hymenoptera: Cimbicidae) were used from the work of Boudinot (2018). These dissections were carried out in 2017 using the same forceps, dish, and Blu-Tack as those recently conducted for *Paraponera*. Lighting for the dissection and photomicrographs was provided by two sources: (1) stably mounted hand-holdable fluorescent work lamps from Home Depot, and (2) a strong fiber optic Leica KL 1500 LCD illuminator with paired goosenecks. The dish was placed on an X–Y mobile stage under a Leica MZ 16A with 115× maximum magnification and a 1.0× Planopo objective. Images were captured using a microscope-mounted JVC KY F75U digital camera, and they were stacked and stitched using Automontage (Synoptics Ltd.).

2.2.2 | SEM

To capture fine-scale detail of surface structure and sensilla form and distribution, we performed SEM with a Hitachi TM4000 Plus Tabletop Microscope for one specimen (SMFHYM0000118) that was hand-dissected under ethanol as for specimen SMFHYM000227 above. The dissection was more complete, with the sternum, cupula, and one gonopod separated. Each structure was mounted to a minuten pin using UHU Sekundenkleber (i.e., super glue). The minuten pins were then pushed into Patafix putty at the bottom of a small plastic container, which was used for simultaneous sputter coating of all of the parts with gold and palladium for ~2.5 min in an Edwards sputter coater. For SEM imaging with a black and noiseless background, we used a "Pohl'nische

Drehspieß" or specimen holder with electron trap (Pohl, 2010), which was machined by Plano GmbH under the product name "Rotationsprobenhalter für Hitachi mit M4-Gewinde." For each view, the minuten pin was observed with a dissecting stereomicroscope and carefully positioned on a piece of trimmed SEM sticky dot placed on the rotating arm of the specimen holder. After taking one to several images at each viewing angle, the specimen holder was removed from the vacuum chamber and the minuten pin repositioned. During this late-stage specimen preparation, the cupula detached from the right-hand gonopod-volsella-penis complex, which was remounted with UHU super glue. The unsputtered portions of the genitalia did not have a grossly negative effect on the resultant images.

2.2.3 | CLSM

CLSM was performed with a Leica DM 2500 CSLM and Leica TCS SPE camera on the same specimen used for photomicrography (SMFHYM0000227). The genital parts were untreated except for further dissection and were placed in a drop of glycerin in a thin cavity well slide, positioned carefully, then sealed with a cover slip. The CLSM system was operated on a Leica TCS SPE computer running LASX 3.5.7.23225. The laser wavelengths were set to 405 and 488 nm following Dal Pos et al. (2023) and the detectors set 5–6 nm above. We assigned the pseudocolor green to the lower channel and red to the higher using Fiji (Schindelin et al., 2012), following Mikó and Deans (2013), resulting in images that were 1.1 × 1.1 mm, which were then stitched using Adobe Photoshop (Adobe Inc.).

2.2.4 | X-ray scanning

Synchrotron microtomography was performed on specimen SMFHYM0005630 at the imaging cluster of the KIT Light Source using a parallel polychromatic X-ray beam produced by an 1.5 T bending magnet. The beam was spectrally filtered by 0.5 mm aluminum with a spectrum peak at about 15 keV. We employed a fast indirect detector system, consisting of a 13 µm LSO:Tb scintillator (Cecilia et al., 2011), and a diffraction limited optical microscope (Optique Peter; Douissard et al., 2012) coupled with a 12 bit pco.dimax high speed camera with 2016 × 2016 pixels (dos Santos Rolo et al., 2014). The specimen was scanned in 95% ethanol. We took 3000 projections at 70 fps and an optical magnification of 2× (scan code: BB312), resulting in an effective pixel size of 6.10 µm. Since the specimen was too large to fit in the vertical field of view, it was scanned in three height steps. The control system concert (Vogelgesang et al., 2016) was used for automated data acquisition and online reconstruction of tomographic slices for data quality assurance. The final tomographic 3D reconstructions were performed with tofu (Faragó et al., 2022) and included phase retrieval (Paganin et al., 2002), ring removal, 8-bit conversion, and blending of phase and absorption 3D reconstructions to increase contrast between the background and homogeneous regions, while at the same time highlighting the edges.

2.3 | 3D reconstruction

2.3.1 | Segmentation and rendering

To reconstruct the three-dimensional anatomy of the male genitalia of *P. clavata*, we manually labeled regions of interest (ROIs) as multi-ROIs with a threshold using Dragonfly software (Comet Technologies Canada Inc.). The labels were exported as TIFF stacks by: (1) extracting ROIs from the multi-ROI label set, (2) inverting each isolated ROI, (3) duplicating the image data set once for each ROI, (4) overwriting each duplicate data set with a scale of 1, and (5) exporting the overwritten data sets into a target directory. The image stacks were then imported into VG Studio (Volume Graphics GmbH) and rendered using Phong shading and two light sources. Clipping planes were used on individual objects for rendering digital dissection.

2.3.2 | 3D printing

Models of the reconstructed genitalia were 3D printed using a Bambu Lab X-1 Carbon printer with an AMS filament feed. To produce these, the segmentations that were done in Dragonfly were used to generate contour meshes for each object (region of interest). The sampling was set to $x = 1$, $y = 1$, $z = 1$ with a threshold of 1 for muscles and $x = 2$, $y = 2$, $z = 2$ with a threshold of 10 for sclerites. The 2, 2, 2 (10) setting for the sclerites resulted in a mesh with fewer holes but also reduced the level of fine detail in the final print. The meshes of each object were then modified and made into manifolds in Blender 4.0 (Blender Foundation). After editing, the objects were then exported as STL files and imported into the Bambu Studio program. From the present study, 3D-printable models of the genital sclerites in isolation and of the sclerites with musculature in various states of digital dissection are available at Zenodo (https://doi.org/10.5281/zenodo.13208662). Example prints are shown in Figure 2.

2.4 | Figure composition

Adobe Photoshop was used to adjust the levels and clean backgrounds for the photographs and SEM images. Some of the SEM images were stitched by hand using this program, which introduced negligible distortion, similar to standard image stacking. Images resulting from all three techniques were assembled in Adobe Illustrator and are available with and without stitching at Zenodo (https://doi.org/10.5281/zenodo.13208662).

2.5 | Morphology: Convention and approach

The technical descriptions were composed while examining 3D printed models, all of which are available for download and printing as STL files from Zenodo (https://doi.org/10.5281/zenodo.13208662). The 3D printed models allowed for straightforward measurements of proportions

FIGURE 2 (See caption on next page).

and for the detection and comparison of structure and shape based on the sense of touch. (Note that we did not use the 3D printed models for metric measurements.) For the convention of this study, we treat the genitalia as they are observed in situ, where the proximal portion of the genital complex is anterior, and the distal portion is posterior. The descriptions therefore proceed from anterior (proximal) to posterior (distal) and dorsal to ventral, with margins described first. The genital appendages (*i.e.*, the genital complex excluding sternum IX) are oriented along the craniocaudal axis of the body at rest; this axis is used to describe structures, although these appendages are processes from the body, so could equally be recognized as having their own proximomedial axis. The abbreviations are constructed such that if they were included as a column in a datasheet, they could be sorted alphabetically with parts of the structures kept together, that is, with the first part of the abbreviation indicating the segmentally numbered sclerite or unique structure, the substructure being second, and the substructure's location following. For example, the anterolateral (=al) apodeme (=A) of sternum IX (S9) is "S9" "A" "al", or "S9Aal." Each noun used in the description is intended to represent an anatomical entity (a "character" *sensu* McKenna et al., 2021; Wagner, 2014), which can be present (developed) or absent (not developed) and have some variation (states). These Wagnerian characters can be dependent on one another in complex ways. In Section 3.1.1 we refine the serial homological classification of structures provided by DiFrisco et al. (2023), and provide further consideration in the Discussion (Section 4.2). The abbreviation and concept set are hierarchically listed in Section 3.1.1 below. The overarching objective of the description is to capture phenotypic information in a structured manner to facilitate future observations and data translation, that is, conversion to matrices for statistical analysis.

3 | RESULTS

3.1 | General part: Concepts and alignment

3.1.1 | Hierarchical concept list used for the genital complex

The concepts used for the sclerites and membranes of the genital complex of *P. clavata* are here listed hierarchically. The label used throughout the text for each term is indicated and the first letters that comprise the label acronym are bolded. Capital letters are used for the primary object (*e.g.*, G for *gonopod*) and secondary object (*e.g.*, C for *coxa* forming GC or *gonocoxa*) concepts. Lowercase letters are used for any tertiary or further nested more concepts. Some letters are used for more than one term (*e.g.*, "a" for "apodeme" and "anterior").

Select synonyms are provided parenthetically for each concept. Unique Resource Identifiers (URIs) from the Hymenoptera Anatomy Ontology (HAO) and, in each case, HAO-preferred terms are indicated in square brackets ("[]") where these are available. As listed, each URI forms a link when appended to "http://purl.obolibrary.org/obo/". The URI search for term matching was done by first viewing all terms as a list via the "Terms" page, then (i) opening each term and copying the URI and (ii) using the "Partonomy" function to find linked terms. By including the URIs, the hierarchy serves as a reference for terms, labels, select synonyms, and the connection to the ontology. Concepts without HAO URIs are indicated by asterisks ("*") on their labels. Note that each figure in which a given body part is visible is indicated, but that these structures may not always be labeled therein. Note also that this hierarchical list is not intended in this form as the universal hierarchy of genitalic structures but is a study-specific pragmatic tool for systematically organizing labels and for synopsis. Our base set of overarching terms and concepts may also be partially linked to available ontologies, in this case Uberon (Haendel et al., 2014; Mungall et al., 2012) and the homology ontology proposed by Roux and Robinson-Rechavi (2010): *Anatomical entity* in the sense of our usage is equivalent to "anatomical structure" (UBERON_0000061); *attributes sensu* DiFrisco et al. (2023) (DLW) may be labeled as "immaterial anatomical entities" (UBERON_0000466); *structures sensu* DLW do not align with Uberon (see Section 4.2.1.2 below for discussion); *homomorphs sensu* DLW are not in available ontologies; *paramorphs sensu* DLW are expressed as "in paramorphism relationship with" in the Relational Ontology (RO:HOM0000074).

Each concept is further classified based on the five categories of serial homology proposed by DiFrisco et al. (2023) (*note*: these categories are defined in Section 4.2.1 of Section 4): Attributes (@), structures ($), replicas (=), homomorphs (!), and paramorphs (%). To account for the observed structural consistencies, we provide further refinements to the DLW system: **(1)** For homomorphs, complexity is categorized, with simple structures having the symbol indicated once (*e.g.*: "**!**" for an individual, positionally indexed carina, and "**!!**" for a separate sclerite, "**!!-!**" for complexes, "**!!-!!**" for a complex of complexes, and "**!!-!!!**" for a supercomplex);

FIGURE 2 Example 3D prints from the present study, which were used for physical manipulation of specimens and for observation and interpretation. (a) The 2-axis specimen manipulator, with SMFHYM0000119 for scale. (b)–(d) Two-material prints of the genital complex, with partial digital dissection. (b) Genital complex in posterolateral dorsal oblique view. (c) Genital complex in posterodorsal view. (d) Volsella in ventral view. (e) and (f) Individually isolated structures of the genitalia printed with a high reflectance plastic. (e) Dorsal view (left and right volsellae switched). (f) Ventral view. **Sclerite abbreviations: C** = cupula; **G** = gonopodite; **GC** = gonocoxite; **G-CSa** = coxostylar attenuation; **GS** = gonostylus; **Ip** = phallotreme; **P** = penite; **S9** = sternum IX; **S9Dd** = dorsal disc of sternum IX; **S9Pm** = posteromedian process (=prong) of sternum IX; **S9Pma** = apicoposteromedian processes of sternum IX; **S9U** = lumen of sternum IX; **V** = volsella; **VLc** = club of the lateropenite; **VLp** = process of the lateropenite, proximomedial; **VLs** = stem of the lateropenite; **VPbda** = basivolsellar apodeme; **VPbdpl** = lateral (portion of the) basivolsellar disc; **VPbdpm** = medial (portion of the) basivolsellar disc; **VPca** = apex of the distivolsella; **VPcs** = stem of the distivolsella; **VPdmdl** = distal margin of the lateral basivolsellar disc; **VPdmdm** = distal margin of the medial basivolsellar disc; **VPsl** = (longitudinal) volsellar sulcus. For **muscle abbreviations**, see Table 1.

(2) pairing or singularity of homomorphs is indicated with "**-||**" and "**-|**," respectively, and replication of a homomorph in a field or along a margin is indicated with "**-R**"; **(3)** sets of homomorphs are indicated with curly brackets ("**!{}**") (note: the phrase "homomorph sets" is used here as it is neutral, allowing for the grouping of similar structures without requiring an explicit hypothesis of paramorphy); **(4)** homomorphs that are formative elements (i.e., positionally defined curvatures of the epidermis and its products, Klass, 1997) are indicated with "**-F**"; (5) geometrical elements of attributes are indicated, namely points ("**-P**"), lines (=margins) ("**-M**"), material areas/surfaces ("**-Am**"), immaterial areas/surfaces ("**-Ai**"), material regions/portions/volumes ("**-Vm**"), immaterial volumes ("**-Vi**"); (6) attributes that are positionally indexed are indicated with "**#**"; (7) subdivisions of attributes are indicated with apostrophes (e.g., "**-M′**"). Procedurally, we constructed the hierarchical list before classifying them with these symbols. The symbols themselves were then used as a sorting tool in Excel to count the homology classes for the purpose of discussion (see Section 4.2 below). The symbols may be ignored by users who are interested in matching label abbreviations to natural language terms.

Where necessary for clarity, definitions are provided with *italics* and double square brackets ("[[]]"). Some basic definitions are as follows: ***process*** (HAO_0000822), or "the [portion of] sclerite that is raised"; ***apodeme*** (HAO_0000142), or "the *process* that is internal [and bears muscular attachment]"; ***carina*** (HAO_0000188), or "the *process* that is elongate and external"; ***lamella*** (=HAO carina), or the carina that is expanded in breadth and solid. We refer to unsclerotized epidermal fields as "**membrane**," which is in this sense synonymous with *conjunctiva/arthrodial membrane/corium* (HAO_0000221) and *membranous layer* (UBERON_0000158).

- **S9** (**!!-|**) = **s**ternum **IX** (Figures 1–6, 8–10, 23, 24, 26) ["abdominal sternum 9," HAO_0000047; see also "acrosternite" in Section 3.1.2 below] (paramorph family 1, *abdominal sternites and tergites* **%**):
  - **S9A*** (**!{}**) = **a**podemes of **s**ternum **IX** (paramorph family 2, *apodemes* **%**):
    - **S9Aal*** (**!-|**) = **a**nterol**a**teral **a**podeme of **s**ternum **IX**.
    - **S9Aam** (**!-||**) = **a**nter**o**median **a**podeme (=spiculum) of **s**ternum **IX** ["spiculum," HAO_0000946].
  - **S9K*** (**!{}**) = carinae of **s**ternum **IX** (paramorph family 3, *carinae* **%**):
    - **S9Kav-aam*** (**!-|**) = **a**pico**v**entral spicular **c**arina of **s**ternum **IX**.
    - **S9Kpd-apm*** (**!-|**) = **p**roxi**m**odorsal prong **c**arina of **s**ternum **IX**.
  - **S9C*** (**@-P**) = **c**orners of **s**ternum **IX**:
    - **S9Cl*** (**@-P#**) = **l**ateral **c**orners of **s**ternum **IX** [[*the points of sternum IX that are situated along the total margin of the sternum and that mark the transition from internal to external*]].
  - **S9D*** (**@-Vm**) = **d**isc of **s**ternum **IX** [[*the portions of sternum IX that directly corresponds to the lumen of the sclerite*]].
    - **S9Dd*** (**@-Am#**) = **d**orsal (surface of the) **d**isc of **s**ternum **IX**.
    - **S9Dv*** (**@-Am#**) = **v**entral (surface of the) **d**isc of **s**ternum **IX**.
  - **S9L***) (**!-|**) = **l**amella of **s**ternum **IX** [[*the lamella that is positioned (develops) along the posterior margin of sternum IX*]] (paramorph family 4, *marginal lamellae* **%**).
  - **S9U*** (**@-Vi#**) = **l**umen of **s**ternum **IX**.
  - **S9M*** (**@-M{}**) = **m**argins of **s**ternum **IX**:
    - **S9Ma*** (**@-M#**) = **a**nterior **m**argin of **s**ternum **IX** [[*the margin of sternum IX that is external and extends between the lateral corners of sternum IX*]].
      - **S9Mal*** (**@-M′#**) = **a**nterol**a**teral **m**argins of **s**ternum **IX**.
      - **S9Mam*** (**@-M′#**) = **a**nter**o**medial **m**argins of **s**ternum **IX**.
    - **S9Mp*** (**@-M#**) = **p**osterior **m**argin of **s**ternum **IX** [[*the margin of sternum IX that is internal and extends between the lateral corners of sternum IX*]].
      - **S9Mpl*** (**@-M′#**) = **p**oster**o**lateral **m**argins of **s**ternum **IX**.
      - **S9Mpm*** (**@-M′#**) = **p**oster**o**median **m**argin of **s**ternum **IX**.
  - **S9P*** (**!{}**) = **p**rocesses of **s**ternum **IX** (paramorph family 5, *evaginations of the cuticle* **%**):
    - **S9Pm*** (**!-|**) = poster**o**median **p**rocess (=prong) of **s**ternum **IX** [*note*: positioned ventrad the lamella of sternum IX].
    - **S9Pma*** (**!-||**) = **a**pico-poster**o**median **p**rocesses of **s**ternum **IX**.
  - **S9R*** (**!{}**) = **r**idges of **s**ternum **IX** [*note*: this set should include the acrosternite, but this was not distinctly observable in the present study; see Section 3.1.2 below] (paramorph family 3, *carinae* **%**):
    - **S9Ral*** (**!-||**) = **a**nterol**a**teral **r**idge of **s**ternum **IX**.
    - **S9Ram*** (**!-||**) = **a**nter**o**medial **r**idge of **s**ternum **IX** [="antecosta," HAO_0000098].
- **Genital appendages** (**!!-!!!-|**) (Figures 1–7, 9, 11–26, 29, 30) ["external male genitalia," HAO_0000312]:
  - **C** (**!!-|**) = **c**upula (Figures 2–6, 9, 11–14, 23–26, 29) ["cupula," HAO_0000238]:
    - **CA*** (**!-|**) = **c**upular **a**podeme [see also "distoventral submedian corner of the cupula," "proximodorsal apodeme of cupula," and "proximolateral apodeme of cupula" in Section 3.1.2 below] (paramorph family 2, *apodemes* **%**).
      - **CAri*** (**@-M#**) = mesal (**i**nternalmost) **r**im of the **c**upular **a**podeme.
      - **CAsa*** (**@-Am#**) = **a**nterior (proximal) **s**urface of the **c**upular **a**podeme.
        - **CAsad*** (**!-F-||**) = **a**nterior (proximal) **d**epression of the **c**upular **a**podeme [*note*: this is the surface curvature of the cupular apodeme as seen in proximal view; see also CAspb].
        - **CAsap** (**!-|**) = posteromedial **p**rocess of the **c**upular **a**podeme **a**nterior **s**urface ["gonocondyle," HAO_0000380].
      - **CAsp*** (**@-Am#**) = **p**osterior (distal) **s**urface of the **c**upular **a**podeme.
        - **CAspb*** (**!-F-||**) = **p**osterior (distal) **b**ulge of the **c**upular **a**podeme [*note*: this is the surface curvature of the cupular apodeme as seen in distal view; see also CAsad].
    - **CD*** (**@-Am#**) = **c**upular **d**isc [[*the portion of the cupula that is positioned between the proximal and distal membranes of the cupula*]].
    - **CL*** (**!{}**) = **c**upular **l**amellae [[*the lamellae that are positioned (develop) proximad or distad the proximal or distal membranes of*

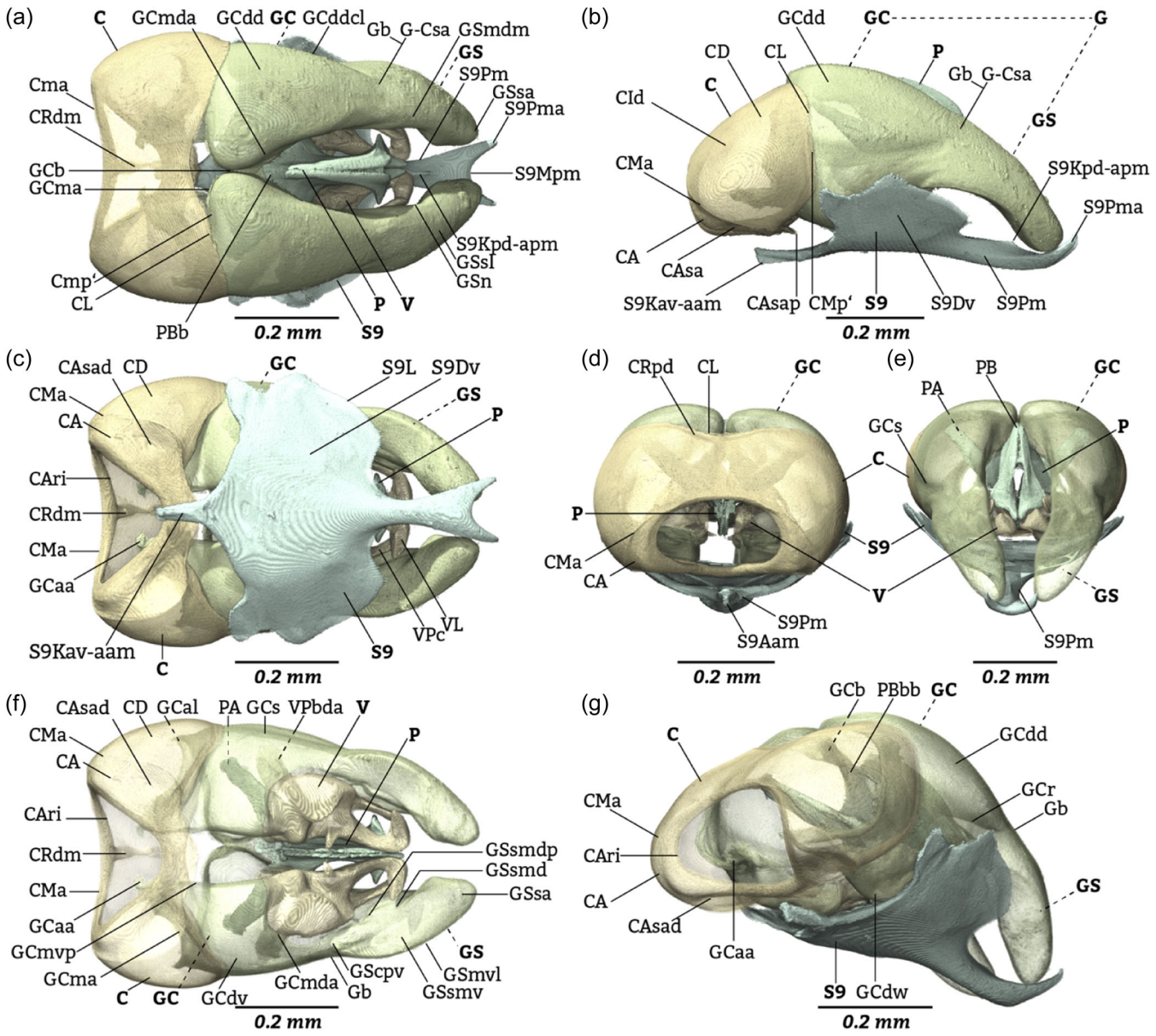

FIGURE 3 The sclerites of the genital complex of *Paraponera clavata* without musculature, in situ. **Parts and views:** (a) Whole genital complex, dorsal view; (b) whole genital complex, lateral view; (c) whole genital complex with sternum IX, ventral view; (d) whole genital complex, anterior (cranial) view; (e) whole genital complex, posterior (caudal) view. (f) Whole genital complex without sternum IX, ventral view. (g) Whole genital complex, anterior ventrolateral view. **Abbreviations: C** = cupula; **CA** = cupular apodeme; **CAri** = mesal (internalmost) rim of the cupular apodeme; **CAsa** = anterior (proximal) surface of the cupular apodeme; **CAsad** = anterior (proximal) depression of the cupular apodeme; **CD** = cupular disc; **CL** = cupular lamella; **CMa** = (true) anterior (proximal) cupular margin; **CMp'** = apparent posterior (distal) cupular margin; **CRdm** = dorsomedian (longitudinal) ridge of cupula; **CRpd** = posterodorsal (marginal) ridge of cupula; **G** = gonopodite; **Gb** = coxostylar boundary; **GC** = gonocoxite; **GCal** = lateral process of the gonocoxal apodeme; **GCb** = gonocoxal bridge; **GCdd** = dorsal disc of the gonocoxa; **GCddcl** = lateral curve of the dorsal gonocoxal disc; **GCdv** = ventral disc of the gonocoxa; **GCma** = anterior gonocoxal margin; **GCmda** = apicodorsal gonocoxal margin; **GCmva** = apicoventral gonocoxal margin; **GCmvp** = proximoventral gonocoxal margin; **GCr** = gonocoxal ridge; **GCs** = gonocoxal sulcus; **G-CSa** = coxostylar attenuation; **GS** = gonostylus; **GScpv** = corner of the gonostylus, proximoventral; **GSmdm** = dorsomedial margin of the gonostylus; **GSmpm** = proximomedial margin of the gonostylar sclerotization; **GSmvl** = ventrolateral margin of the gonostylus; **GSn** = notch, proximodorsal of gonostylus; **GSsa** = apical surface of the gonostylus (=gonostylar apex); **GSsmd** = dorsomedial gonostylar surface; **GSsmdp** = (medial) process of the dorsomedial gonostylar surface; **GSsmv** = ventromedial gonostylar surface; **P** = penite; **PA** = valvura; **PB** = valviceps; **S9** = sternum IX; **S9Aam** = spiculum; **S9Dv** = ventral disc of sternum IX; **S9Kav-aam** = apicoventral spicular carina of sternum IX; **S9Kpd-apm** = proximodorsal prong carina of sternum IX; **S9Pm** = posteromedian process (=prong) of sternum IX; **V** = volsella; **VL** = lateropenite; **VPc** = distivolsella.

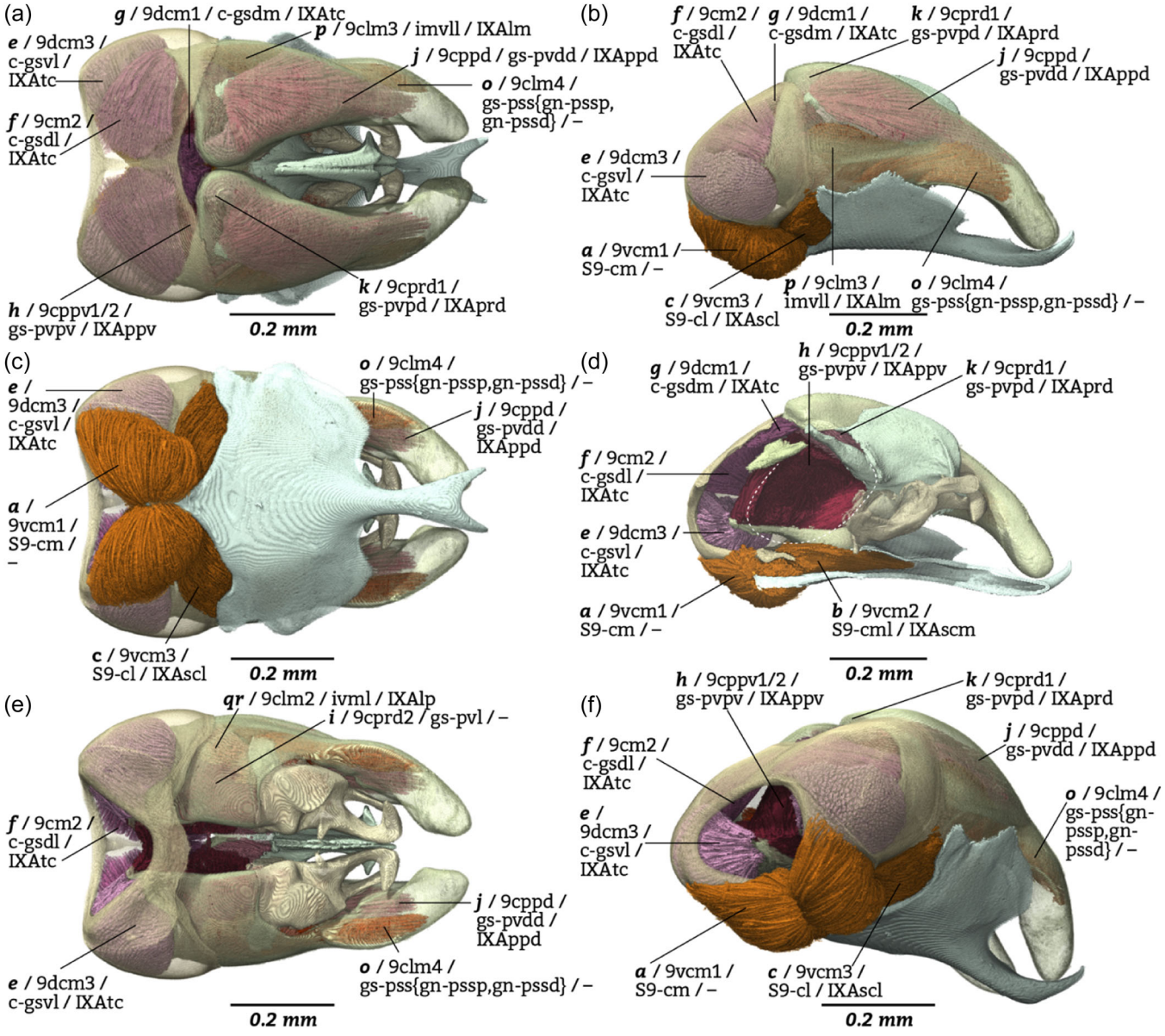

FIGURE 4 Volume renders of the genital sclerites of *Paraponera clavata* with musculature. **Parts and views:** (a) Whole genital complex, dorsal view; (b) whole genital complex, lateral view; (c) whole genital complex with sternum IX, ventral view; (d) genital complex in lateral view with left gonopod digitally removed and sternum IX sagittally sectioned; (e) whole genital complex without sternum IX, ventral view; (f) whole genital complex, anterior ventrolateral view. **Abbreviations:** ***a*** = "anteromedian sterno-cupular muscle"; ***b*** = "posteromedian sterno-cupular muscle"; ***c*** = "anterolateral sterno-cupular muscle"; ***e*** = "ventrolateral cupulo-coxal muscle"; ***f*** = "dorsolateral cupulo-coxal muscle"; ***g*** = "dorsomedial cupulo-coxal muscle"; ***h*** = "apicoventral coxo-penial muscle"; ***i*** = "proximoventral coxo-penial muscle"; ***j*** = "apicodorsal coxo-penial muscle"; ***k*** = "proximoventral coxo-penial muscle"; ***o*** = "coxo-basivolsellar muscle"; ***p*** = "coxo-distivolsellar muscle"; ***qr*** = "basivolsellar-distivolsellar muscle."

the cupula, respectively]] (paramorph family 4, *marginal lamellae* **%**).

- **CLi** (**@-Am#**) = posterior (distal) **c**upular **i**nflection ["proximodorsal inflection of cupulal margin," HAO_0002523] [*note*: a proximal cupular lamella is not distinguishable in *Paraponera*, hence is excluded from this list].

- **CF*** (**@-Ai{}**) = **f**oramina of the **c**upula:
  - **CFa** (**@-Ai#**) = **a**nterior (proximal) **c**upular **f**oramen ["foramen genitale," HAO_0000346].
  - **CFp*** (**@-Ai#**) = **p**osterior (distal) **c**upular **f**oramen.
- **CI*** (**@-Am**) = **i**mpressions of the **c**upula [*note*: classified as a material area rather than a formative element because this appears to be simply where the two lateral halves of the cupular disc (CD) meet]:
  - **CId** (**@-Am#**) = "**d**orsal submedian **i**mpression of **c**upula" [HAO_0002037].
- **CM*** (**@-M{}**) = **m**argins of the **c**upula:
  - **CMa*** (**@-M#**) = (true) **a**nterior (proximal) **c**upular **m**argin.
    - **CMan*** (**@-Am{}**) = **n**otches of the **a**nterior (proximal) **c**upular **m**argin [*note*: classified as a material area rather

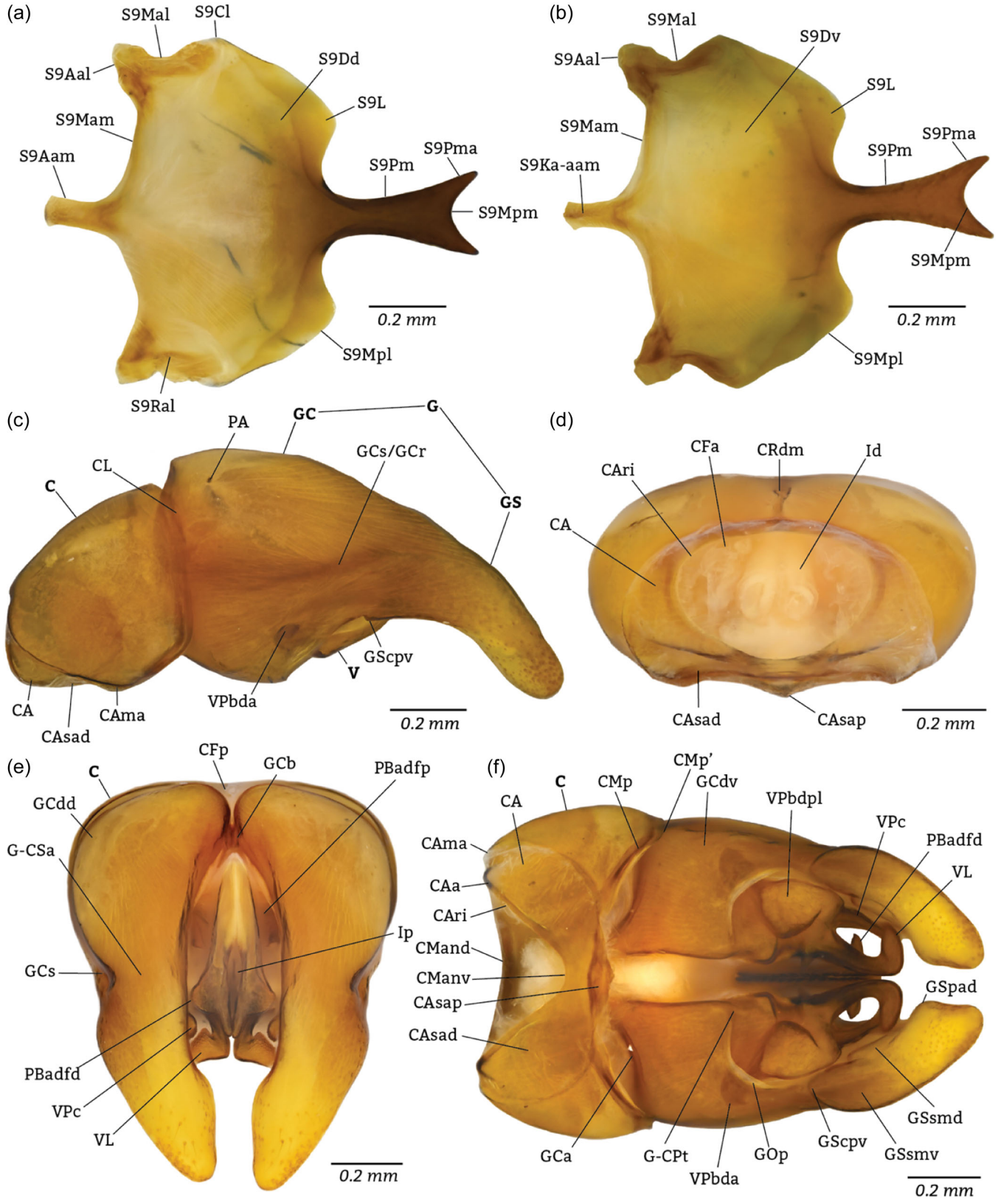

FIGURE 5 (See caption on next page).

than a formative element because this appears to be simply be portions of the curve formed by the anterior (proximal) cupular margin].
- **CMand** (**@-Am#**) = "proximodorsalnotch of thecupula" [HAO_0002048].
- **CManv** (**@-Am#**) = "proximoventralnotch of thecupula" [HAO_0002395].

- **CMp*** (**@-M#**) = (true) **p**osterior (distal) **c**upular **m**argin [*note*: this corresponds to the location of the cupular-gonopodal membrane].
- **CMp′*** (**@-M#**) = apparent **p**osterior (distal) **c**upular **m**argin [*note*: this corresponds to the distal margin of the posterior (apical) cupular lamella].

- **CO*** (**$**) = membranes (=**co**rium) of the **c**upula:
  - **COc*** (**$#**) = **c**upulo-**c**oxal membrane.
- **CR*** (**!{}**) = **r**idges of the **c**upula (paramorph family 3, *carinae* **%**):
  - **CRa*** (**!-|**) = **a**nterior (marginal) **r**idge of **c**upula.
  - **CRdm*** (**!-|**) = **d**orso**m**edian (longitudinal) **r**idge of **c**upula.
  - **CRpv*** (**!-|**) = **p**ostero**v**entral (marginal) **r**idge of **c**upula.
  - **CRpd*** (**!-|**) = **p**ostero**d**orsal (marginal) **r**idge of **c**upula.

o **Gonopod–volsellar complex** (**!!-!!-|**) (Figures 1–5, 7, 9, 12, 14–21, 23–26, 29, 30) [in part matching "gonostipes-volsella complex," HAO_0000168]:
- **G-CPt*** (**@-Am#**) = **c**oxo-**p**arossicular **t**ransition.
- **G-CSa*** (**@-Am#**) = **c**oxo**s**tylar **a**ttenuation.
- **G** (**!!-||**) = **g**onopodite (=gonopod) (Figures 1–5, 7, 9, 12, 14, 15, 17, 19–21, 23, 24, 25, 26, 29) ["gonostyle," HAO_0000389] (paramorph family 6, *appendages* **%**):
  - **Gb*** (**@-Am#**) = coxostylar **b**oundary.
  - **GC** (**!!′-||**) = **g**ono**c**oxite (=gonocoxa) ["gonostipes," HAO_0000386]:
    - **GCa*** (**!-|**) = **g**ono**c**oxal **a**podeme:
      - **GCaa*** (**@-P{}**) = **a**pices of the **g**ono**c**oxal **a**podeme:
        - **GCaad*** (**@-P#**) = **d**orsal (proximomedial) **a**pex of the **g**onocoxal **a**podeme.
        - **GCaav** (**@-P#**) = **v**entral (proximomedial) **a**pex of the **g**onocoxal **a**podeme ["gonostipital arm," HAO_0000387].
      - **GCal*** (**!-|**) = **l**ateral **p**rocess of the **g**ono**c**oxal **a**podeme.
    - o **GCb*** (**@-Am#**) = **g**ono**c**oxal **b**ridge.
    - o **GCcpm*** (**@-P#**) = **g**ono**c**oxal **c**orner, proximomedial.
    - o **GCd*** (**@-Vm{}**) = **g**ono**c**oxal **d**isc.
      - **GCdd*** (**@-Vm′#**) = **d**orsal **d**isc of the **g**ono**c**oxa [see "parapenis" and "parapenisjugum" in Section 3.1.2 below].
        - **GCddc*** (**@-M{}**) = **c**urves of the **d**orsal **g**ono**c**oxal **d**isc.
          - o **GCddcl*** (**@-M#**) = **l**ateral **c**urve of the **d**orsal **g**ono**c**oxal **d**isc.
          - o **GCddcm*** (**@-M#**) = **m**edial **c**urve of the **d**orsal **g**ono**c**oxal **d**isc.
        - **GCddi*** (**@-Am#**) = (medial) **i**nflection of the **d**orsal **g**ono**c**oxal **d**isc.
      - **GCdv*** (**@-Vm′#**) = **v**entral **d**isc of the **g**ono**c**oxa [see "apex gonostipitis" in Section 3.1.2 below].
    - o **GCm*** (**@-M{}**) = **g**ono**c**oxal **m**argins:
      - **GCma*** (**@-M#**) = **a**nterior (proximal) **g**ono**c**oxal **m**argin.
      - **GCmda*** (**@-M#**) = **a**pico**d**orsal (medial) **g**ono**c**oxal **m**argin.
      - **GCmvp*** (**@-M#**) = **p**roximo**v**entral (medial) **g**ono**c**oxal **m**argin.
      - **GCmva*** (**@-M#**) = **a**pico**v**entral **g**ono**c**oxal **m**argin.
    - o **GCr*** (**!-|**) = **g**ono**c**oxal **r**idge (=**coxostylar ridge**, ="coxal apodeme"/"Cxaapd" of Boudinot, 2018) (paramorph family 3, *carinae* **%**).
    - o **GCs*** (**!′-|**) = **g**ono**c**oxal **s**ulcus [*note*: the sulcus is dependent on formation of the ridge].
- **GS** (**!!′-||**) = **g**ono**s**tylus ["harpe," HAO_0000395; see also "distolateral projection of the harpe" in Section 3.1.2 below]:

FIGURE 5 Photomicrographs of the genital sclerites of *Paraponera clavata* (SMFHYM0000227). Setation omitted through masking. **Views** (a) Lateral, (b) dorsal, (c) ventral, (d) anterior (cranial); (e) posterior (caudal). **Abbreviations: C** = cupula; **CA** = cupular apodeme; **CAri** = mesal (internalmost) rim of the cupular apodeme; **CAsad** = anterior (proximal) depression of the cupular apodeme; **CAsap** = posteromedial process of the cupular apodeme anterior surface; **CD** = cupular disc; **CL** = cupular lamella; **CMa** = (true) anterior (proximal) cupular margin; **CMand** = proximodorsal notch of the cupula; **CManv** = proximoventral notch of the cupula; **CMp** = (true) posterior (distal) cupular margin; **CMp′** = apparent posterior (distal) cupular margin; **CRa** = anterior (marginal) ridge of cupula; **CRdm** = dorsomedian (longitudinal) ridge of cupula; **G** = gonopodite; **GC** = gonocoxite; **GCa** = gonocoxal apodeme; **GCb** = gonocoxal bridge; **GCdd** = dorsal disc of the gonocoxa; **GCdv** = ventral disc of the gonocoxa; **G-CPt** = coxo-parossicular transition; **GCr** = gonocoxal ridge; **GCs** = gonocoxal sulcus; **G-CSa** = coxostylar attenuation; **GOp** = coxo-parossicular membrane; **GS** = gonostylus; **GScpv** = corner of the gonostylus, proximoventral; **GSsmd** = dorsomedial gonostylar surface; **GSsmv** = ventromedial gonostylar surface; **Id** = ductus ejaculatorius; **Ip** = phallotreme; **PA** = valvura; **PBadfd** = distal flange of the dorsal valviceps region; **PBadfp** = proximal flange of the dorsal valviceps region; **S9Aal** = anterolateral apodeme of sternum IX; **S9Aam** = spiculum; **S9Cl** = lateral corners of sternum IX; **S9Dd** = dorsal disc of sternum IX; **S9Dv** = ventral disc of sternum IX; **S9Kav-aam** = apicoventral spicular carina of sternum IX; **S9Kpd-apm** = proximodorsal prong carina of sternum IX; **S9L** = lamella of sternum IX; **S9Mal** = anterolateral margins of sternum IX; **S9Mam** = anteromedial margins of sternum IX; **S9Mpl** = posterolateral margins of sternum IX; **S9Mpm** = posteromedian margin of sternum IX; **S9Pm** = posteromedian process (=prong) of sternum IX; **S9Pma** = apico-posteromedian processes of sternum IX; **S9Ral** = anterolateral ridge of sternum IX; **V** = volsella; **VL** = lateropenite; **VPbda** = basivolsellar apodeme; **VPbdpl** = lateral (portion of the) basivolsellar disc; **VPc** = distivolsella.

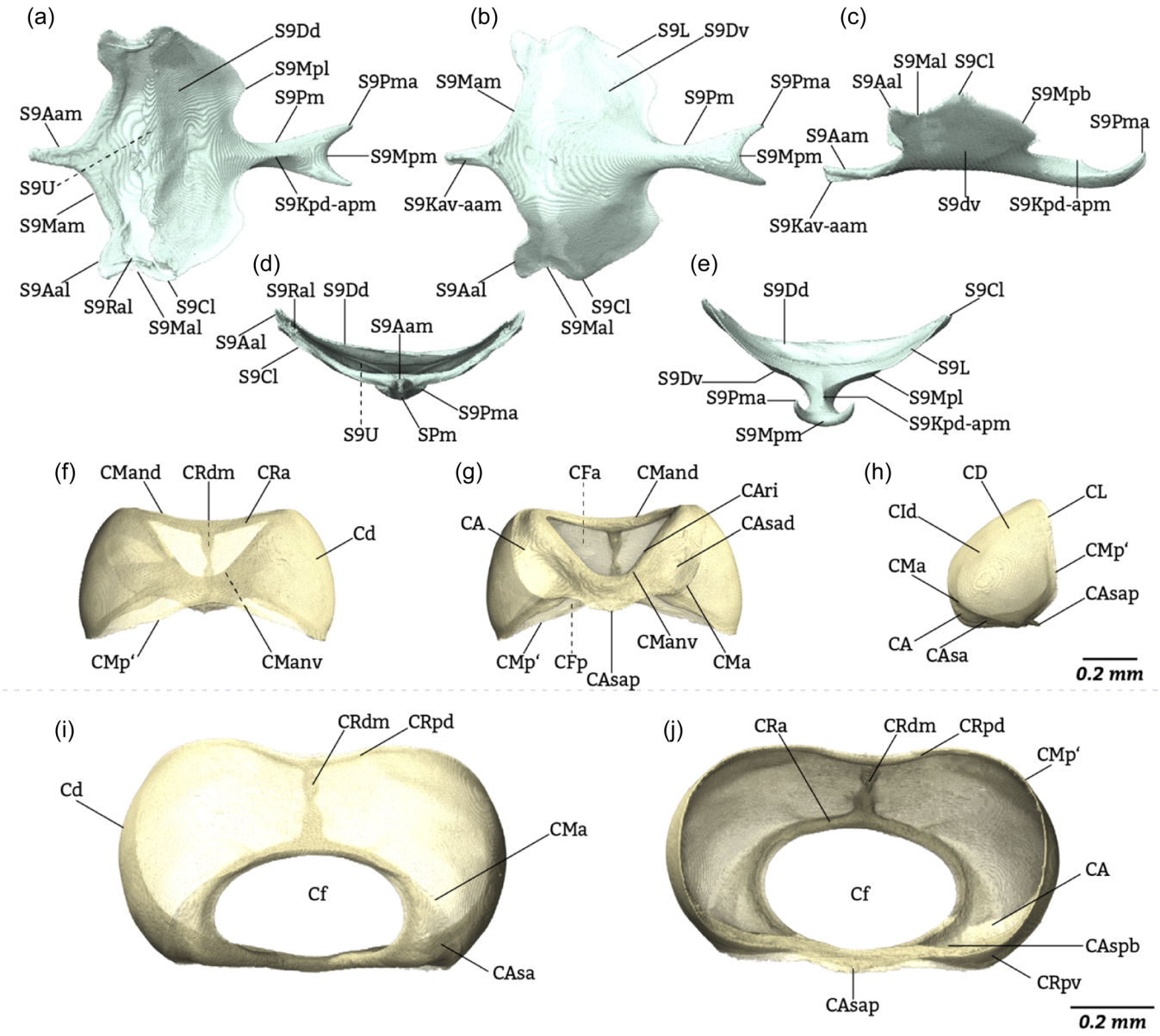

FIGURE 6 Volumetric renders of the genital sclerites of *Paraponera clavata* in isolation, without musculature. **Sclerites**: (a)–(e) Sternum IX. (f)–(j) Cupula. **Views: (c), (h)**: Lateral; **(d), (i)**: anterior (cranial); **(e), (j)**: posterior (caudal). **Abbreviations: C** = cupula; **CA** = cupular apodeme; **CAri** = mesal (internalmost) rim of the cupular apodeme; **CAsa** = anterior (proximal) surface of the cupular apodeme; **CAsad** = anterior (proximal) depression of the cupular apodeme; **CAsap** = posteromedial process of the cupular apodeme anterior surface; **CAsp** = posterior (distal) surface of the cupular apodeme; **CAspb** = posterior (distal) bulge of the cupular apodeme; **CD** = cupular disc; **CF** = foramina of the cupula; **CFa** = anterior (proximal) cupular foramen; **CFp** = posterior (distal) cupular foramen; **CL** = cupular lamella; **CLi** = posterior (distal) cupular inflection; **CMa** = (true) anterior (proximal) cupular margin; **CMp′** = apparent posterior (distal) cupular margin; **S9** = sternum IX; **S9Aal** = anterolateral apodeme of sternum IX; **S9Aam** = spiculum; **S9Cl** = lateral corners of sternum IX; **S9Dd** = dorsal disc of sternum IX; **S9Dv** = ventral disc of sternum IX; **S9Kav-aam** = apicoventral spicular carina of sternum IX; **S9Kpd-apm** = proximodorsal prong carina of sternum IX; **S9L** = lamella of sternum IX; **S9Mal** = anterolateral margins of sternum IX; **S9Mam** = anteromedial margins of sternum IX; **S9Mpl** = posterolateral margins of sternum IX; **S9Mpm** = posteromedian margin of sternum IX; **S9Pm** = posteromedian process (=prong) of sternum IX; **S9Pma** = apico-posteromedian processes of sternum IX; **S9Ral** = anterolateral ridge of sternum IX; **S9U** = lumen of sternum IX.

- **GScpv*** (**!-F-|**) = **c**orner of the **g**onostylus, **p**roximo**v**entral [see also "squama" in Section 3.1.2].
- **GSm*** (**@-M{}**) = **m**argins of the **g**onostylus:
  - **GSmdm*** (**@-M#**) = **d**orso**m**edial **m**argin of the **g**onostylus.
  - **GSmpm*** (**@-M#**) = **p**roximo**m**edial **m**argin of the **g**onostylar sclerotization.
  - **GSmvl*** (**@-M#**) = **v**entrolateral **m**argin of the **g**onostylus.
- **GSn** (**!-F-|**) = **n**otch, proximodorsal of **g**onostylus ["proximodorsal notch of harpe," HAO_0002049].
- **GSpad** (**!-F-|**) = **p**rocess of the **g**onostylus, apicodorsal [see "proximodorsal projection of harpe" in Section 3.1.2].

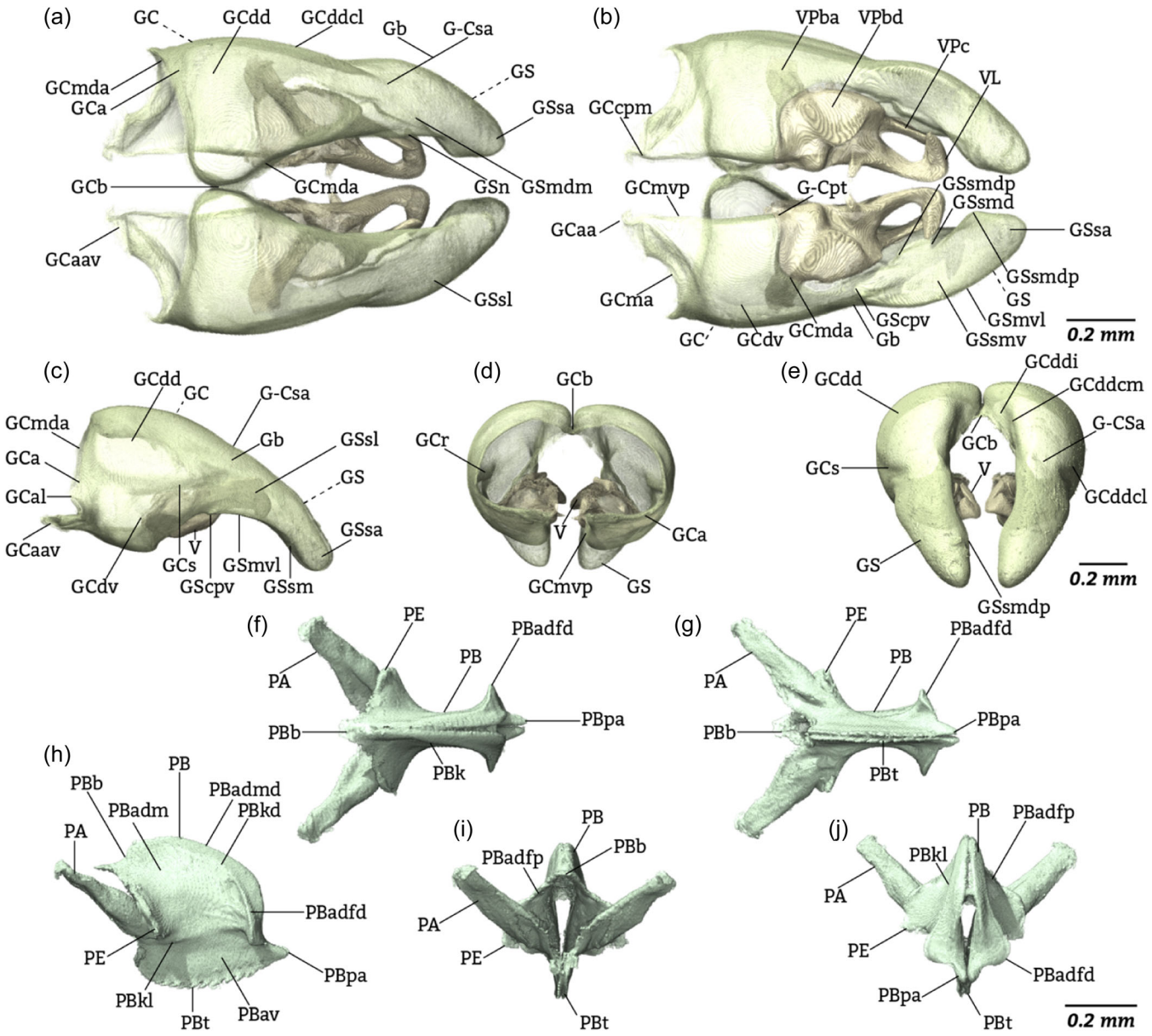

FIGURE 7 Volumetric renders of the genital sclerites of *Paraponera clavata* in isolation, without musculature. **Sclerites**: (a)–(e) Gonopod-volsellar complexes; (f)–(j) penites. **Views:** (a), (e): dorsal; (b), (f): ventral; (c), (g): lateral; (d), (h): anterior (proximal/cranial). (e), (i): posterior (distal/caudal). **Abbreviations: Gb** = coxostylar boundary; **GC** = gonocoxite; **GCa** = gonocoxal apodeme; **GCaa** = apex of the gonocoxal apodeme; **GCaad** = dorsal (proximomedial) apex of the gonocoxal apodeme; **GCaav** = ventral (proximomedial) apex of the gonocoxal apodeme; **GCal** = lateral process of the gonocoxal apodeme; **GCb** = gonocoxal bridge; **GCcpm** = Gonocoxal corner, proximomedial; **GCdd** = dorsal disc of the gonocoxa; **GCddcl** = lateral curve of the dorsal gonocoxal disc; **GCddcm** = medial curve of the dorsal gonocoxal disc; **GCddi** = (medial) inflection of the dorsal gonocoxal disc; **GCdv** = ventral disc of the gonocoxa; **GCma** = anterior gonocoxal margin; **GCmda** = apicodorsal gonocoxal margin; **GCmva** = apicoventral gonocoxal margin; **GCmvp** = proximoventral gonocoxal margin; **G-CPt** = coxo-parossicular transition; **GCr** = gonocoxal ridge; **GCs** = gonocoxal sulcus; **G-CSa** = coxostylar attenuation; **GS** = gonostylus; **GScpv** = corner of the gonostylus, proximoventral; **GSmdm** = dorsomedial margin of the gonostylus; **GSmpm** = proximomedial margin of the gonostylar sclerotization; **GSmvl** = ventrolateral margin of the gonostylus; **GSn** = notch, proximodorsal of gonostylus; **GSs** = surfaces of the gonostylus; **GSsa** = apical surface of the gonostylus; **GSsl** = lateral surface of the gonostylus; **GSsm** = medial surface of the gonostylus; **GSsmd** = dorsomedial gonostylar surface; **GSsmdp** = (medial) process of the dorsomedial gonostylar surface; **GSsmv** = ventromedial gonostylar surface; **PA** = valvura; **PB** = valviceps; **PBad** = dorsal region/area of the valviceps; **PBadf** = flanges of the dorsal valviceps region/area; **PBadfd** = distal flange of the dorsal valviceps region; **PBadfp** = proximal flange of the dorsal valviceps region; **PBadm** = margins of the dorsal valviceps region/area; **PBadmd** = dorsal margin of the dorsal valviceps region; **PBadmp** = proximal margin of the dorsal valviceps region; **PBav** = ventral region/area of the valviceps; **PBavm** = margins of the ventral valviceps region/area; **PBavmp** = proximal margin of the ventral valviceps region; **PBavmv** = ventral margin of the ventral valviceps region; **PBb** = bridge of the valviceps; **PBkd** = dorsal (marginal) carina of the valviceps; **PBkl** = lateral (longitudinal) carina of the valviceps; **PBpa** = apical process of the valviceps; **PBt** = teeth of the valviceps; **PE** = ergot; **V** = volsella; **VL** = lateropenite; **VP** = parossiculus; **VPb** = basivolsella; **VPbd** = basivolsellar disc; **VPbda** = basivolsellar apodeme; **VPc** = distivolsella.

- **GSs*** (**@-Am{}**) = **s**urfaces of the **g**ono**s**tylus:
  - **GSsa*** (**@-Am#**) = **a**pical **s**urface of the **g**ono**s**tylus (=gonostylar apex).
  - **GSsl*** (**@-Am#**) = **l**ateral **s**urface of the **g**ono**s**tylus.
  - **GSsm*** (**@-Am#**) = **m**edial **s**urface of the **g**ono**s**tylus.
    - **GSsmd*** (**!-F-|**) = **d**orsomedial **g**ono**s**tylar **s**urface (=cupping disc) [“gonomacula,” HAO_0000382; see also “gonomacula” in Section 3.1.2 for comment].
      - **GSsmdp*** (**!-F-|**) = (medial) **p**rocess of the **d**orsomedial **g**ono**s**tylar **s**urface.
    - **GSsmv*** (**@-Am#**) = **v**entromedial **g**ono**s**tylar **s**urface.
  - **GSsv*** (**@-Am#**) = **v**entral **s**urface of the **g**ono**s**tylus (=gonostylar heel).
- **GO** (**$**) = membrane (=**co**rium):
  - **GOe** (**$#**) = coxo-**p**enial membrane.
  - **GOp** (**$#**) = coxo-**p**arossicular membrane.
  - **GOv** (**$#**) = **v**entromedial coxo-stylar membrane.

- **V** (**!!-!-||**) = **v**olsella (Figures 2–5, 7, 9, 14–21, 23–25, 29, 30) (=volsellar complex):
  - **VP** (**!!-|**) = **p**arossiculus [“parossiculus,” HAO_0000703; see also “intervolsellar process” in Section 3.1.2]:
    - **VPb** (**@-Vm**) = **b**asivolsella [“basivolsella,” HAO_0001085; see also “basivolsellar bridge” in Section 3.1.2].
      - **VPbda*** (**!-|**) = **b**asivolsellar **a**podeme.
        - **VPbdaa*** (**@-P#**) = **a**pex of the **b**asivolsellar **a**podeme.
      - **VPbd*** (**@-Vm#**) = **b**asivolsellar **d**isc.
        - **VPdm*** (**@-M{}**) = **m**argins of the **b**asivolsellar **d**isc.
          - **VPdmd*** (**@-M#**) = **d**istal **m**argin of the **b**asivolsellar **d**isc.
          - **VPdmdl*** (**@-M#**) = **d**istal **m**argin of the **l**ateral **b**asivolsellar **d**isc.
          - **VPdmdm*** (**@-M#**) = **d**istal **m**argin of the **m**edial **b**asivolsellar **d**isc.
          - **VPdmll*** (**@-M#**) = **l**ateral **m**argin of the **l**ateral **b**asivolsellar **d**isc.
        - **VPbdp*** (**@-Vm′{}**) = **p**ortions of the **b**asivolsellar **d**isc.
          - **VPbdpl*** (**@-Vm′#**) = **l**ateral (**p**ortion of the) basivolsellar **d**isc.
          - **VPbdpm*** (**@-Vm′#**) = **m**edial (**p**ortion of the) basivolsellar **d**isc.
    - **VPc** (**@-Vm**) = distivolsella (=**c**uspis) [“cuspis,” HAO_0000239] (paramorph family 4, *marginal lamellae* **%**).
      - **VPcA** (**!-|**) = **a**podeme of the distivolsella [“distivolsellar apodeme,” HAO_0000249] (paramorph family 2, *apodemes* **%**).
      - **VPca*** (**@-P#**) = **a**pex of the distivolsella.
      - **VPcs*** (**@-Vm#**) = **s**tem of the distivolsella.
    - **VPr*** (**!{}**) = **r**idges of the **p**arossiculus (paramorph family 3, *carinae* **%**).
      - **VPrd*** (**!-|**) = **d**istal **p**arossicular **r**idge.
      - **VPrl*** (**!-|**) = (longitudinal) **v**olsellar **r**idge (=carina volsellaris, Schulmeister, 2001; =**l**ongitudinal volsellar ridge) [“volsellar ridge,” HAO_0001086].
    - **VPs*** (**!-F{}**) = **p**arossicular **s**ulci.
      - **VPsd*** (**!-F-|**) = **d**istal **p**arossicular **s**ulcus.
      - **VPsl*** (**!-F-|**) = (**l**ongitudinal) volsellar **s**ulcus.
  - **VL** (**!-||**) = **l**ateropenite (=digitus, =gonossiculus) [“gonossiculus,” HAO_0000385; see also “apiceps,” “basiura,” “digital spine,” “distal projection of the parossiculus,” and “dorsalmost digital spine” in Section 3.1.2]:
    - **VLc*** (**@-Vm#**) = **c**lub of the **l**ateropenite.
    - **VLs*** (**@-Vm#**) = **s**tem of the **l**ateropenite.
    - **VLp*** (**!-|**) = **p**rocess of the **l**ateropenite, proximomedial [see also “basal hooklet” in Section 3.1.2].
  - **VM*** (**!-R**) = **m**icrotrichial **f**ield of the **v**olsella.

- **P** (**!!-||**) = **p**enite(s) (Figures 2–5, 7, 9, 14, 17, 19–26, 29, 30) (=penial sclerite, =penisvalve) [“penisvalva,” HAO_0000707] (paramorph family 6, *appendages* **%**):
  - **PA** (**!-|**) = valvura (=**p**enital **a**podeme) [“valvura,” HAO_0001050] (paramorph family 2, *apodemes* **%**).
  - **PE** (**!-|**) = **e**rgot (=lateral **p**enital apodeme) [“ergot,” HAO_0000308].
  - **PB** (**!-|**) = valviceps (=**p**enital **b**lade) [“valviceps,” HAO_0001047; see also “ergot,” “pseudoceps,” “valvar strut,” and “valvispina” in Section 3.1.2]:
    - **PBpa** (**!-|**) = **a**pical **p**rocess of the valviceps [“distal projection of the penisvalva,” HAO_0002391].
    - **PBb*** (**!-F-|**) = **b**ridge of the valviceps.
    - **PBk*** (**!{}**) = carinae of the valviceps:
      - **PBkd*** (**!-|**) = **d**orsal (marginal) carina of the valviceps.
      - **PBkl*** (**!-|**) = **l**ateral (longitudinal) carina of the valviceps.
    - **PBa*** (**@-Am{}**) = regions/**a**reas of the valviceps:
      - **PBad*** (**@-Am#**) = **d**orsal region/**a**rea of the valviceps.
        - **PBadm*** (**@-M#**) = **m**argins of the **d**orsal valviceps region/**a**rea.
          - **PBadmd*** (**@-M′#**) = **d**orsal **m**argin of the **d**orsal valviceps region (=dorsal margin of the valviceps).
          - **PBadmp*** (**@-M′#**) = **p**roximal **m**argin of the **d**orsal valviceps region.
        - **PBadf*** (**!-F{}**) = **f**langes of the **d**orsal valviceps region/**a**rea.
          - **PBadfd** (**!-F-|**) = **d**istal **f**lange of the dorsal valviceps region [see also “paravalva” in Section 3.1.2].
          - **PBadfp*** (**!-F-|**) = **p**roximal **f**lange of the dorsal valviceps region.
      - **PBav*** (**@-Am#**) = **v**entral region/**a**rea of the valviceps.
        - **PBavm*** (**@-M#**) = **m**argins of the **v**entral valviceps region/**a**rea.
          - **PBavmv*** (**@-M′#**) = **v**entral **m**argin of the **v**entral valviceps region (=ventral margin of the valviceps).
          - **PBavmp*** (**@-M′#**) = **p**roximal **m**argin of the **v**entral valviceps region.

- **PBt*** (**!-R**) = **t**eeth of the valviceps [*note*: individual teeth are replicas (=); in *Paraponera*, it appears that there are three partially individuated sections of valviceps teeth, defined along the proximodistal axis of the ventral penital margin] (paramorph family 7, *marginal processes* **%**).
- **POv*** (**$**) = **p**enial membrane (=**co**rium), **v**entral.

o **I** (**!!-!-|**) = **i**nternal genitalia (Figures 5,14,19,23-26) [“internal male genitalia,” HAO_0000427] (paramorph family 8, *internal genitalia* **%**):

- **Ia** (**!!-||**) = **a**ccessory gland [“accessory gland,” HAO_0000078].
- **Id** (**!!-|**) = **d**uctus ejaculatorius [“ejaculatory duct,” HAO_0000283].
- **Ie** (**!!-|**) = **e**ndophallus [“endophallus,” HAO_0000291]:
  - **Ieb*** (**!-|**) = **e**ndophallic **b**ladder (=endophallic bladder, Boudinot, 2013).
  - **Iec*** (**!-|**) = endophallic **c**hamber, distal.
  - **Ied*** (**!-|**) = **e**ndophallic **d**uct.
    - **Iedd*** (**@-Vm#**) = **e**ndophallic **d**uct, **d**istal.
    - **Iedp*** (**@-Vm#**) = **e**ndophallic **d**uct, **p**roximal.
  - **Ies** (**!!-|**) = **e**ndophallic **s**clerite (=Sperrkeil, =wedge sclerite) [“fibula ducti,” HAO_0000328].
    - **Iesa*** (**!-||**) = **a**rms of the **e**ndophallite.
    - **Iesra*** (**@-Vm{}**) = **r**egions of the **e**ndophallite.
      - **Iesrd*** (**@-Vm#**) = **d**istal **e**ndophallite **r**egion.
      - **Iersp*** (**@-Vm#**) = **p**roximal **e**ndophallite **r**egion.
        - **Iesrpi*** (**!-F-||**) = **i**mpressions of the **p**roximal **e**ndophallite **r**egion.
        - **Iesrpl*** (**!-F-|**) = (dorsomedian) **l**amella of the **p**roximal **e**ndophallite **r**egion [*note*: not independent from the ventromedian sulcus (Iesrps)].
        - **Iesrps*** (**!-F-|**) = (ventromedian) **s**ulcus of the **p**roximal **e**ndophallite **r**egion [*note*: dependent on the dorsomedian lamella (Iesrpl)].
    - **Iess*** (**!-F-|**) = **s**ulcus of the **e**ndophallite, dorsal.
- **Ig** (**@-Ai#**) = **g**onopore [“primary gonopore,” HAO_0000821].
- **Ip** (**@-Ai#**) = **p**hallotreme [“phallotrema,” HAO_0000714].
- **It** (**!!-||**) = **t**estis [“testis,” HAO_0001007].
  - **Its*** (**!-|**) = peritoneal **s**heath (e.g., fig. 292 of Snodgrass, 1935).
  - **Itf*** (**!-R**) = **t**esticular **f**ollicles (=spermatic tube, Snodgrass, 1935).
- **Iv** (**@-Vm#**) = **v**as deferens [“vas deferens,” HAO_0001052; see also “proximal lobe of vas deferens” in Section 3.1.2 below].
- **Is** (**@-Vm#**) = vesicula **s**eminalis [“seminal vesicle,” HAO_0001081].

3.1.2 | HAO concepts not recognizable for *Paraponera*

Some concepts found in the HAO using the partonomy search appear may or may not apply to the male genitalia *Paraponera* but could not be recognized during our present study. These are listed here, with notes.

- “Acrosternite 9” [HAO_0001614]. *Note*: Using the concept of acrosclerite from Snodgrass (1935, e.g., fig. 87), which is a sclerotic continuation of a sclerite anterad (i.e., anteriorly past) a costa, no such structure was observable for *Paraponera*.
- “Apex gonostipitis” [HAO_0000134]. *Note*: The “apex gonostipitis” is defined as “the apodeme that … [bears the] origin of the ventral … penisvalval muscles.” We prefer not to recognize the ventral disc of the gonocoxa (GCdv) as the “apex gonostipitis,” as it is exposed and not an internal process, that is, it is not an apodeme.
- “Apiceps” [HAO_0000141]. *Note*: The lateropenite/gonossiculus/digitus of *Paraponera* is dissimilar in specific form relative to symphytan Hymenoptera, for which an apiceps/digiceps and basiura/digiura have been recognized (e.g., Schulmeister, 2001).
- “Proximomedian apodeme of the harpe” [HAO_0002050]. *Note*: Muscle ***t*** (“gs-hrd”) is absent in *Paraponera*, and no obvious internal process is developed from the gonostylus, thus we do cannot recognize this structure. (See “pah,” fig. 17 of Mikó et al., 2013.)
- “Basal hooklet” [HAO_0001179]. *Note*: It is not clear from the illustration of Evans (1950, fig. 2 therein) whether his basal hooklet corresponds to our proximomedial process of the lateropenite (VLp).
- “Basiura” [HAO_0000179]. *Note*: See “apiceps” above.
- “Basivolsellar bridge” [HAO_0000165]. *Note*: A sclerotization that connects the left and right parossiculi is not present in *Paraponera*.
- “Distal projection of the parossiculus” [HAO_0002386]. *Note*: As *Paraponera* lacks an apical parossicular seta [HAO_0000138], the distal projection of the parossiculus is by definition absent.
- “Digital spine” [HAO_0001574]. *Note*: We are unsure of the correspondence of distal structures between *Paraponera* and Chalcidoidea.
- “Distolateral projection of the harpe” [HAO_0002035]. *Note*: The gonostylus of *Paraponera* is not divided into two lobes, thus this label does not apply.
- “Distoventral submedian corner of the cupula” [HAO_0002414]. *Note*: There is an apparent corner of the cupula in *Paraponera* when seen in lateral view. Because the reference article for label usage was not findable, we were unsure whether our observed corner is the corner observed by the HAO authorities.
- “Dorsalmost digital spine” [HAO_0002062]. *Note*: We are uncertain whether the dorsalmost digital spine of Ceraphronoidea (Mikó et al., 2013) corresponds to any specific structure in *Paraponera*.
- “Gonomacula” [HAO_0000382]. *Note*: We tentatively recognize the dorsomedial surface of the gonostylus as the cupping disc (Snodgrass, 1941) or gonomacula (Crampton, 1919). The homology of this element of the gonostylus is uncertain, however, as its continuity of form throughout the Aculeata and parasitican Apocrita should be evaluated.

- "Intervolsellar process" [HAO_0001799]. *Note*: We are uncertain about the correspondence of this chalcidoid structure with respect to *Paraponera*.
- "Parapenis" [HAO_0000692]. *Note*: The dorsal disc of the gonocoxa (GCdd) does bear the origins of the "distidorsal and proximodorsal … penisvalval muscles." We prefer not to use "parapenis" for this region as this term is anatomically vague, that is, it does not specify location and is not conceptually connected to other terms, hence reasoning out its identity with a specimen at hand would be difficult. Additionally, the term was initially applied to symphytan Hymenoptera (Crampton, 1919), which have a specific form relative to Apocrita and other Holometabola, for which reason we would prefer to recognize this as a state of the dorsal disc.
- "Parapenisjugum" [HAO_0000693]. *Note*: Given that the form of the "parapenis" is characteristic of certain groups of symphytan Hymenoptera and not the whole order or other Holometabola (see "parapenis" above), we prefer to recognize this only for those taxa that have that specific modification.
- "Paravalva" [HAO_0000698]. *Note*: We are uncertain about the exact identity of the paravalva (Ross, 1945), thus we are unable to evaluate the possible homology with *Paraponera*. Based on the definition of this term in the HAO, we tentatively associate it with the distal flange of the penite (PBadfd).
- "Proximodorsal apodeme of cupula" [HAO_0002522]. *Note*: It is possible that our cupular apodeme (CA) corresponds to the proximodorsal, proximolateral, and proximodorsal apodemes of the cupula from the HAO. However, because three concepts are included in the HAO for apodemes of the cupula and as no reference figure or paper were available, we could not determine which of the three was synonymous with our concept, or whether our concept applies to all of them.
- "Proximodorsal projection of harpe" [HAO_0002049]. *Note*: The apicodorsal process of the gonostylus (GSpad) of *Paraponera* appears to match the definition of this term from the HAO: "the median projection of the proximodorsal region of the harpe (=gonostylus) that accommodates the gonossiculus (=digitus, lateropenite) when it is pressed against the harpe." The process in *Paraponera* is distal rather than proximal, and no comparable figures are known. We therefore recognize correspondence but not synonymy and homology of these processes.
- "Proximolateral apodeme of cupula" [HAO_0000878]. *Note*: See "Proximodorsal apodeme of cupula" above.
- "Proximomedial brush of the harpe" [HAO_0002525]. *Note*: This appears to define a state of gonostylar sensilla that is observed in certain Ceraphronidae.
- "Proximomedian apodeme of the harpe" [HAO_0002050]. *Note*: The gonostylus of *Paraponera* was not observed to have a muscle-bearing extension. A similar structure is present in various holometabolan outgroups, forming an abductor swelling.
- "Proximal lobe of vas deferens" [HAO_0002047]. *Note*: We could not recognize this structure in *Paraponera*, which has markedly derived internal genitalia.
- "Pseudoceps" [HAO_0000880]. *Note*: We are uncertain of the exact structural identity of the pseudoceps, valvar strut, and valviceps of (Ross, 1945), thus we have not provided any further association than the valviceps.
- "Sensillar ring of harpe" [HAO_0002392]. *Note*: We do not observe a distinct row of setae along the dorsomedial margin of the gonostylus in *Paraponera*.
- "Squama" [HAO_0001224]. *Note*: The squama was recognized by Evans (1950) for the Pompilidae. This label applies to a bulge on the proximoventral margin of the gonostylus that corresponds in location to the proximoventral corner of the gonostylus (GScpv) recognized here for *Paraponera*. Because of this positional correspondence, we consider these structures to be tentative homologs, which should be evaluated with a broader comparison across Aculeata, and with reference to special quality of structure (Remane, 1952, p. 42).
- "Valvar strut" [HAO_0001046]. *Note*: See "pseudoceps" above.
- "Valvispina" [HAO_0001048]. *Note*: See "pseudoceps" above.

3.1.3 | Hymenopteran muscle system alignment

Five principal systems have been developed for the muscle system of the Hymenoptera. The homologies of the muscles among the systems are generally clear, and all systems follow the example of Boulangé (1924), which was modified by Schulmeister (2001, 2003). The alignment of these systems recognizing individual muscle homologs is provided in Table 1 below.

3.2 | Specific part: Anatomy of *P. clavata*

3.2.1 | Male genital complex

The male genital complex as treated here includes the sternum IX (**S9**, Figures 1–6, 8–10, 23, 24, 26; Section 3.2.2), which is sexually dimorphic relative to the female (S9 absent), and the genital capsule, which comprises the cupula (**C**, Figures 2–6, 9, 11–14, 23–26, 29; Section 3.2.3), the gonopods (**G**, Figures 1–5, 7, 9, 12, 14, 15, 17, 19–21, 23–26, 29, 30; Section 3.2.4), the volsellae (**V**, Figures 2–5, 7, 9, 14–21, 23, 24, 25, 29, 30; Section 3.2.5), the penites (**P**, Figures 2–5, 7, 9, 14, 17, 19–26, 29, 30; Section 3.2.6), and the internal genitalia (**I**, Figures 5,14,19,23-26; Section 3.2.7).

3.2.2 | Sternum IX

Sclerite

Sternum IX is concave dorsally and convex ventrally (**S9**); this sternum cups the genital capsule ventrally. The *lateral corners of sternum IX* (**S9Cl**) divide the perimeter of the sternum into the *anterior* and *posterior margins of sternum IX* (**S9Ma**, **S9Mp**). The *anterior margin of sternum IX* (**S9Ma**) bears the *anterior ridge of sternum IX* (**S9Ra**) along its length.

TABLE 1 Muscular label equivalencies (=synonymies) and occurrence in *Paraponera clavata*.

B24/S01/S03	S41	G23	D23	B18	HAO URI	*P. clavata*
1. Sterno-cupular muscles (Figures 2, 4, 9, 10).						
a	1	9vcm1	S9-cm	–	HAO_0000516	Present
b	2	9vcm2	S9-cml	IXAscm	HAO_0000533	Present
c	3	9vcm3	S9-cl	IXAscl	HAO_0000464	Present
2. Sternal intrinsic muscles						
–		9vvim	–	–	–	Absent
3. Cupulo-coxal muscles (Figures 2, 4, 12).						
d	4	9dcm4	c-gsvm	IXAtc	HAO_0001075	Present
e	5	9dcm3	c-gsvl	[IXAtc]	HAO_0001074	Present
f	7	9dcm2	c-gsdl	[IXAtc]	HAO_0000278	Present
g	6	9dcm1	c-gsdm	[IXAtc]	HAO_0000279	Present
4. Coxo-stylar muscles.						
–	–	9csm1	–	–	–	Absent
w	16	9csm2	gs-gs	IXAxad	HAO_0002581	Absent
t	15	[9csm2]	gs-hrd	[IXAxad]	HAO_0000336	Absent
t′	[15]	[9csm2]	gs-hrp	[IXAxad]	HAO_0000926	Absent
u	–	9csm3	ga-hra	IXAxab	HAO_0000246	Absent
v	17	9csm4	ha-gon	–	HAO_0000396	Absent
5. Coxo-volsellar muscles (Figures 2, 17, 18).						
o	18	9clm4	gs-pss	–	HAO_0002041	Present
o′	[18]	[9clm4]	gn-pssp	–	HAO_0000876	
o″	[18]	[9clm4]	gn-pssd	–	HAO_0000247	
p	19	9clm3	imvll	IXAlm	HAO_0002580	Present
qr	21	9clm2	imvl	IXAlp	HAO_0000473	Present
s	23	9clm1	imvm	–	HAO_0000517	Absent
6. Volsello-volsellar muscles.						
y	–	9ccm	vl-vl	–	HAO_0000441	Absent
7. Penial-volsellar muscles.						
si	–	9cprv1	pss-pv	IXAppv	HAO_0000701	Absent
m	22	10plm1	pv-gssl	–	HAO_0002579	Absent
n	–	10plm2	ps-gssm	–	HAO_0002578	Absent
nb	24		pv-ph	–	HAO_0000710	Absent
nd	–	–	gss-ph	–	HAO_0002577	Absent
nl	–	–	pss-ph	–	HAO_0000702	Absent
8. Coxo-penial muscles (Figures 2, 4, 20, 21).						
h	8	9cppv1	gs-pvpv	IXAppv	HAO_0000879	Present
h′	–	9cppv2	–	[IXAppv]	–	
i	9	9cprv2	gs-pvdv	IXAprv	HAO_0000251	Present
j	10	9cppd	gs-pvdd	IXAppd	HAO_0000250	Present

TABLE 1 (Continued)

B24/S01/S03	S41	G23	D23	B18	HAO URI	*P. clavata*
k	11	9cprd1	gs-pvpd	IXAprd	HAO_0000877	Present
l	12	9cprd2	gs-pvl	—	HAO_0000472	Present
9. Pene-penial muscles.						
x	13	10ppm1	pv-pv	—	HAO_0000433	Absent
z	14	10ppm2	pv-mss	—	HAO_0002582	Absent

Note: B24 = Boulangé (1924), S01 = Schulmeister (2001), S03 = Schulmeister (2003), S41 = Snodgrass (1941), G23 = Griebenow et al. (2023), D = Dal Pos et al. (2023), B18 = Boudinot (2018), HAO URI, Hymenoptera Anatomy Ontology Unique Resource Identifier (forms a link when appended to http://purl.obolibrary.org/obo/). Alignment of B24, S41, and B18 follows the interpretations of Griebenow et al. (2023). The colors are used across all tables to indicate observed presence/absence, versus theoretical occurrence.

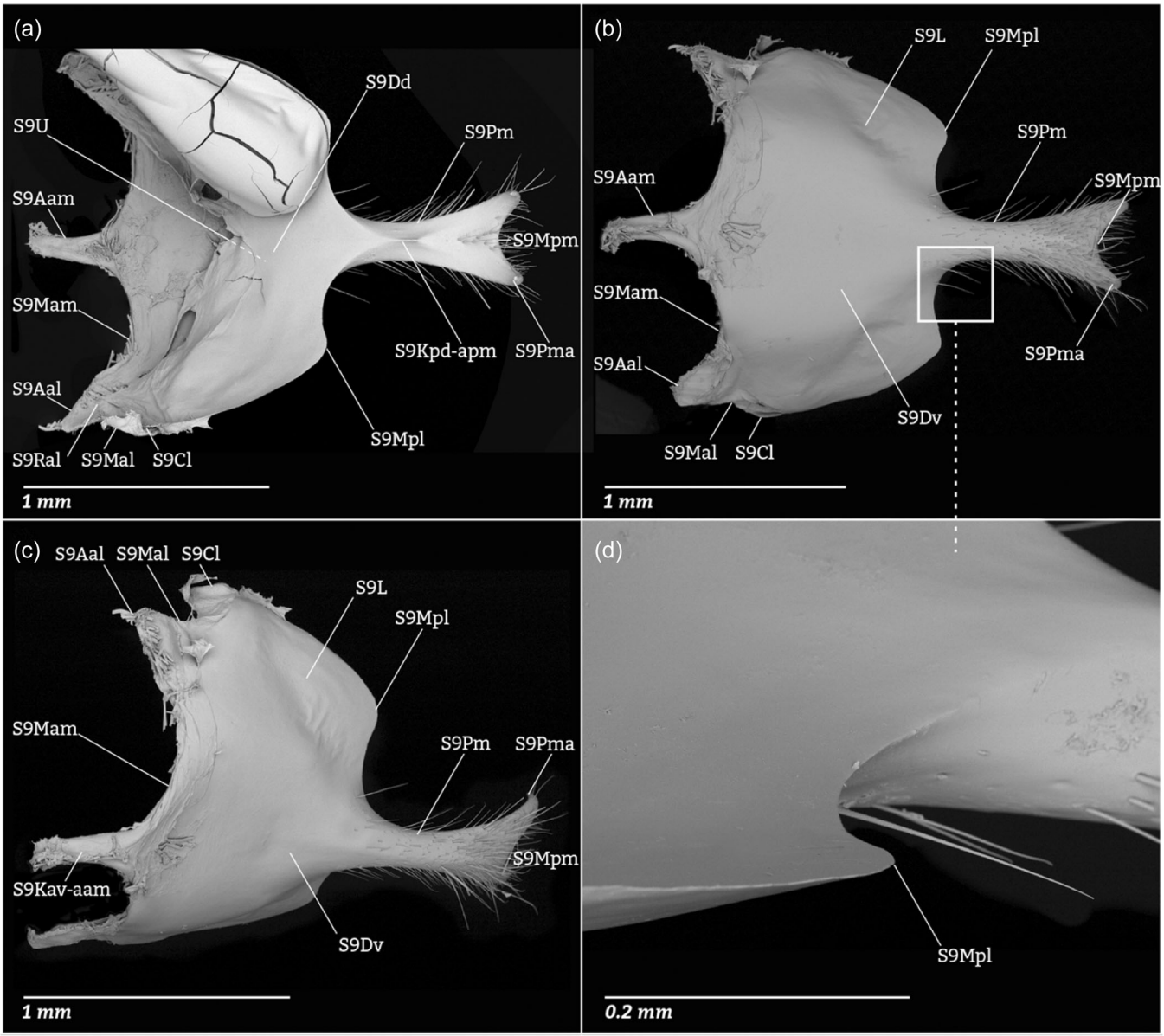

FIGURE 8 Scanning electron micrographs of the male sternum IX of *Paraponera clavata* (SMFHYM0000118). **Views:** (a) Dorsal, (b) ventral, (c) anterior ventrolateral oblique view, (d) detail of the lamella. **Abbreviations: S9Aal** = anterolateral apodeme of sternum IX; **S9Aam** = spiculum; **S9Cl** = lateral corners of sternum IX; **S9Dd** = dorsal disc of sternum IX; **S9Dv** = ventral disc of sternum IX; **S9Kav-aam** = apicoventral spicular carina of sternum IX; **S9Kpd-apm** = proximodorsal prong carina of sternum IX; **S9L** = lamella of sternum IX; **S9Mal** = anterolateral margins of sternum IX; **S9Mam** = anteromedial margins of sternum IX; **S9Mpl** = posterolateral margins of sternum IX; **S9Mpm** = posteromedian margin of sternum IX; **S9Pm** = posteromedian process (=prong) of sternum IX; **S9Pma** = apico-posteromedian processes of sternum IX; **S9Ral** = anterolateral ridge of sternum IX; **S9U** = lumen of sternum IX.

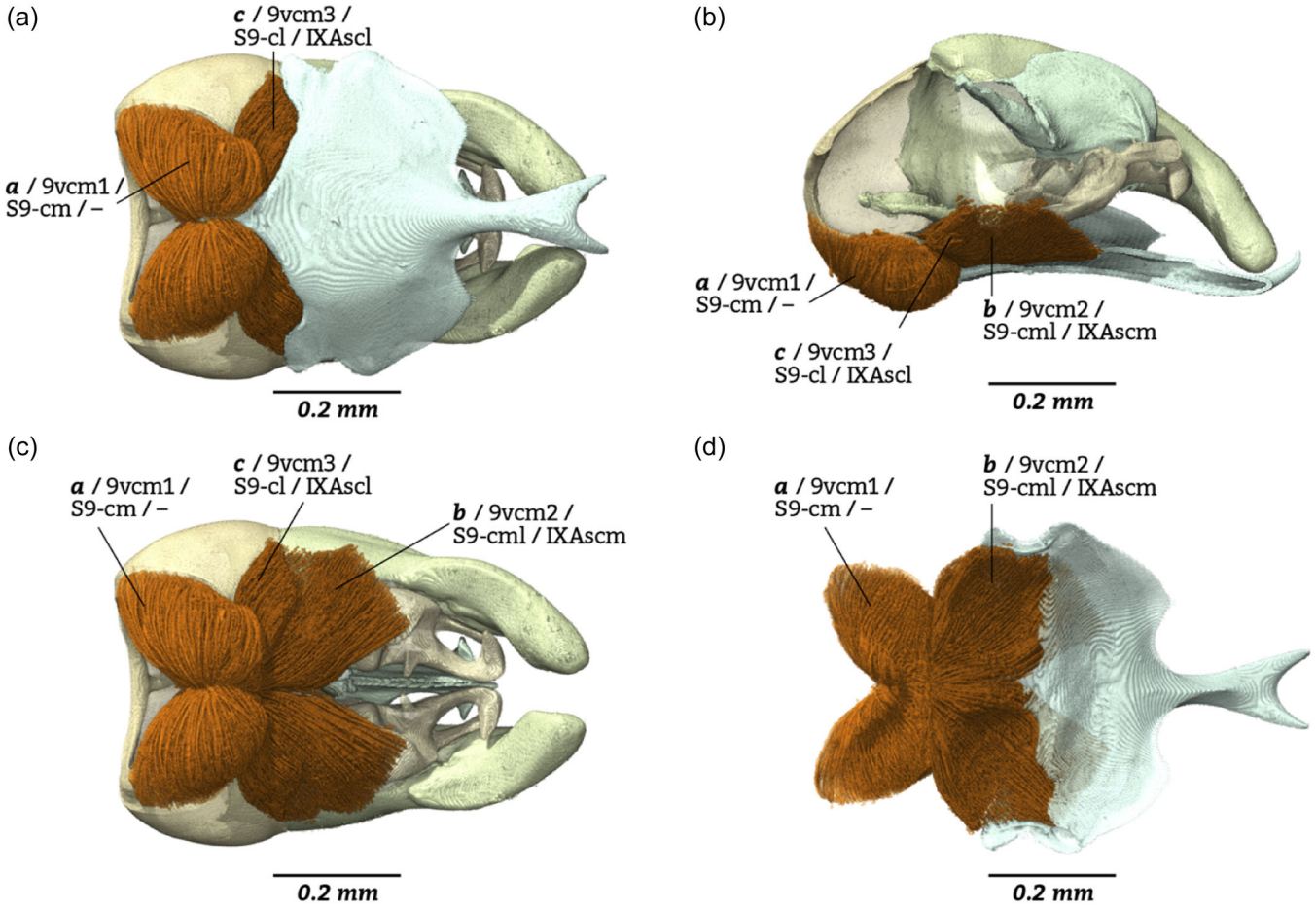

FIGURE 9 Volume renders of the sterno-cupular musculature of *Paraponera clavata*. **Views:** (a) Ventral, (b) lateral with left gonopod digitally removed and sternum IX sagittally sectioned, (c) ventral with sternum IX digitally removed, (d) sternum IX and its musculature in isolation, dorsal. **Abbreviations:** ***a*** = "anteromedian sterno-cupular muscle"; ***b*** = "posteromedian sterno-cupular muscle"; ***c*** = "anterolateral sterno-cupular muscle."

The sternum bears three processes anteriorly: (1) an anteromedian apodeme (the *spiculum*, **S9Aam**) that is digitate, about 3× as long as broad at its base and bears a distinct yet weak anteroventral (apical) keel (the *apicoventral spicular carina*, **S9Kav-aam**), and (2) a pair of *anterolateral apodemes of sternum IX* (**S9Aal**) that are dorsoventrally flattened and asymmetrically lobate, with their apices directed anterolaterally.

The *anteromedial margins of sternum IX* (**S9Mam**) are marked by the spiculum and anterolateral apodemes and correspond to the *anteromedial ridge of sternum IX* (**S9Ram**); they are longer than the spiculum and are weakly sinuate. The *anterolateral margins of sternum IX* (**S9Mal**) are situated between the anterolateral apodemes and the *lateral corners of sternum IX* (**S9C**); these margins are short, weakly concave, and delimited dorsomedially by a short ridge, the *anterolateral ridge of sternum IX* (**S9Ral**). The *posterior margin of sternum IX* (**S9Mp**) is complex, bearing a median forked process that divides the margin into the broadly and asymmetrically sinuate *posterolateral margins of sternum IX* (**S9Mpl**) and the *posteromedian margin of sternum IX* (**S9Mpm**).

The posteromedian forked process is the *prong of sternum IX* (**S9Pm**); it is long and narrow, with its maximum width (which is between the apices of the distal prongs) being about 5–6× is minimum width in ventral or dorsal view; it bears the *proximodorsal carina of the posterior process of sternum IX* (**S9Kpd-apm**), which is longitudinally oriented, posteriorly narrowing, wedge-like, and acute, and it bears the paired *apicomedian processes of the sternum IX prong* (**S9Pma**), which are acutely triangular, long, and narrow, with their lengths being somewhat more than 2× their proximal widths.

The *lumen of sternum IX* (**S9U**) is indicated ventrally by a median bulge, the *ventral disc of sternum IX* (**S9Dv**), and dorsally by the *dorsal disc of sternum IX* (="cranial apodeme," cf. references in Boudinot, 2013) (**S9Dd**), which is inflected over the posterior margin and extends toward the ventral base of the gonopod. Posterolaterad the lumen, the sternum is produced as a flat, translucent lamella, the *posterolateral lamellae of sternum IX* (**S9L**), which are extremely thin at their posterior apices (Figure 8d).

Setation

Sternum IX is largely devoid of setae. Long, thin setae are present on the ventral surface of the sternum, extending from the base of the posteromedial prong to the apex of the prong with density increasing apically. Similar setae are present in a triangle on the

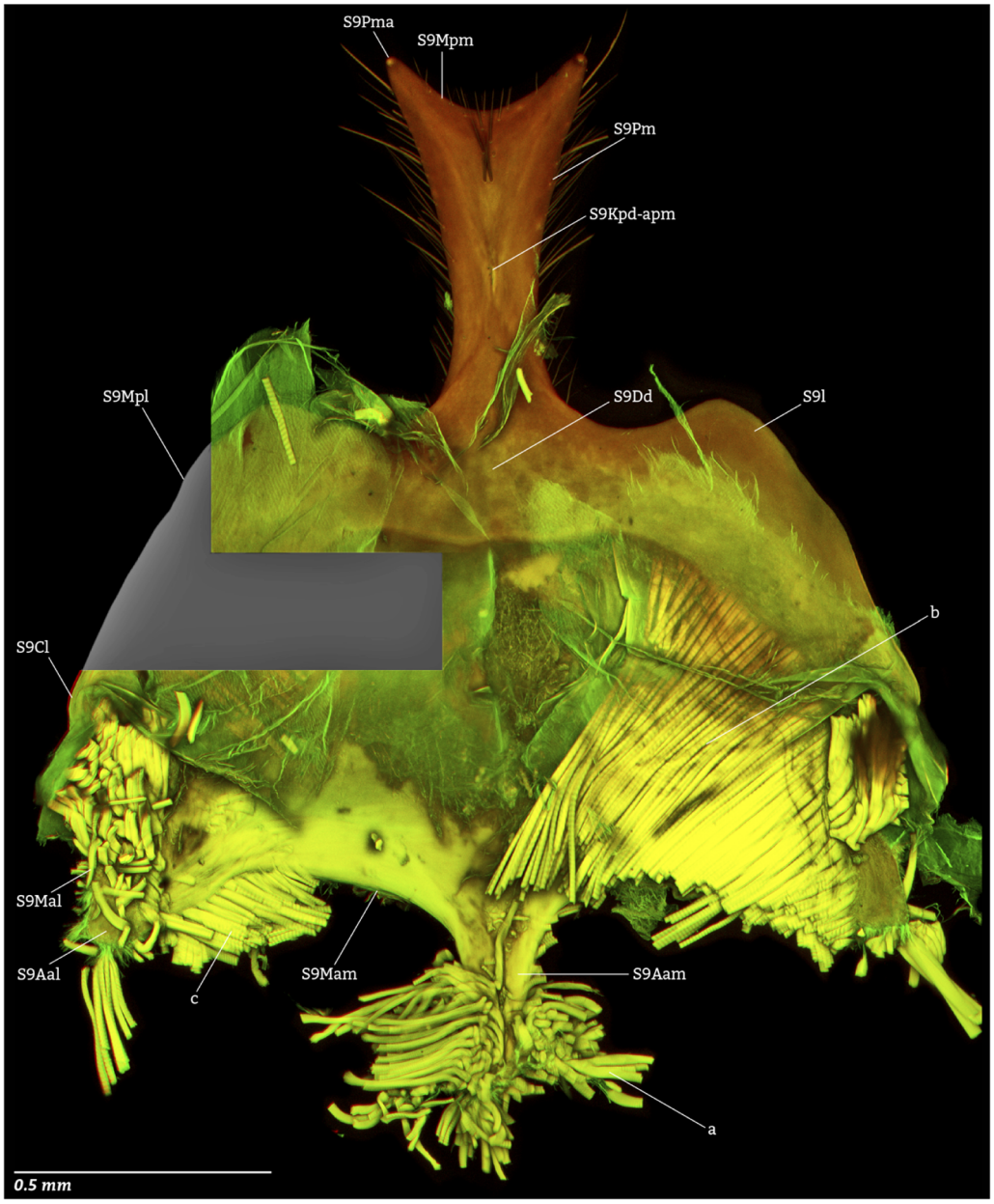

FIGURE 10 CLSM max intensity render of sternum IX of *Paraponera clavata* (SMFHYM0000227) in dorsal view. Gray indicates missing data. **Abbreviations: S9Aal** = anterolateral apodeme of sternum IX; **S9Aam** = spiculum; **S9Dd** = dorsal disc of sternum IX; **S9L** = lamella of sternum IX; **S9Mal** = anterolateral margins of sternum IX; **S9Mam** = anteromedial margins of sternum IX; **S9Pm** = posteromedian process (=prong) of sternum IX; **S9Pma** = apico-posteromedian processes of sternum IX.

apicodorsal surface of the prong distal to the dorsal median longitudinal carina.

Muscles

Sternum IX bears the origins of three muscles that insert on the cupula (Figures 4, 9, 10); these muscles control the retraction and protraction of the genitalia. (*Note*: The long-form names provided here are informal and intended to be descriptive; the muscle labels are provided in the following sequence after Table 1: #1 = Boulangé (1924) as modified by Schulmeister (2001, 2003), #2 = Griebenow et al. (2023), #3 = Dal Pos et al. (2023), #4 = Boudinot (2018).)

Muscle *a* (**9vcm1**, **S9**-cm, –), the *anteromedian sterno-cupular muscle*: **O** (=origin): Along the length of the apicoventral spicular carina of sternum IX (S9Kav-apm). **I** (=insertion): Across the anterior (proximal) depression of the CA (CAsad). **S** (=shape): Paired; directed dorsolaterally. **F** (=function): Retractor of the external genitalia; antagonist of muscles ***b***, ***c***.

Muscle *b* (**9vcm2**, **S9-cml**, **IXAscm**), the *posteromedian sterno-cupular muscle*: **O**: Parasagittally within the lumen of sternum IX (S9L).

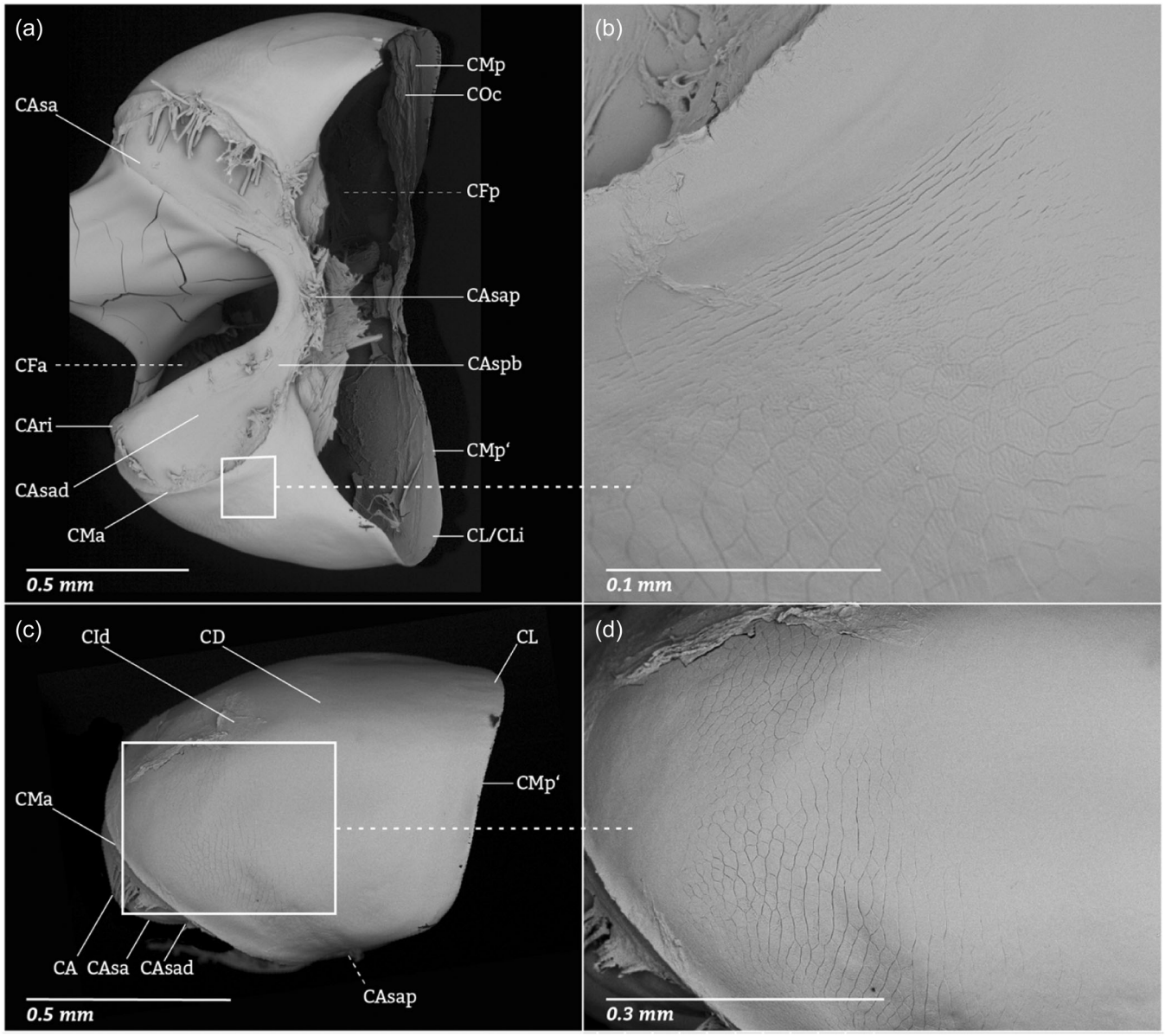

FIGURE 11 Scanning electron micrographs showing the shape and surface structure of the cupula of *Paraponera clavata* (SMFHYM0000118). **Views:** (a) Ventral; (b) detail of ventrolateral surface, near the juncture of the sterno-cupular membrane; (c) lateral view; (d) detail of the anterolateral surface, near the juncture of the sterno-cupular membrane. **Abbreviations: CA** = cupular apodeme; **CAri** = mesal (internalmost) rim of the cupular apodeme; **CAsa** = anterior (proximal) surface of the cupular apodeme; **CAsad** = anterior (proximal) depression of the cupular apodeme; **CAsap** = posteromedial process of the cupular apodeme anterior surface (=gonocondyle); **CD** = cupular disc; **CFa** = anterior (proximal) cupular foramen; **CFp** = posterior (distal) cupular foramen; **CL** = cupular lamella; **CLi** = posterior (distal) cupular inflection; **CMa** = (true) anterior (proximal) cupular margin; **CMp** = (true) posterior (distal) cupular margin; **CMp′** = apparent posterior (distal) cupular margin; **COc** = cupulo-coxal membrane.

I: Ventromedially on the gonocondyle (CAsap). **S**: Paired; broad, shallow fans. **F**: Protractor of the external genitalia; antagonist of muscle ***a***, functionally integrated with muscle ***c***.

Muscle c (**9vcm**, **Sp-cl**, **IXAscl**), the *anterolateral sterno-cupular muscle*: **O**: On the anteromedial margins of sternum IX (S9Mam), including the anterior base of the anterolateral apodemes of sternum IX (S9Aal). **I**: Laterad the gonocondyle on the anterior surface of the CA (CAsa). **S**: Paired; somewhat more than half the width of ***b*** and about half the length of ***b***. **F**: Protractor of the external genitalia; antagonist of muscle ***a***, functionally integrated with muscle ***b***.

The *intrinsic muscles of sternum IX* (**–**, **9vvim**, **–**, **–**) are absent.

3.2.3 | Cupula

Sclerite

The *cupula* forms a complete ring (**C**); its anterior opening is the *anterior cupular foramen* (=*foramen genitale*) (**CFa**) and its posterior opening is the *posterior cupular foramen* (**CFp**); posteriorly (distally), it is connected by membrane to the bases of the gonopods distally and

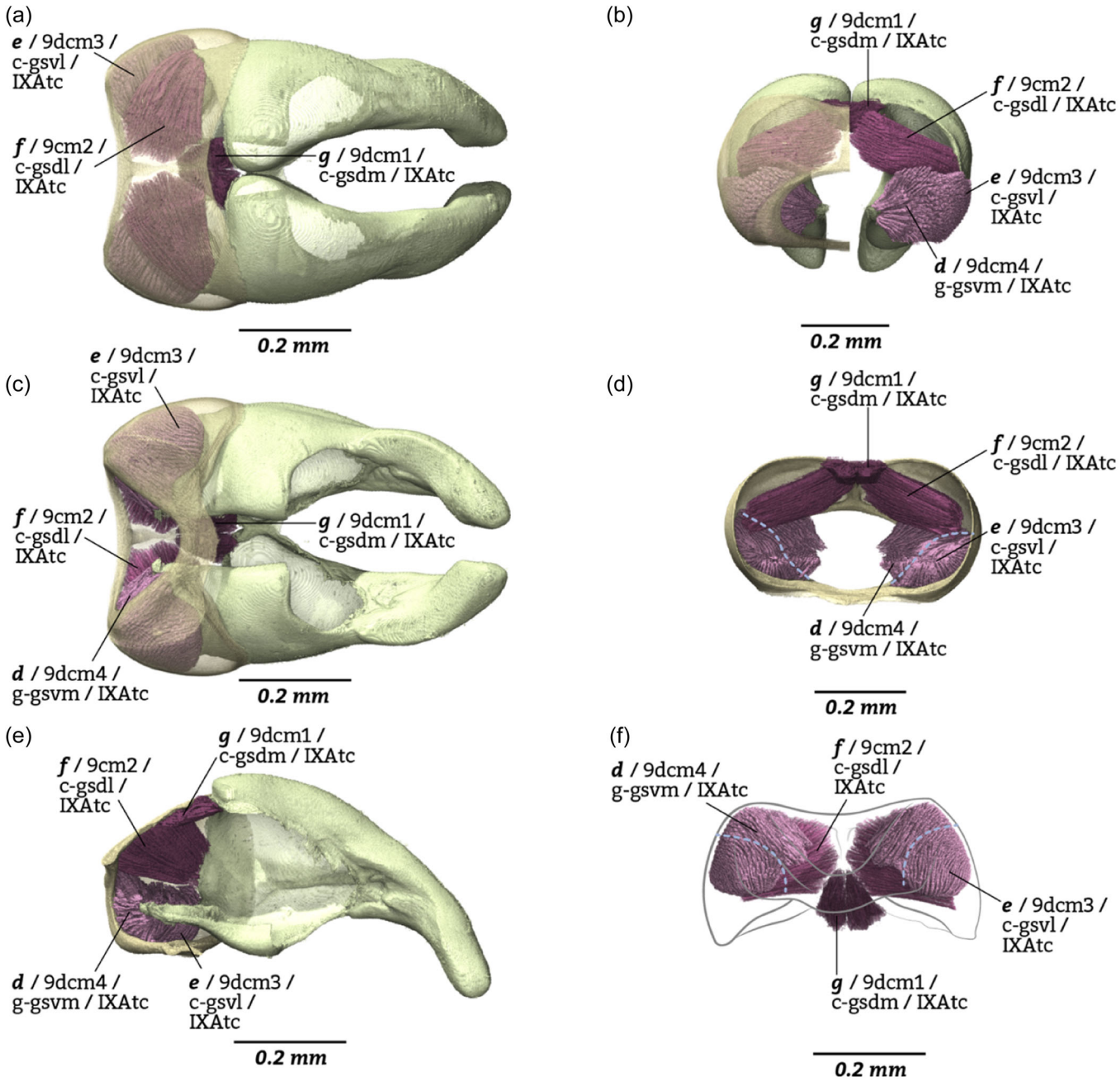

FIGURE 12 Volume renders of the cupulo-coxal musculature of *Paraponera clavata*, with the volsellae and penites digitally removed. **Views:** (a) Dorsal; (b) medial, with cupula digitally sectioned in the sagittal plane and the left gonopod removed; (c) ventral; (d) anterior (cranial) view with the left half of the cupula digitally removed; (e) posterior (caudal) view of the cupula and its musculature in isolation; (f) illustration of the cupula in ventral view. **Abbreviations:** ***d*** = "ventromedial cupulo-coxal muscle"; ***e*** = "ventrolateral cupulo-coxal muscle"; ***f*** = "dorsolateral cupulo-coxal muscle"; ***g*** = "dorsomedial cupulo-coxal muscle."

sternum IX proximally; it cups the bases of the gonopods, and it is cupped ventrally by sternum IX. The cupula has three main components: The CD, the cupular lamella, and the CA.

(1) The **CD** is the portion of the cupula between the anteriorly attached *genital chamber membrane*, which forms the true *anterior (proximal) margin of the cupula* (**CMa**), and the posteriorly (distally) attached *cupulo-gonopodal membrane*, which forms the true *posterior (distal) margin of the cupula* (**CMp**). The *anterior/proximal margin of the cupula* (CMa) is concave dorsally, forming the *proximodorsal notch of the cupula* (**CMand**), and is concave ventrally, forming the *proximoventral notch of the cupula* (**CManv**). The CD is somewhat more than 2× as wide lateromedially as long anteroposteriorly; it is about 5× as long dorsally as ventrally; in dorsal view, it is divided into left and right halves as the anterior and posterior margins are medially concave, and each half is only slightly longer than wide; in lateral view, it is parabolic in shape, with the vertex of the curve located

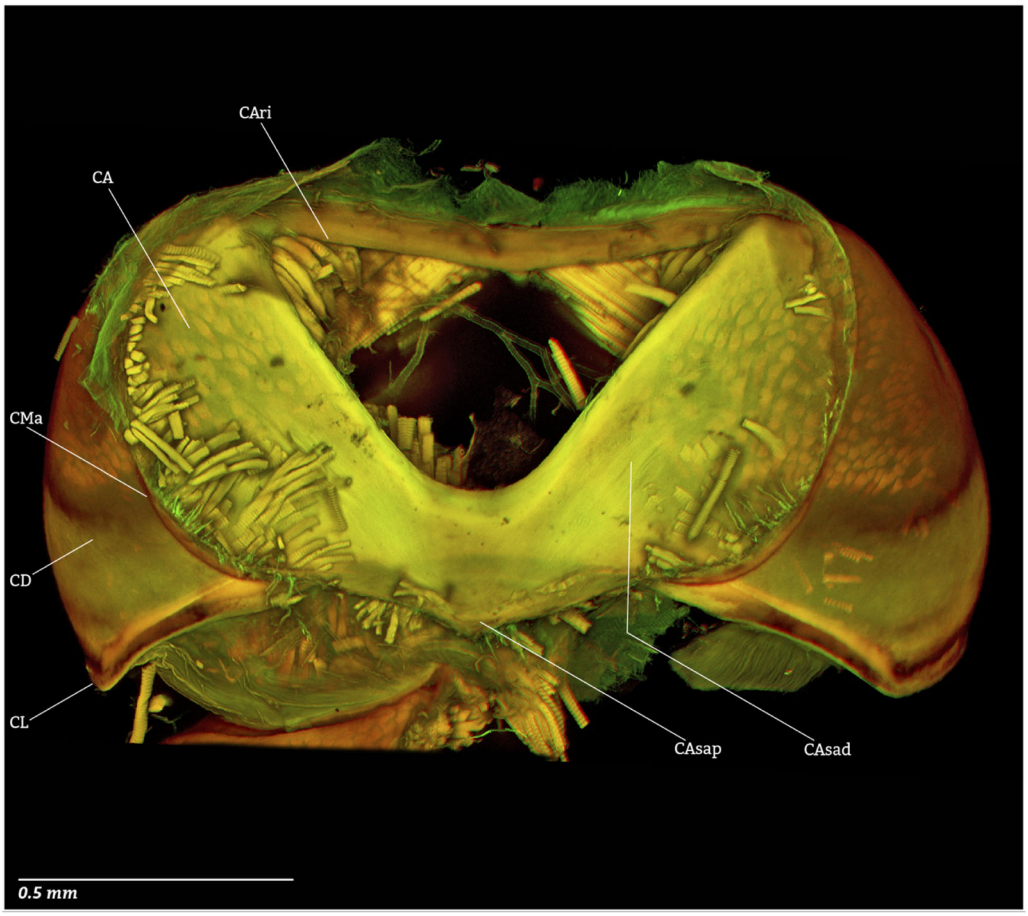

FIGURE 13 CLSM max intensity render of the cupula of *Paraponera clavata* (SMFHYM0000227) in anteroventral oblique view. **Abbreviations: C** = cupula; **CA** = cupular apodeme; **CAri** = mesal (internalmost) rim of the cupular apodeme; **CAsa** = anterior (proximal) surface of the cupular apodeme; **CAsad** = anterior (proximal) depression of the cupular apodeme; **CAsap** = posteromedial process of the cupular apodeme anterior surface; **CD** = cupular disc; **CL** = cupular lamella; **CMa** = (true) anterior (proximal) cupular margin.

anteriorly; in ventral view, it is extremely narrow and overlapped by the CA. Internally, the CD bears the *dorsomedian longitudinal ridge* (**CRdm**), which extends from the CA anteriorly to the *posterodorsal ridge of the cupula* (**CRpd**), which itself follows the contour of the true and apparent posterior margins of the cupula and is thickest medially and becomes obsolete laterally where contact is made with the gonocoxa during motion. The cupula is weakly impressed in its anterior half, with this impression corresponding to the origins of cupulo-coxal muscles, thus matching the HAO concept of "dorsal submedian impression of cupula" (**CId**).

(2) The *cupular lamella* (**CL**) is the flange-shaped portion of the cupular sclerite that projects posteriorly beyond the cupulo-gonopodal membrane, forming the *apparent posterior margin of the cupula* (**CMp′**), which directly contours the true posterior margin, hence is equivalent in shape but not in precise location, and the *posterior cupular inflection* (**CLi**), which is the surface of the lamella that contacts the gonocoxae.

(3) The **CA** is the internal ridge that bears muscles, subtends the true anterior cupular margin hence forming a secondary rim around the anterior cupular foramen. In *Paraponera*, it is considerably broadened, being thick but anteroposteriorly narrow dorsally and broadening ventrolaterally until narrowing again ventromedially. The *mesal rim of the cupular apodeme* (**CAri**) marks the limit of the *anterior (proximal) surface* (**CAsa**) and *posterior (distal) surface* (**CAsp**) *of the cupular apodeme*. The ventrolateral areas of the anterior surface of the cupular apodeme are concave externally, forming the *anterior (proximal) depressions of the cupular apodeme* (**CAsad**), which correspond internally to the *posterior (distal) bulges of the cupular apodeme* (**CAspb**). Ventromedially, the apodeme is produced posteriorly as the *posteromedial process of the cupular apodeme anterior surface* (=gonocondyle) (**CAsap**); this process bears the attachment of sterno-cupular membrane; as seen in ventral view, this process overlaps the posterior (distal) cupular margin, which bears the attachment of the cupulo-coxal membrane.

Setation

The cupula is devoid of setation.

Sculpture

Cellular outlines ("scutes" *sensu* Mikó et al., 2016) are visible externally on the cupula, particularly adjacent to the sclerotic swelling

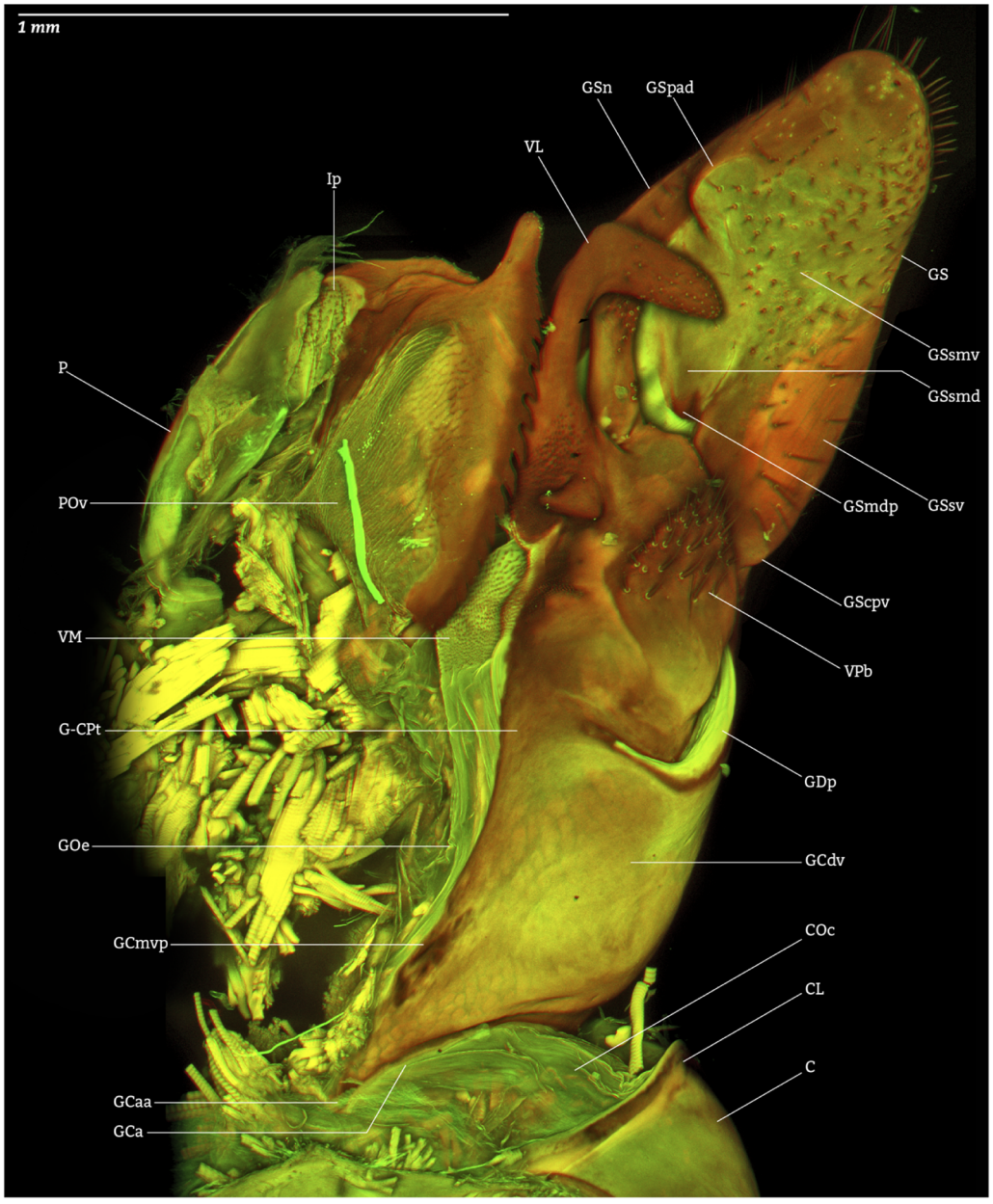

FIGURE 14 CLSM max intensity render of the genital appendages of *Paraponera clavata* (SMFHYM0000227) in ventrolateral posterior oblique view. **Abbreviations: C** = cupula; **CL** = cupular lamella; **COc** = cupulo-coxal membrane; **GCa** = gonocoxal apodeme; **GCcpm** = gonocoxal corner, proximomedial; **GCdv** = ventral disc of the gonocoxa; **GCmvp** = proximoventral gonocoxal margin; **G-CPt** = coxo-parossicular transition; **GOe** = coxopenial membrane; **GOp** = coxo-parossicular membrane; **GS** = gonostylus; **GScpv** = corner of the gonostylus, proximoventral; **GSn** = notch, proximodorsal of gonostylus; **GSpad** = process of the gonostylus, apicodorsal; **GSsmd** = dorsomedial gonostylar surface; **GSsmdp** = (medial) process of the dorsomedial gonostylar surface; **GSsmv** = ventromedial gonostylar surface; **GSsv** = ventral gonostylar surface; **Ip** = phallotreme; **P** = penite; **VL** = lateropenite; **VM** = microtrichial field of the volsella; **VPb** = basivolsella.

to which the sterno-cupular membrane attaches. The outlines become faint and disappear altogether by the midlength of the cupula.

Muscles

The cupula bears the origins of four muscles that insert on the gonocoxites (Figures 4 and 12); these muscles control the opening (abduction), closing (adduction), and stability of the gonopods.

Muscle *g* (**9dcm1**, **c-gsdm**, **IXAtc**-part), the *dorsomedial cupulo-coxal muscle*: **O**: Posterodorsomedially on the internal surface of the cupula, immediately laterad the dorsomedian (longitudinal) ridge (CRdm) and immediately posterad the posterodorsal (marginal) ridge (CRpd). **I**: Marginally on the dorsal apex of the gonocoxal apodeme (GCaav), laterad the gonocoxal bridge (GCb). **S**: Paired; small and parallel; broadening to their insertion. **F**: Stabilizer of the gonocoxal bridge (GCb).

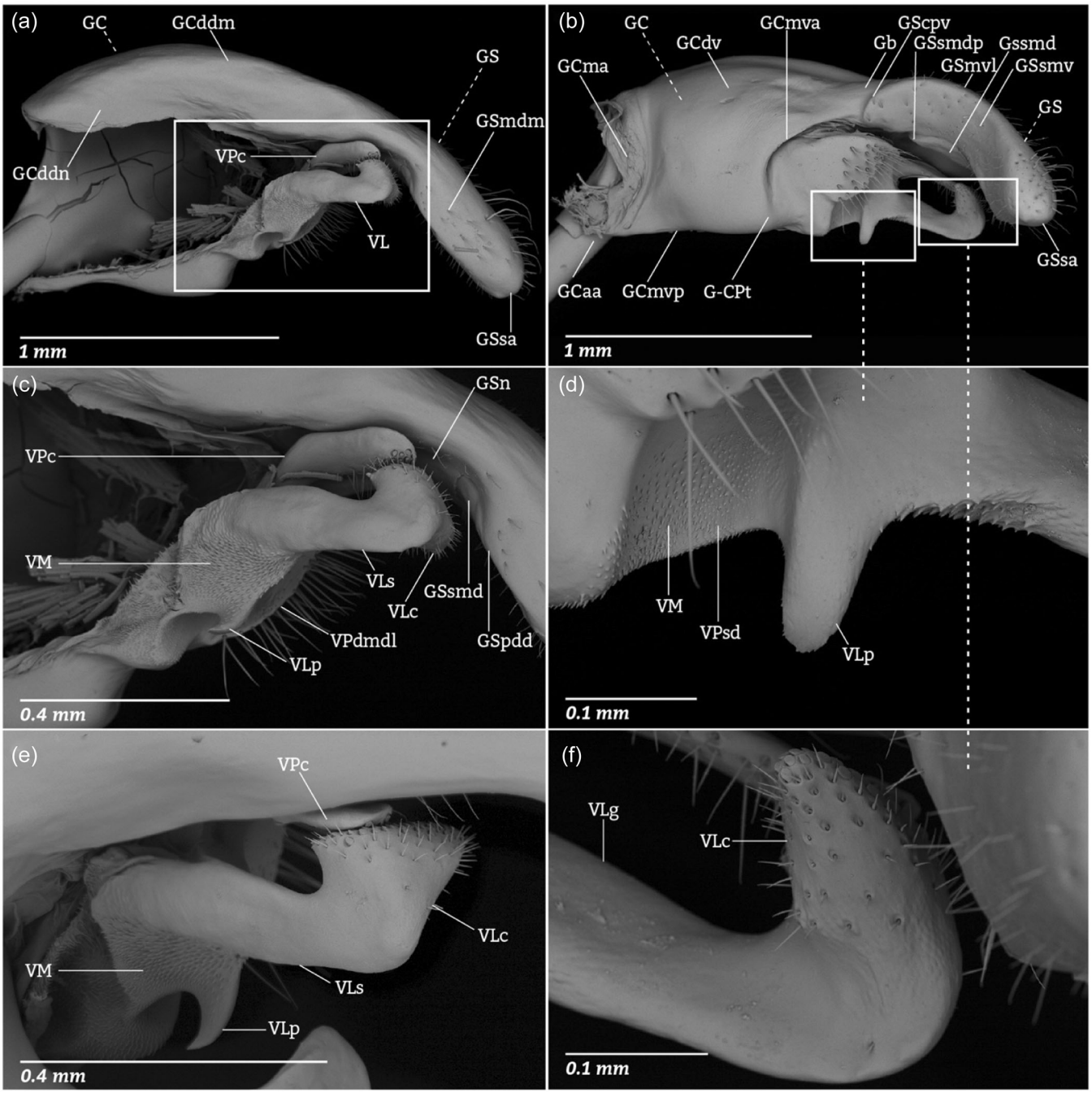

FIGURE 15 Scanning electron micrographs showing shape, surface structure, and spatial relationships of the volsellar complex of *Paraponera clavata* (SMFHYM0000118). **Structures and views:** (a, c, e) Gonopod–volsellar complex in medial posterodorsal oblique view; (b, d, f) gonopod–volsellar complex in ventral posterior-oblique view. **Abbreviations: GC** = gonocoxite; **GCaa** = apex of the gonocoxal apodeme; **GCdd** = dorsal disc of the gonocoxa; **GCddc** = curves of the dorsal gonocoxal disc.; **GCddcm** = medial curve of the dorsal gonocoxal disc; **GCddi** = (medial) inflection of the dorsal gonocoxal disc; **GCdv** = ventral disc of the gonocoxa; **GCma** = anterior gonocoxal margin; **GCmva** = apicoventral gonocoxal margin; **GCmvp** = proximoventral gonocoxal margin; **G-CPt** = coxo-parossicular transition; **GS** = gonostylus; **GScpv** = corner of the gonostylus, proximoventral; **GSmdm** = dorsomedial margin of the gonostylus; **GSmpm** = proximomedial margin of the gonostylar sclerotization; **GSmvl** = ventrolateral margin of the gonostylus; **GSn** = notch, proximodorsal of gonostylus; **GSpad** = process of the gonostylus, apicodorsal; **GSsa** = apical surface of the gonostylus; **GSsmd** = dorsomedial gonostylar surface; **GSsmdp** = (medial) process of the dorsomedial gonostylar surface; **GSsmv** = ventromedial gonostylar surface; **V** = volsella; **VL** = lateropenite; **VLc** = club of the lateropenite; **VLp** = process of the lateropenite, proximomedial; **VLs** = stem of the lateropenite; **VM** = microtrichial field of the volsella; **VPc** = distivolsella; **VPs** = sulcus; **VPsd** = distal parossicular sulcus; **VPsl** = (longitudinal) volsellar sulcus.

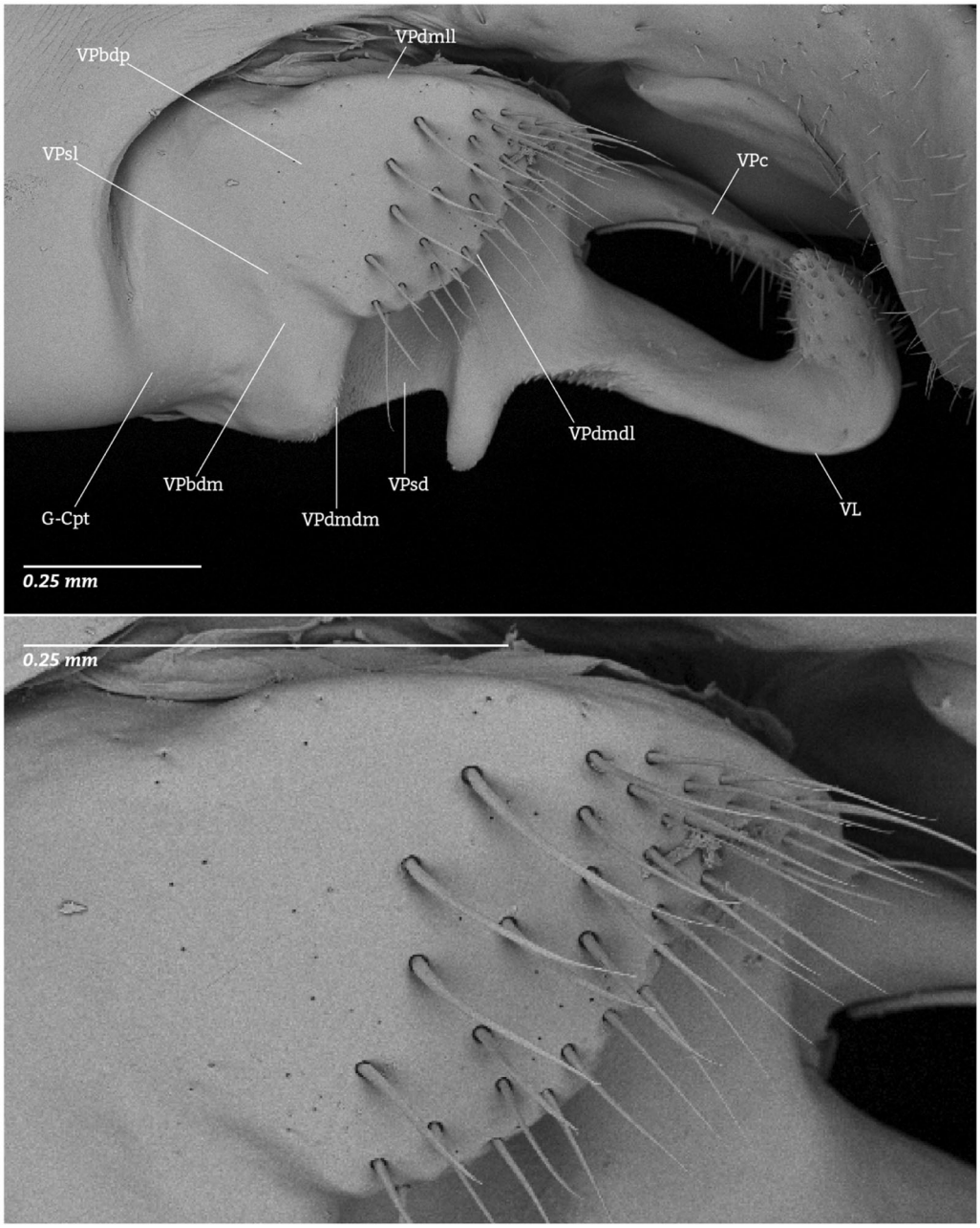

FIGURE 16 Scanning electron micrographs of the volsella of *Paraponera clavata* (SMFHYM0000118), both in ventral view. **Views:** (a) Overview of the volsella. (b) Detail of basivolsella. **Abbreviations: G-CPt** = coxo-parossicular transition; **VL** = lateropenite; **VPbdpl** = lateral (portion of the) basivolsellar disc; **VPbdpm** = medial (portion of the) basivolsellar disc; **VPc** = distivolsella; **VPdmdl** = distal margin of the lateral basivolsellar disc; **VPdmdm** = distal margin of the medial basivolsellar disc; **VPdmll** = lateral margin of the lateral basivolsellar disc; **VPsd** = distal parossicular sulcus; **VPsl** = (longitudinal) volsellar sulcus.

Muscle *f* (**9dcm2**, **c-gsdl**, **IXAtc**-part), the *dorsolateral cupulo-coxal muscle*: **O**: Anterodorsally immediately laterad the dorsomedian (longitudinal) ridge (CRdm), anterad (proximad) ***g*** and dorsad ***e*** and ***d***. **I**: Laterally on the gonocoxal apodeme (GCa), immediately dorsad the anterior (proximal) apex of the coxostylar ridge (GCr). **S**: Paired; broad and fan-shaped; narrowing to their insertion. **F**: Abductor of the gonopod; antagonist of ***e***, ***d***.

Muscle *e* (**9dcm3**, **c-gsvl**, **IXAtc**-part), the *ventrolateral cupulo-coxal muscle*: **O**: Ventrolaterally in the proximal half of the cupula, immediately ventrad ***f***, anterad the cupular apodeme (GCa), and dorsoproximad ***d***. **I**: Ventrolaterally on the gonocoxal apodeme (GCa), immediately ventrad ***f***. **S**: Paired; forming large, thick bundles. **F**: Adductor of the gonopod; antagonist of ***f***, functionally integrated with ***d***.

Muscle *d* (**9dcm4**, **c-gsvm**, **IXAtc**-part), the *ventromedial cupulo-coxal muscle*: **O**: Ventrally on the CD, ventrad ***f***. **I**: Ventral apex of the gonocoxal apodeme (GCaav). **S**: Paired; smaller than ***e***; forming thick bundles. **F**: Adductor of the gonopod; antagonist of ***f***, functionally integrated with ***d***.

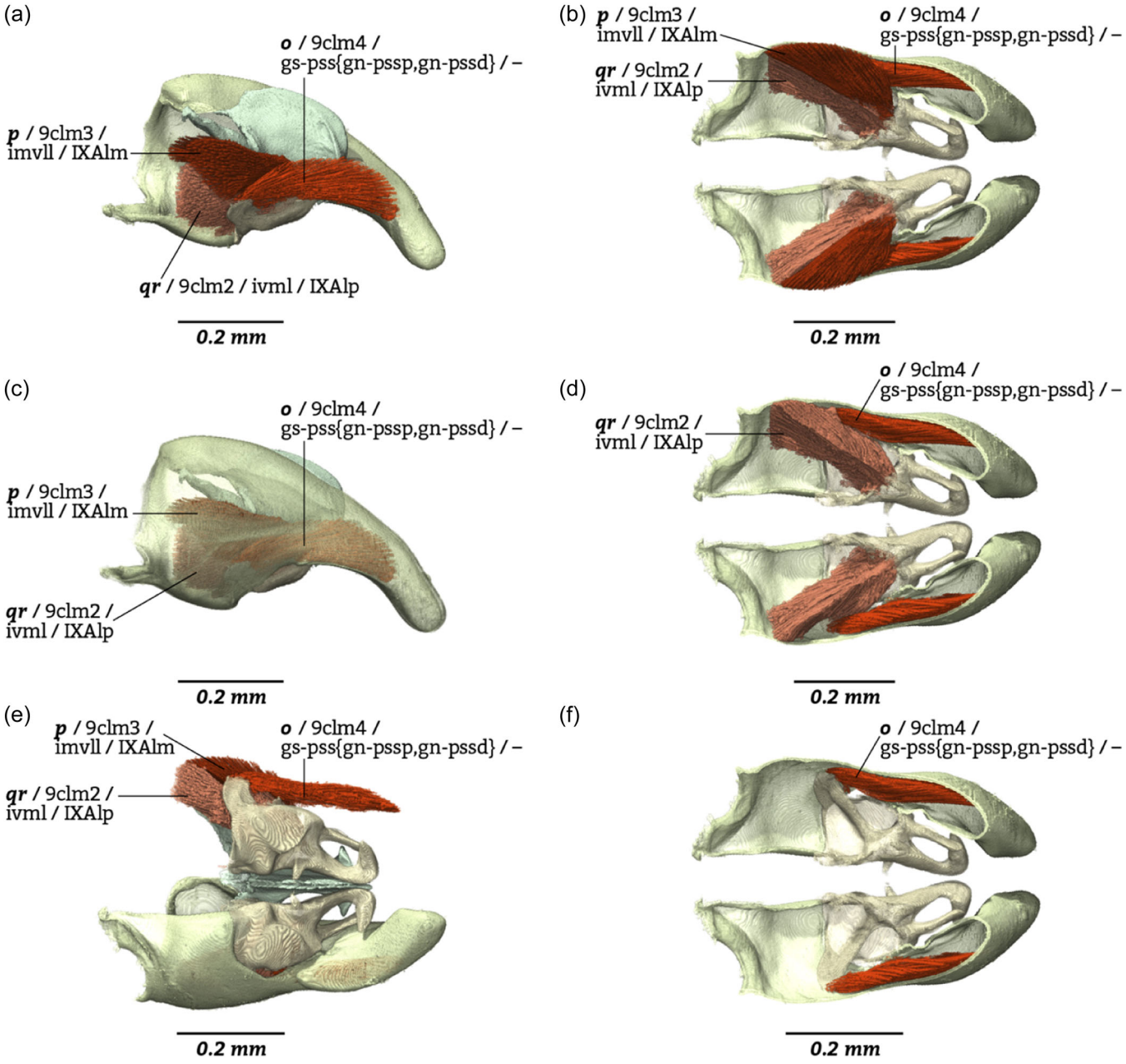

FIGURE 17 Volume renders of the volsellar musculature of *Paraponera clavata*. **Parts and views:** (a) Left volsella, both penites, and right gonopod in medial view; (b, d, f) gonopod–volsellar complex with gonopods digitally dissected approximately in the frontal plane, dorsal view; (c) left gonopod, volsella, and penite in lateral view; (e) gonopod–volsellar complex with left gonopods digitally removed. **Abbreviations:** ***o*** = "coxo-basivolsellar muscle"; ***p*** = "coxo-distivolsellar muscle"; ***qr*** = "basivolsellar-distivolsellar muscle."

3.2.4 | Gonopod

Sclerite

The ***gonopodites*** (here forward, *gonopods*) (**G**) are paired appendages that are divided into the proximal *gonocoxites* (here forward, *gonocoxae*) (**GC**) and the distal *gonostyli* (**GS**); the gonocoxae and gonostyli are similar in length as seen in lateral view. The *coxostylar boundary* (**Gb**) is identifiable by phenotypic elements visible in the four primary views:

(Gb-1) In dorsal view, the coxostylar boundary is marked by the *lateral* (**GCddcl**) and *medial curves of the dorsal gonocoxal disc* (**GCddcm**); these also partially delimit the *gonocoxal disc*, which bears most of the origin of the penial depressor muscle (***j***).

(Gb-2) In medial view, the coxostylar boundary is marked by: (a) the medial curve of the gonocoxal disc, (b) the *proximomedial margin of the gonostylar sclerotization* (**GSmpm**), and (c) the associated *ventromedial coxostylar membrane* (**GOv**).

(Gb-3) In lateral view, the coxostylar boundary is marked dorsally by: (a) the *dorsal coxostylar attenuation* (**G-CSa**), which is a distal narrowing of the dorsal gonocoxal disc; (b) ventrally the *proximoventral corner of the gonostylus* (**GScpv**), and (c) especially the apex

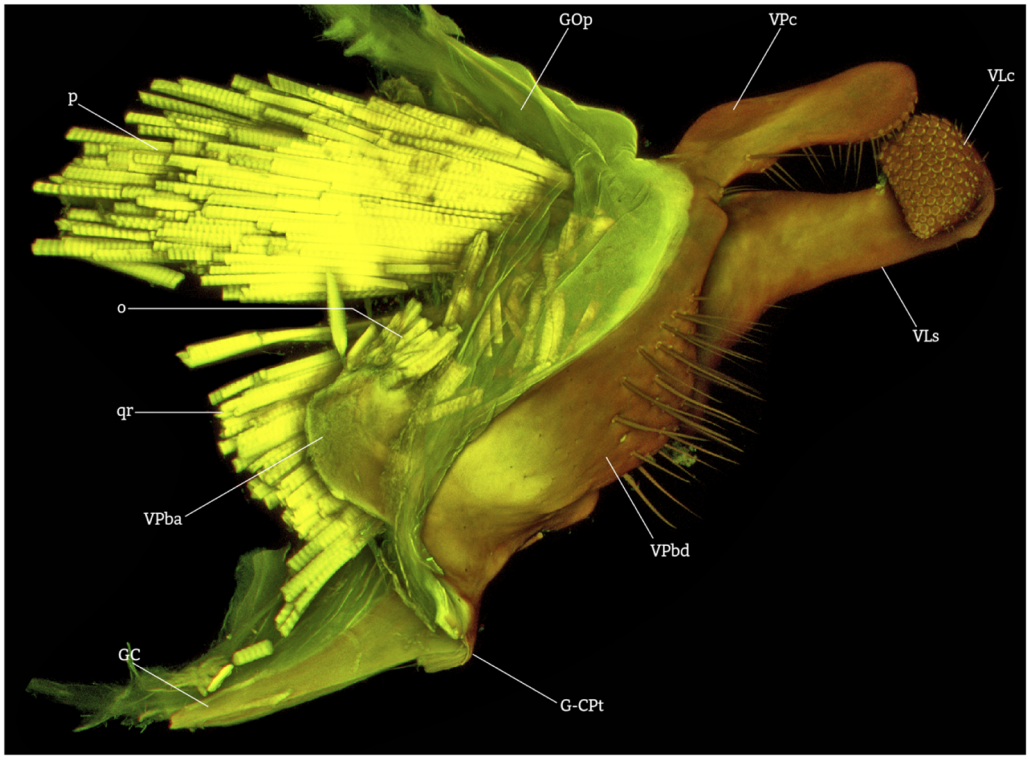

FIGURE 18 CLSM max intensity render of the volsella of *Paraponera clavata* (SMFHYM0000227) in ventrolateral anterior oblique view, that is, looking towards the midline of the body from below and somewhat forward. **Abbreviations: G-CPt** = coxo-parossicular transition; **GOp** = coxo-parossicular membrane; ***o*** = "coxo-basivolsellar muscle"; ***p*** = "coxo-distivolsellar muscle"; ***qr*** = "basivolsellar-distivolsellar muscle"; **VL** = lateropenite; **VLc** = club of the lateropenite; **VLs** = stem of the lateropenite; **VPb** = basivolsellar apodeme; **VPbd** = basivolsellar disc; **VPc** = distivolsella.

of the *ventrolateral gonocoxal sulcus* (**GCs**), which gently curves posterodorsally from the anterolateral gonocoxal margin, and corresponds to the internal *ventrolateral gonocoxal ridge* (=*coxostylar ridge*) (**GCr**).

(Gb-4) In ventral view, the coxostylar boundary is marked by (a) the *ventrolateral margin of the gonostylus* (**GSmvl**) and (b) the proximomedial margin of the gonostylar sclerotization.

The ***gonocoxae*** (**GC**) are fused proximo-dorsomedially, forming the *dorsal gonocoxal bridge* (**GCb**). In anterior view, each gonocoxa is half-pipe shaped, with the vertex of the parabola describing their curve directed laterally. Each gonocoxa has an anterior (proximal) *gonocoxal apodeme* (**GCa**), which is delimited by the *cupulo-coxal membrane* (**COc**) and bears the short and obtuse *lateral process of the gonocoxal apodeme* (**GCal**). Each gonocoxa is divided into *dorsal* (**GCdd**) and *ventral gonocoxal discs* (**GCdv**) by the longitudinally oriented *coxostylar ridge* (**GCr**), which early completely extend anteriorly to meet the gonocoxal apodeme. The *dorsal gonocoxal disc* (GCdd) is roughly parabolic in dorsal view; its medial curve (GCddcm) is shallowly sinuate, and its lateral curve (GCddcl) is shallowly convex; it is about 1.25× as long as broad in dorsal view; its surface is inflected ventrad medial to the medial curve of the gonocoxa, forming the *medial inflection of the dorsal gonocoxal disc* (**GCddi**). The *ventral gonocoxal disc* (GCdv) is subrectangular in ventral view; is about as long as broad; it is slightly bulging along the middle of its surface. Each gonocoxa has four margins defined by sclerite-to-membrane transition:

(GCm-1) The *anterior (proximal) gonocoxal margin* (**GCma**) extends dorsally from the *ventral proximomedial apex of the gonocoxal apodeme* (**GCaav**) to the *dorsal proximomedial apex of the gonocoxal apodeme* (**GCaad**).

(GCm-2) The *proximoventral (medial) gonocoxal margin* (**GCmvp**) extends posteriorly (distally) from the ventral proximomedial apex of the gonocoxal apodeme to the *coxo-parossicular transition* (**G-CPt**), itself recognizable as a curved surface of sclerite between the *gonocoxal disc* (**GCd**) and the *parossiculus* (**VP**); this medial margin is weakly sinuate and more-or-less parallel along its length. The boundary between the *anterior* and *proximoventral gonocoxal margins* is the *proximomedial gonocoxal corner* (**GCcpm**).

(GCm-3) The *apicoventral gonocoxal margin* (**GCmva**) contours along the *coxo-parossicular membrane* (**GOp**) from the coxo-parossicular transition to the proximoventral corner of the gonostylar medial surface.

(GCm-4) The *apicodorsal gonocoxal margin* (**GCmda**) contours along the *coxo-penial membrane* (**GOe**), extending from the dorsal gonocoxal bridge to the proximomedial margin of the gonostylar sclerotization.

The ***gonostyli*** (**GS**) are finger-like and ventromedially curved from base to tip. Each gonostylus is roughly divided into proximal and distal portions as seen in dorsal view due to the medial expansion of the gonostylus distad the volsellar apex. In lateral view, each gonostylus is about 2× as long as tall, with dorsoventral height

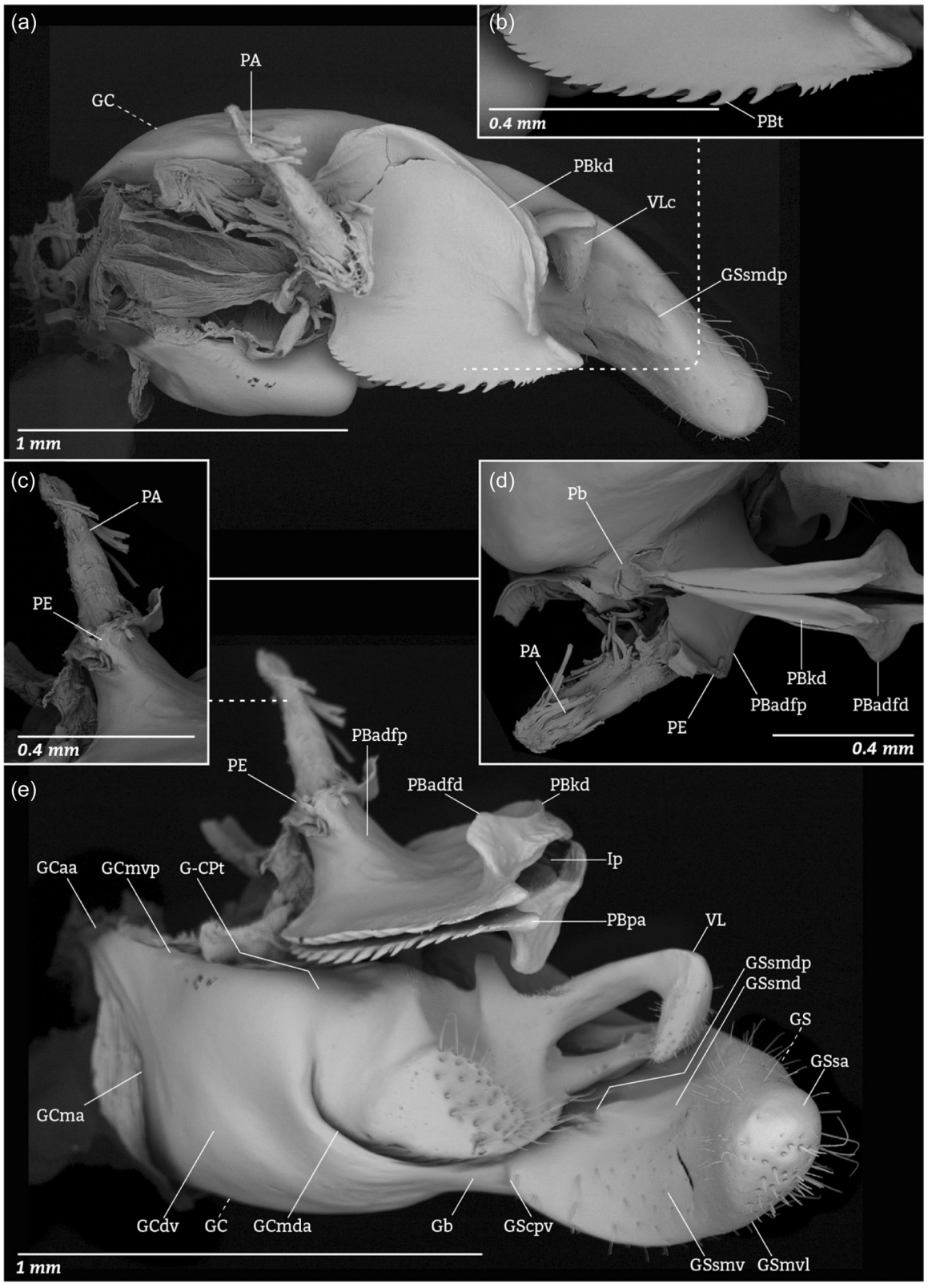

FIGURE 19 (See caption on next page).

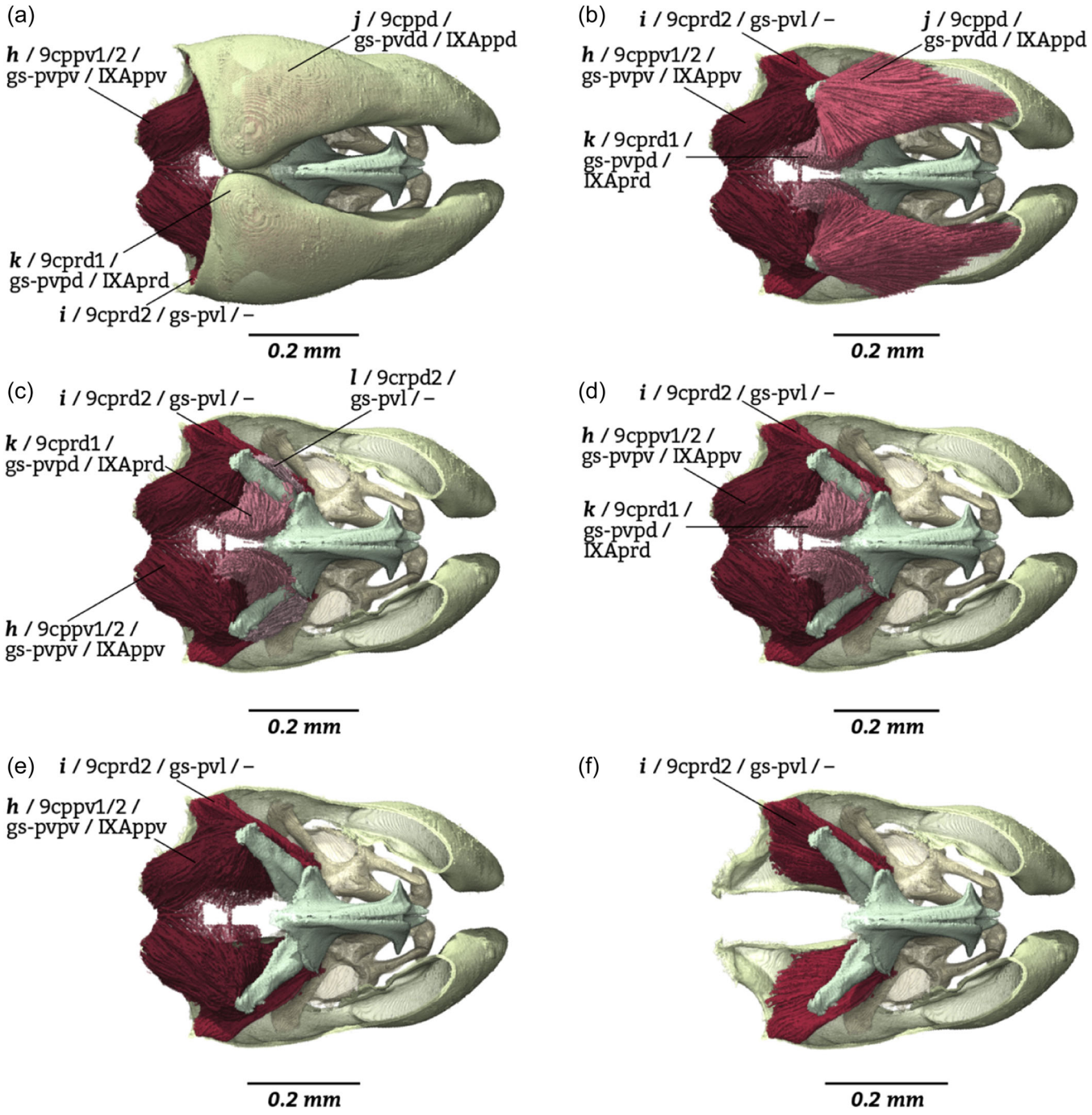

FIGURE 20 Volume renders of the penial musculature of *Paraponera clavata*. **Parts and views:** (a) Gonopod–volsellar complex and penites, dorsal view; (b–f) gonopod–volsellar complex and penites with gonopods digitally sectioned in the frontal plane, dorsal view. **Abbreviations:** ***h*** = "apicoventral coxo-penial muscle"; ***i*** = "proximoventral coxo-penial" muscle; ***j*** = "apicodorsal coxo-penial muscle"; ***k*** = "proximoventral coxo-penial muscle"; ***l*** = "apicolateral coxo-penial muscle."

FIGURE 19 Scanning electron micrographs showing shape, surface structure, and spatial relationships of the penites of *Paraponera clavata* (SMFHYM0000118). **Parts and views:** (a) Both penites and right gonopod–volsellar complex in posteromedial oblique view; (b) detail of the penital teeth; (c) both penites and right gonopod–volsellar complex in ventral posteromedial oblique view; (d) detail of valvura in the same view as (c); (e) both penites and right gonopod–volsellar complex in posterodorsal oblique view. **Abbreviations: GC** = gonocoxite; **GS** = gonostylus; **GScpv** = corner of the gonostylus, proximoventral; **GSmdm** = dorsomedial margin of the gonostylus; **GSmpm** = proximomedial margin of the gonostylar sclerotization; **GSmvl** = ventrolateral margin of the gonostylus; **GSsa** = apical surface of the gonostylus; **GSsl** = lateral surface of the gonostylus; **GSsm** = medial surface of the gonostylus; **GSsmd** = dorsomedial gonostylar surface; **GSsmdp** = (medial) process of the dorsomedial gonostylar surface; **GSsmv** = ventromedial gonostylar surface; **PA** = valvura; **PB** = valviceps; **PBb** = bridge of the valviceps; **PBkd** = dorsal (marginal) carina of the valviceps; **PBpa** = apical process of the valviceps; **PBt** = teeth of the valviceps; **PE** = ergot; **VL** = lateropenite; **VLc** = club of the lateropenite.

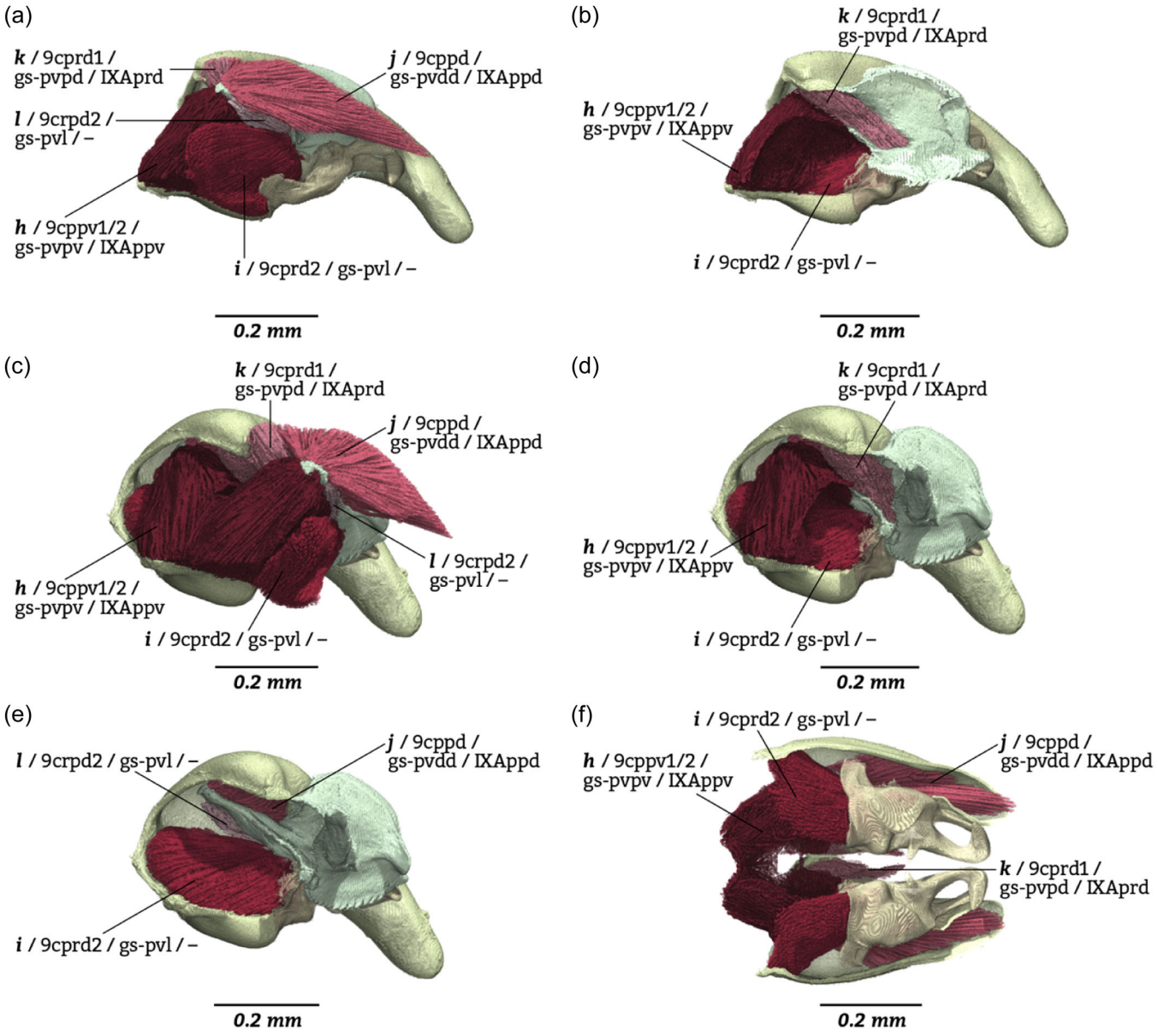

FIGURE 21 Volume renders of the penial musculature of *Paraponera clavata*. **Parts and views:** (a) Both penites and right gonopod–volsellar complex, medial view; (b) right penite and gonopod-volsellar complex, medial view; (c, d, e) both penites and left gonopod-volsellar complex in anterolateral oblique view; (f) gonopod–volsellar complex with gonopods digitally sectioned in frontal plane, ventral view. **Abbreviations:** ***h*** = "apicoventral coxo-penial muscle"; ***i*** = "proximoventral coxo-penial" muscle; ***j*** = "apicodorsal coxo-penial muscle"; ***k*** = "proximoventral coxo-penial muscle"; ***l*** = "apicolateral coxo-penial muscle."

measured from the proximoventral corner of the stylus (GSsmc) to the dorsal coxostylar attenuation (G-CSa). Each gonostylus is divided into the *lateral* (**GSsl**) and *medial* (**GSsm**) *gonostylar surfaces* by a pair of margins: (1) The *dorsomedial gonostylar margin* (**GSmdm**) is more-or-less continuous with the medial curve of the dorsal gonocoxal disc (GCddcm) and extends to the bluntly rounded *gonostylar apex* (**GSsa**), and (2) the *ventrolateral gonostylar margin* (GSmvl) extends from the proximoventral gonostylar corner (**GScpv**) to the gonostylar apex (GSsa). The *lateral gonostylar surface* (**GSsl**) is convex across most of its area. The *medial gonostylar surface* (**GSsm**) is complex and sclerotized, but weakly and variably so (Figure 14); it is divided into the *ventromedial* (GSmv) and the *dorsomedial* (GSmd) *gonostylar surfaces* by a longitudinal curvature, which is a visible as a line of decreased sclerotization (Figure 14). The *ventromedial gonostylar surface* (**GSsmv**) is roughly triangular, concave, and curved along its length, and it proximally appears as the *gonostylar heel* (**GSsv**). The *dorsomedial gonostylar surface* (**GSsmd**) is roughly triangular, concave, and has a low yet bulging *medial process of the proximomedial gonostylar surface* (**GSsmdp**). Where the curvature separating the dorsomedial and ventromedial gonostylar surfaces meets with the dorsomedial gonostylar margin apically, the gonostylus becomes expanded and club-like, with the medial margins being subparallel at

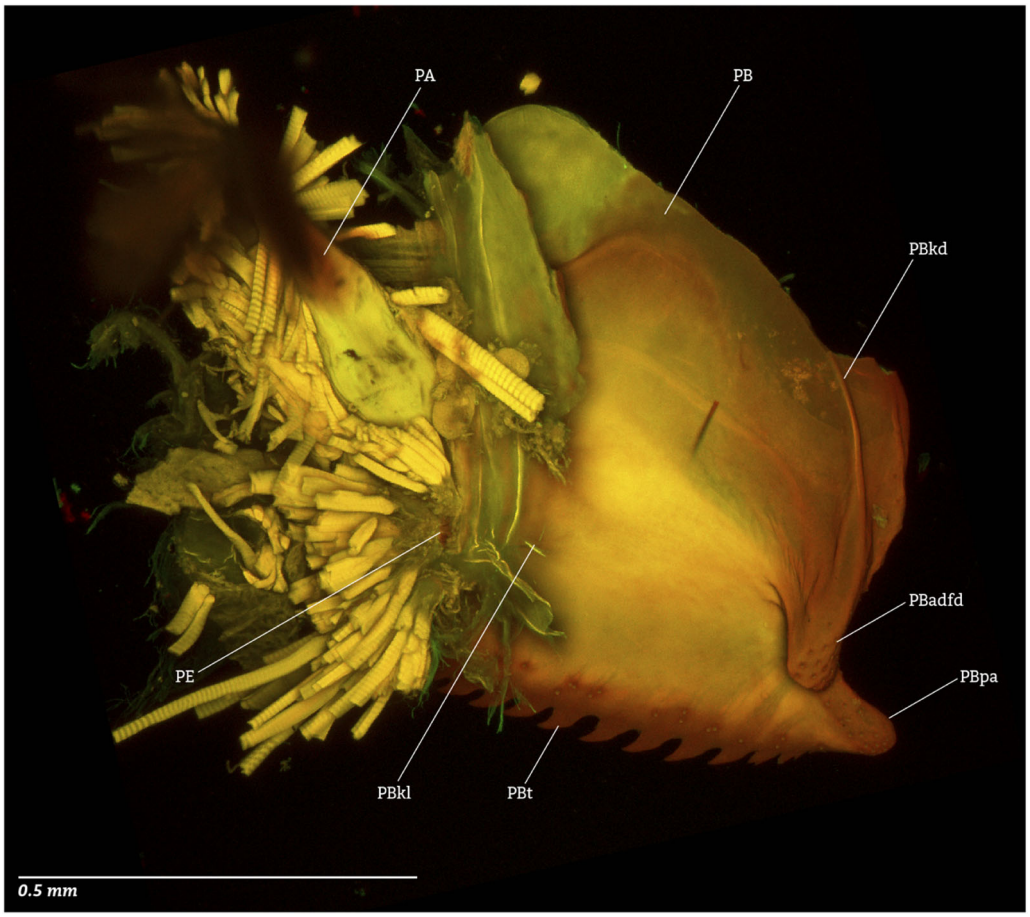

FIGURE 22 CLSM max intensity render of the right penite of *Paraponera clavata* (SMFHYM0000227) in lateral view. **Abbreviations: PA** = valvura; **PE** = ergot; **PB** = valviceps; **PBadfd** = distal flange of the dorsal valviceps region; **PBkd** = dorsal (marginal) carina of the valviceps; **PBkl** = lateral (longitudinal) carina of the valviceps; **PBpa** = apical process of the valviceps; **PBt** = teeth of the valviceps.

rest as seen in dorsal view. In dorsal view, the portion of the *dorsomedial gonostylar margin* that is concave and receives the volsella is the *proximodorsal notch of the gonostylus* (**GSn**). In ventromedial view, the medial expansion of the *dorsomedial gonostylar margin* is proximally convex, forming the *apicodorsal process of the gonostylus* (**GSpad**).

Setation

The gonocoxa is devoid of setation. The gonostylus has long, dilute setae on in the apical half of its lateral surface, some smaller setae on the dorsomedial surface of the club-like apex, and has short, prickly appearing setae along the ventromedial gonostylar surface, where this surface is less heavily sclerotized (GSsmv, Figure 14).

Muscles

The gonopodites bear the origins of the *coxo-stylar*, *coxo-volsellar*, and *coxo-penial muscles*. For the latter two sets, see Sections 3.2.5 and 3.2.6. No *coxo-stylar* muscles were observed in *Paraponera*, that is, muscles – (**9csm1**, –, –), ***w*** (**9scm2**, **gs-gs**, **IXAxad**), ***t*** (**9csm2**, **gs-hrd**, **IXAxad**), ***t′*** (**9csm2**, **gs-hrp**, **IXAxad**), ***u*** (**9csm3**, **ga-hra**, **IXAxab**), and ***v*** (**9csm4**, **ha-gon**, –) are absent.

3.2.5 | Volsella

Sclerite

The ***volsellar complex*** (**V**) comprises the *parossiculus* (**VP**) and the *lateropenite* (=*gonossiculus*, =*digitus*) (**VL**), all of which are fused together and connected to the gonocoxa via the *coxo-parossicular transition* (**G-CPt**), which is a continuous surface of sclerite.

The ***parossiculus*** (**VP**) is divisible into the proximal *basivolsella* (**VPb**) and *distivolsella* (=*cuspis*) (**VPc**) by the *distal parossicular sulcus* (**VPsd**), which corresponds internally to the *distal parossicular ridge* (**VPrd**) (*note*: this is not generally the case in Hymenoptera; see Schulmeister, 2001). The ***basivolsella*** (**VPb**) has an internal *basivolsellar apodeme* (**VPba**), which extends laterally at an obliquely anterior angle into the gonocoxa, and an external *basivolsellar disc* (**VPbd**). The more-or-less longitudinally oriented *volsellar ridge* (=*carina volsellaris*) (**VPrl**), which corresponds externally to the *volsellar sulcus* (**VPsl**), extends from the *apex of the basivolsellar apodeme* (**VPbaa**) distally to the *distal parossicular ridge* (VPrd) and divides the basivolsellar disc into the *medial* (**VPbdpm**) and the *lateral (portions of the) basivolsellar disc* (**VPbdpl**). The *distal margin of the basivolsellar disc* (**VPdmd**) is concave where it is met by the volsellar sulcus, and

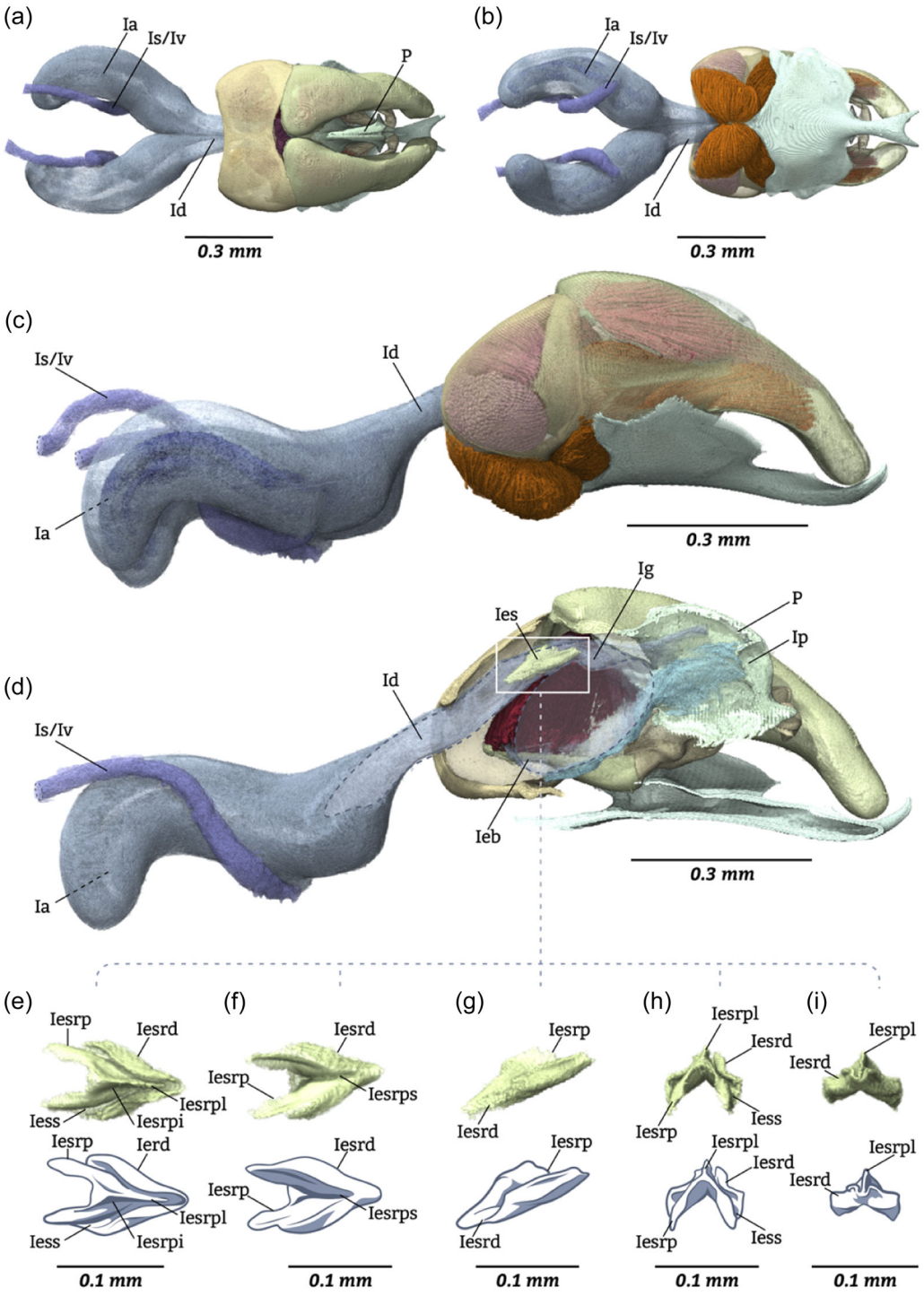

FIGURE 23 Volume renders and diagrams of the male internal genitalia of *Paraponera clavata*; accessory glands partially cropped. ***Structures***: (a–c) Complete genitalia, (d) genitalia with left half of genital appendages digitally removed, (e–i) endophallic sclerite (=fibula ducti). ***Views***: (a) Dorsal, (b) ventral, (c, d) lateral, (e) dorsal, (f) ventral, (g) posterolateral, (h) anterodorsal oblique, (i) posterior. **Abbreviations: Ia** = accessory gland; **Id** = ductus ejaculatorius; **Ieb** = endophallic bladder; **Ies** = endophallic sclerite; **Iesa** = arms of the endophallite; **Iesra** = regions of the endophallite; **Iesrd** = distal endophallite region; **Iersp** = proximal endophallite region; **Iesrpi** = impressions of the proximal endophallite region; **Iesrpl** = (dorsomedian) lamella of the proximal endophallite region; **Iesrps** = (ventromedian) sulcus of the proximal endophallite region; **Iess** = sulcus of the endophallite, dorsal; **Ig** = gonopore; **Ip** = phallotreme; **It** = testis; **Iv** = vas deferens; **Is** = vesicula seminalis; **S9** = sternum IX; **P** = penite; **V** = volsella.

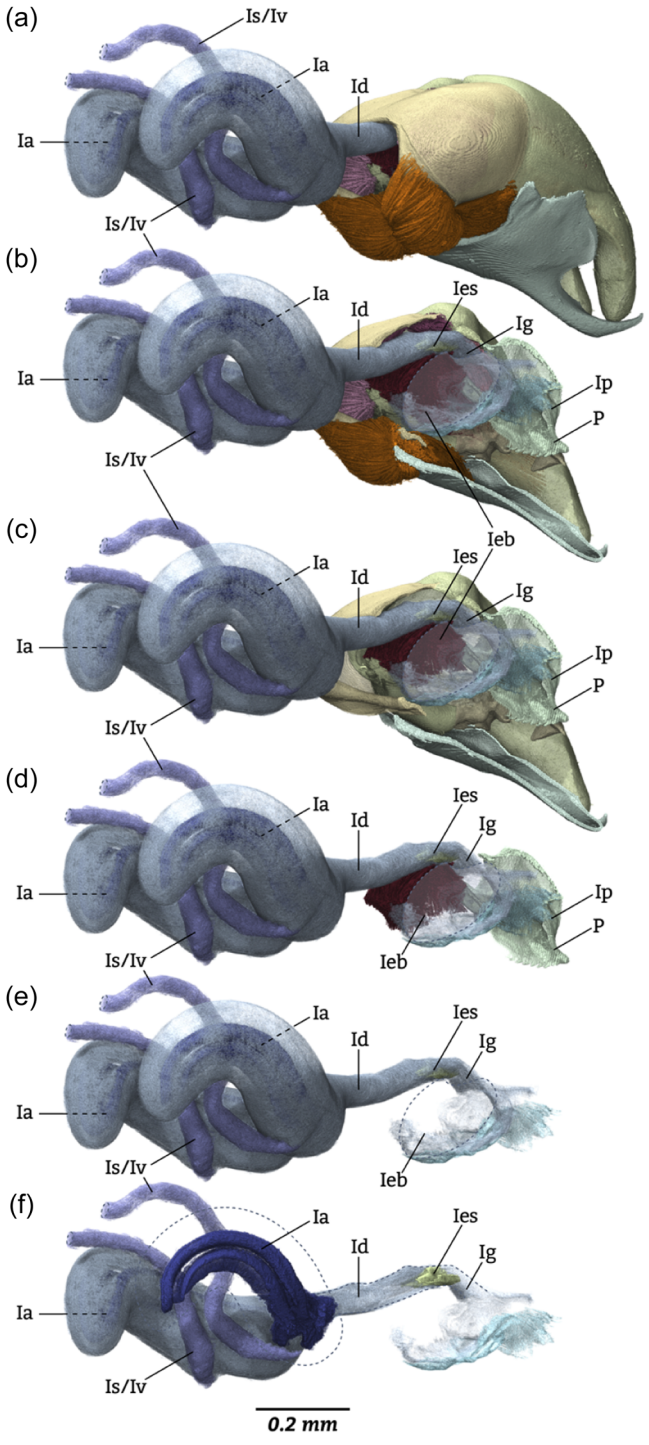

FIGURE 24 Volume renders of the male internal genitalia of *Paraponera clavata*; testes and vas deferens cropped. *Structures*: (a) Complete genitalia, (b) genitalia with left genital appendages removed, (c) genitalia with left genital appendages and further soft tissue removed, (d) internal genitalia and penites, (e) internal genitalia, (f) internal genitalia with left side digitally removed, exposing the spermatic tubes and endophallic sclerite. *Views*: All in anterolateral ventral oblique. **Abbreviations: Ia** = accessory gland; **Id** = ductus ejaculatorius; **Ieb** = endophallic bladder; **Ies** = endophallic sclerite; **Iess** = sulcus of the endophallite, dorsal; **Ig** = gonopore; **Ip** = phallotreme; **It** = testis; **Iv** = vas deferens; **Is** = vesicula seminalis.

convex laterally and medially, with these convexities forming the *distal margins of the medial* (**VPdmdm**) and *lateral* (**VPdmdl**) *basivolsellar discs*. The *lateral margin of the lateral basivolsellar disc* (**VPdmll**) is curved and contours with the *apicoventral gonocoxal margin* (GCmva). The ***distivolsella*** (**VPc**) is digitate, being about 2.5× as long as tall in medial view and is narrow with its height being about 2× its width in dorsal view; due to its length the proximal portion can be referred to as the *distivolsellar stem* (**VPcs**) and the distal portion as the *distivolsellar apex* (**VPa**); internally it bears the *apodeme of the distivolsella* (VPcA).

The ***lateropenite*** (**VL**) is digitate and strongly hooked apically. The proximal ***stem of the lateropenite*** (**VLs**) is narrow, long, and somewhat flattened lateromedially, while the distal ***club of the lateropenite*** (**VLc**) is conical, with its apex directed ventrolaterad and expanded dorsomedially, forming an apparent notch in dorsal view. At the base of the lateropenital stem is the *proximomedial process*, which is thorn-shaped, directed medially, and is slightly upturned.

Surface features

The lateral portion of the basivolsellar disc (VPbdpl) bears a dilute series of pores across its surface (Figure 16b), and in its distal half a brush of setae that extend along the lateral basivolsellar margin toward the distivolsella (Figure 16a). The distivolsellar stem has a few setae clustered on its ventral margin and its apex also with a few setae. The distivolsellar apex has very short, pointed chaetae (=traction setae; =peg setae) on its medial surface where it opposes the lateropenital club. The lateropenital stem is devoid of setae but its club has bears a vestiture of short setae on several surfaces. The lateropenital apex also bears chaetae of a similar quality to those of the distivolsella, with these being along its apex and lateral surface, which opposes the distivolsellar apex. The distal parossicular sulcus bears a field of medially oriented microtrichia (the *microtrichial field of the volsella*, **VM**) that continue onto the volsellar-penial membrane; this microtrichial field also extends onto the lateropenital stem and dorsal surface of the proximomedial lateropenital process; each microtrichium is sclerotized, as best seen in (Figure 14). All of the microtrichiae are directed toward the penis, and the field varies continuously in length.

Muscles

The volsella bears the insertion of two muscles (***p***, ***qr***) and the origin of one (***o***) (Figures 2, 4, 17, 18); these muscles control the closing (adduction) of the distivolsella and lateropenite/gonossiculus/digitus, the medial rotation of the volsella, and the flexion of the gonostylus.

Muscle *o{o′,o″}* (**9clm4**, **gs-pss{gn-pssp, gn-pssd}**, –), the *coxo-basivolsellar muscle*: **O**: Proximo-dorsolaterally on the lateral surface of the gonostylus (GSsl), distolaterad ***j*** and just distad the coxostylar boundary (Gb). **I**: Basivolsellar apodeme (VPba). **S**: Paired; long, thin, fanning narrowly. **F1**: If the gonopod is held in place, contraction of ***o*** would act as the in force for a primary lever of the volsella, with the fulcrum being the coxostylar transition (G-CSt), rotating the volsella medially and likely engaging the proximomedial lateropenital process

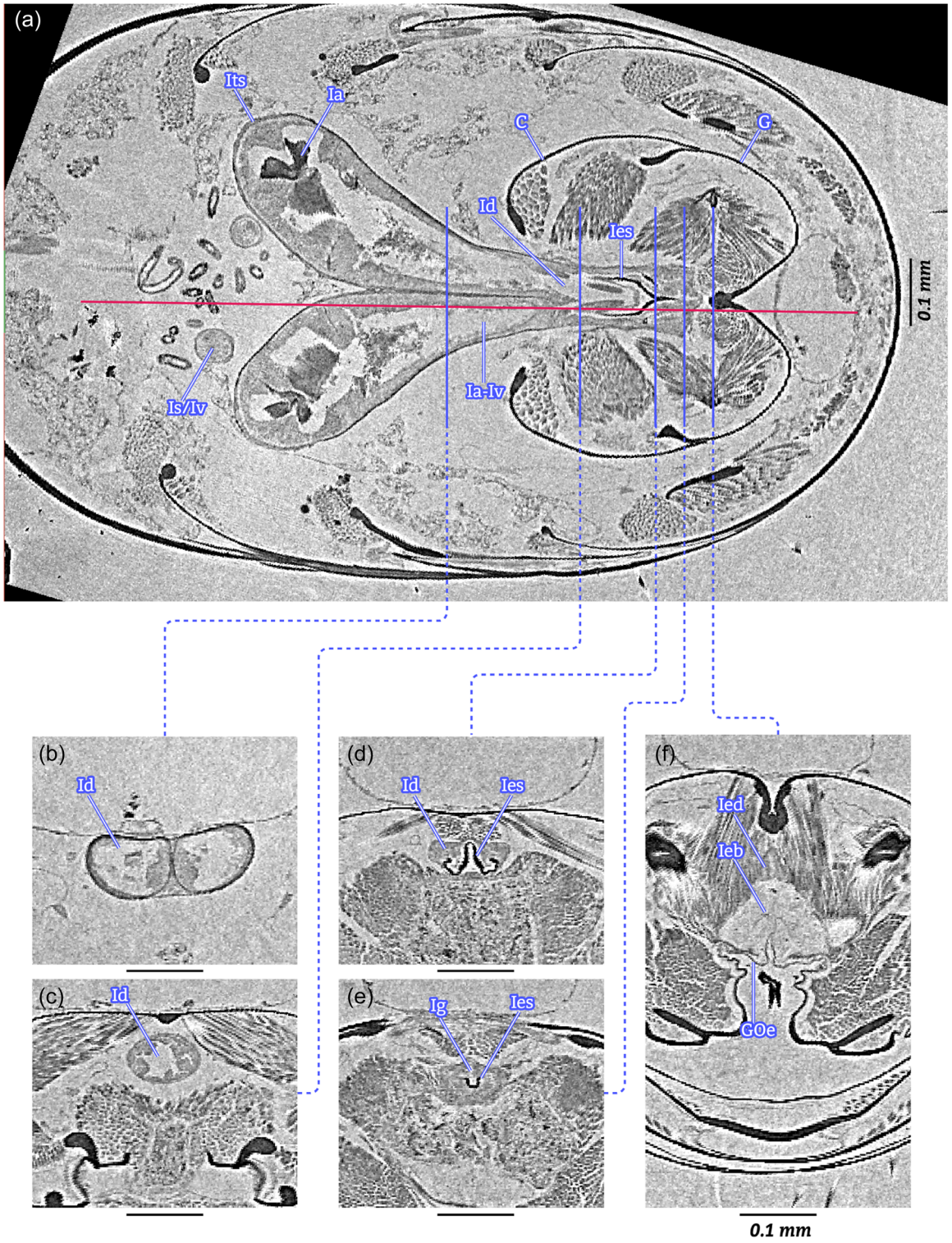

FIGURE 25 Digital sections of the male genitalia of *Paraponera clavata*. (b–f) to same scale. **Views:** (a) Metasoma in frontal plane, (b–f) metasoma in cross-section, showing iterative slices of the soft tissue. **Abbreviations: C** = cupula; **G** = gonopod; **GOe** = coxo-penial membrane; **Ia** = accessory gland; **Id** = ductus ejaculatorius; **Ieb** = endophallic bladder; **Ied** = endophallic duct; **Ies** = endophallic sclerite; **Ig** = gonopore; **It** = testis; **Its** = peritoneal sheath; **Itf** = testicular follicles; **Iv** = vas deferens; **Is** = vesicula seminalis

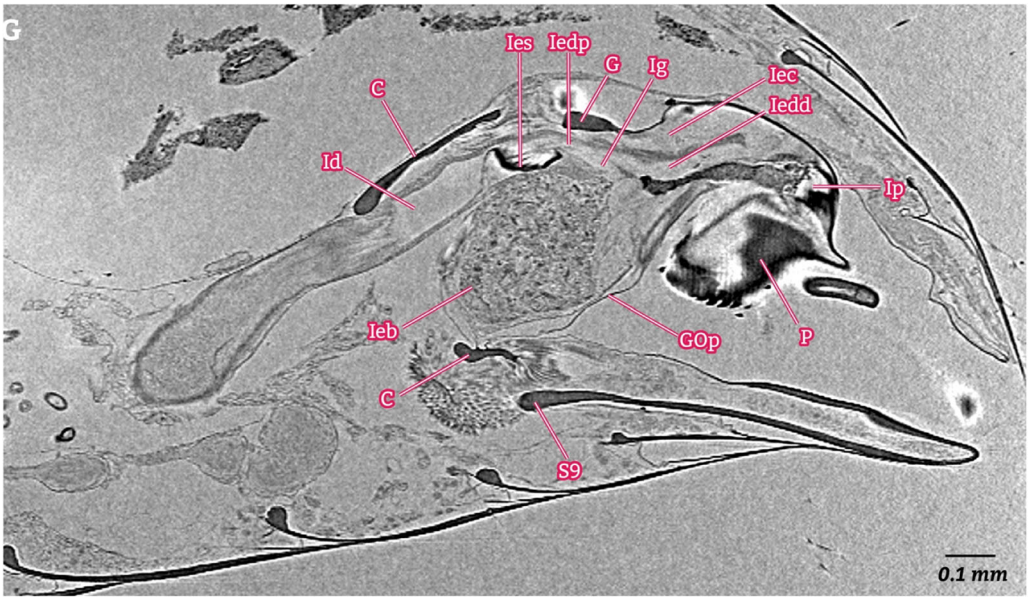

FIGURE 26 Digital parasagittal section of the male genitalia of *Paraponera clavata*. The plane of the cut is indicated in Figure 25a. **Abbreviations: C** = cupula; **G** = gonopodite; **GOp** = coxo-parossicular membrane; **Id** = ductus ejaculatorius; **Ieb** = endophallic bladder; **Iec** = endophallic chamber, distal; **Iedd** = endophallic duct, distal; **Iedp** = endophallic duct, proximal; **Ies** = endophallic sclerite; **Ig** = gonopore; **Ip** = phallotreme; **It** = testis; **S9** = sternum IX; **P** = penite.

(VLp) and the surrounding microtrichial surface with any soft tissue of the female caught between the volsella and penis. **F2**: If the volsella is held in place, contraction of ***o*** would act as an in force for a primary lever of the gonopod, with the fulcrum being the coxostylar attenuation (G-CSa), flexing the gonostylus ventromediad, hence performing a "clasping" function. ***Note 1***: We recognize ***o*** here as a broad category including ***o′*** (gn-pssp) and ***o″*** (gn-pssd) because the muscle is formed from a single fascicle and transitional forms linking our ***o*** to those of sawflies are not yet documented. ***Note 2***: This muscle is homologous with that of *Veromessor andrei* (Mayr, 1886) which was labeled "*t*" in fig. 10 of Boudinot (2013); the latter is in error. Preliminary observations across the Formicidae based on μ-CT scans (unpubl. data) indicate to us that the musculature attaching to the gonostylus needs to be carefully evaluated, due to variation in the orientation of ***o***. ***Note 3***: The second inferred function (F2) is likely a neofunctionalization due to the derived area of origin for muscle ***o***. Examining preliminary data of other taxa, we observed that ***o*** is oriented vertically (i.e., originating on the gonocoxa) in *Platythyrea* and *Rhytidoponera metallica*; we were also informed by Ziv Lieberman (personal communication, May 3, 2024) that the muscle also originates in the gonocoxa of *Liometopum*.

Muscle *p* (**9clm3**, **imvll**, **IXAlm**), the *coxo-distivolsellar muscle*: **O**: Lateral gonocoxal surface, surrounding the anterior (proximal) terminus of the coxostylar ridge (GCr) and positioned dorsad ***qr***. **I**: Distivolsellar apodeme (VPcA). **S**: Broadly fan shaped. **F**: Abduction of the lateropenite club (VLc) to the distivolsellar apex (VPca), protagonist with ***qr***.

Muscle *qr* (**9clm2**, **ivml**, **IXAlp**), the *basivolsellar-distivolsellar muscle*: **O**: Basivolsellar apodeme and ventrolaterad the coxostylar ridge (GCr). **I**: Distivolsellar apodeme (VPcA). **S**: Narrowly fan shaped. **F**: Abduction of the lateropenite club (VLc) to the distivolsellar apex (VPca), protagonist with ***p***.

Muscle *s* (**9clm1**, **imvm**, –), a coxo-volsellar muscle, is **absent**.

Muscle *y* (**9ccm**, **vl-vl**, –), a volsello-volsellar muscle, is **absent**.

Muscle *si* (**9cprv1**, **pss-pv**, **IXAppv**), a penial-volsellar muscle, is **absent**.

Muscle *m* (**10plm1**, **pv-gssl**, –), a penial-volsellar muscle, is **absent**.

Muscle *n{nb,nd,nl}* (**10plm2**, **ps-gss{pv-ph**, **gss-ph**, **pss-ph}**, –), a penial-volsellar muscle, is **absent**.

3.2.6 | Penis

Sclerite

The sclerites of the penis are the paired *penites* (=penial sclerites, =penisvalvae, =penis valves) (**P**) and are situated medially between the gonopodal-volsellar complex. The membrane that connects the penites to the gonopod, cupula, and volsellae divides each penite into the anterior (proximal) and internal *valvura* (PU) and posterior (distal) and external *valviceps* (PV).

The ***valvura*** (=penital apodeme) (**PA**) is digitate, dorsoventrally flattened, and directed obliquely anterodorsally and laterally, at about a 45° angle relative to the valviceps as seen in lateral view; it is distinct from the lateral penital process, the *ergot* (PE), which bears the insertion of the proximal penital muscles.

The ***valviceps*** (=penital blade) (**PB**) is about 1.2× as tall (dorsoventrally) as long (proximodistally/anteroposteriorly); it is divided into

the *dorsal* (PBad) and *ventral* (PBav) *valviceps region/area* by the longitudinally oriented *lateral carina of the valviceps* (**PBkl**), which is nearly obsolete in *Paraponera*. The *dorsal region of the valviceps* (**PBad**) has two margins, the *proximal* (PBadmp) and *dorsal* (PBadmd) *margins of the dorsal valviceps region*, both of which are sinuate. The *proximal margin of the dorsal valviceps region* (**PBadmp**) as seen in postero-(distal-)lateral view is convex where it covers the valvura and is concave where it extends to the dorsal gonocoxal bridge (GCb), and where itself is sclerotized, forming the *bridge of the valviceps* (**PBb**). The *dorsal margin of the valviceps* (**PBadmd**) is concave and short proximally and is asymmetrically arcuate distally. The *dorsal region of the valviceps* (PBad) is curved proximolaterally at the bases of the valvura, forming the *proximal valviceps flange* (**PBadfp**), which is best seen in a posterior/distal view; this region also bears a *dorsal (marginal) of the dorsal valviceps region* (**PBkd**), which follows the contour of the dorsal valviceps margin and, where becomes vertically oriented and expanded distally, forming the lobate *distal valviceps flange* (**PBadfd**). The *ventral region of the valviceps* (**PBav**) has two margins, the *proximal* (**PBavmp**) and *ventral* (**PBavmv**) *margins of the ventral valviceps region*. The *proximal margin of the ventral valviceps region* (**PBavmp**) is short and edentate. The *ventral margin of the ventral valviceps region* (**PBavmv**) is long, shallowly convex, and is serrate, with the serration comprising the *teeth of the valviceps* (**PBt**). The *valviceps teeth* (**PBt**) are divided into three subseries: The proximal series includes about 15 teeth, which are are directed proximally, short proximally and becoming longer and more widely spaced distally, and extend over 4/5 of the ventral margin of the valviceps; the second series of teeth include five teeth, which are directed proximally, but are finer and are much extend over much less than 4/5 of the ventral valviceps margin; the distal series includes six teeth, which are distally directed, very small, and extend over much less than 4/5 of the ventral valviceps margin. The *apical process of the valviceps* (**PBpa**) is conical, directed distally, and short-digitate as seen in dorsal view (Figure 19e). In the CLSM image (Figure 22), it is possible to see that the proximodorsal lobe of the penite is less sclerotized; the distal flange (PBadfd) and apical process (PBpa) bear roughly even fields of extremely short sensilla; and similar sensilla are developed along the ventral margin of the sclerite, at the transition between the less sclerotized ventral portion of the penite and the strongly sclerotized ventral teeth (PBt).

Muscles

The penis bears the insertions of five muscles (Figures 4, 20, 21), although the one of these (***h***) has an origin that spans multiple surfaces; these muscles control the motion of the penites, as well as the compression of the endophallic bladder.

Muscle *h* (**9cppv1**/**9cppv2**, **gs-pvpv**, **IXAppv**), the *apicoventral coxo-penial muscle*: **O**: Proximomedially of the ventral gonocoxal disc (GCdv), along the ventral (proximomedial) apex of the gonocoxal apodeme (GCaav), and along the anterior (proximal) and dorsal surfaces of the endophallic bladder. **I**: Apicoventrally on the valvura (PA). **S**: Paired; broad, thin, and fan-like. **F1**: Contraction of the portion of ***h*** that originates on the gonocoxa would draw the valvura (PA) down hence act as a primary lever elevating the apex of the valviceps (PB) (antagonistically relative to ***j***), with the fulcrum being the bridge of the valviceps (PBb) as stabilized against the gonocoxal bridge (GCb); this action may also compress the endophallic bladder due to the downward swing of the valvura. **F2**: Contraction of the portion of ***h*** that originates on the endophallic bladder would compress the bladder by pulling the anterior (proximal) surfaces of the bladder toward the distal endophallic chamber (Iec) between the penites (P). ***Note***: Although ***h*** originates on multiple surfaces, there is no apparent separation of this muscle into multiple fascicles. We therefore interpret this as a single muscle.

Muscle *i* (**9cprv2**, **gs-pvpdv**, **IXAprv**), the *proximoventral coxo-penial muscle*: **O**: Across the ventral surface of the ventral gonocoxal disc (GCdv), laterad ***h***. **I**: Ventrally on the ergot (PE). **S**: Paired; thick, weakly fan shaped. **F**: With the fulcrum being the bridge of the valviceps (PBb) as stabilized against the gonocoxal bridge (GCb) and the out-force being translated through the ventral serrations (PBt) and distal flange (PBadfd), contraction of ***i*** would adduct the penites away from one another, resulting in splaying of the ventral valviceps margins relative to the dorsal valviceps margins; antagonist of ***k***.

Muscle *j* (**9cppd**, **gs-pvdd**, **IXAppd**), the *apicodorsal coxo-penial muscle*: **O**: Medially along the medial inflection of the dorsal gonocoxal disc (GCddcm), apically across the width of the dorsal gonocoxal disc (GCdd), and across the coxostylar attenuation (G-CSa) onto the proximal lateral surface of the gonostylus (GSsl). **I**: Dorsally on the apex of the valvura (VA). **S**: Paired; elongate fan-shaped, with the strands that reach into the gonostylus being twice as long as those largely restricted to the dorsal disc of the gonocoxa (GCdd). **F**: Depression of the valviceps; antagonist of ***h***.

Muscle *k* (**9cprd1**, **gs-pvpd**, **IXAprd**), the *proximoventral coxo-penial muscle*: **O**: Proximodorsally in the dorsal gonocoxal disc (GCdd), immediately laterad the gonocoxal bridge (GCb) and anterad the insertion of muscle ***g***. **I**: Proximomedially along the ventral region of the valviceps (PBav), on the opposite side of the penite from ***i***. **S**: Paired; thick, nearly cylindrical. **F**: With the fulcrum being the valviceps bridge (PBb) as stabilized by the gonocoxal bridge (GCb), contraction of ***k*** would abduct the ventral margins of the valviceps together and draw them proximad; antagonist of ***i***.

Muscle *l* (**9cprd2**, **gs-pvl**, –), the *apicolateral coxo-penial muscle*: **O**: Membrane immediately distad the ergot (PE). **I**: Apicodorsally on the valvura (VA), at the base of ***j***. **S**: Paired; a thin, small band of fibers. **F**: Possibly stabilizing the penial-gonopodal membrane.

3.2.7 | Internal genitalia

The paired *testes* (**It**), containing the *testicular follicles* (**Itf**) and surrounded by the *peritoneal sheaths* (**Its**), are small and hemispherical; it appears that there are six follicles. The *vas deferens* (**Iv**) and *vesicula seminalis* (**Is**) are continuous, tube-like, and end proximally at the base of the massive, long, and shallowly coiled *accessory glands* (**Ia**). The *ductus ejaculatorius* (=*ejaculatory duct*) (**Id**) is paired distally for a short

distance before becoming a shared duct; it runs the length of the cupula (C) before meeting the *endophallic sclerite* (=*fibula ducti*) (**les**).

The ***endophallic sclerite*** (**les**) is complex in form: In dorsal or ventral view, it is wedge- or V-shaped, with the apex directed posteriorly (distally); each arm of the V is convex in cross-section, with the vertices being directed dorsolaterally; as the arms of the V come into closer proximity, their medial margins raise until they come into contact, where they form a median, longitudinally oriented lamella, while the lateral margins become upcurved; these lateral margins then continue posteriorly (distally) beyond the median lamella, ending at a narrowly rounded point. Based on the 3D reconstructions, the *endophallic sclerite* can be seen to be divided into *proximal* (**lesrp**) and *distal* (**lesrd**) *endophallite regions* by the split *dorsal sulcus of the endophallite* (**less**), which is a deep groove that runs along the dorsal surface of each *endophallite arm* (**lesa**) and meets medially near the posterior (distal) apex of the *endophallic sclerite*. The *proximal endophallite region* (lesrp) is dorsally convex, with lateromedially paired *impressions of the proximal endophallite region* (**lesrpi**), which subtend the longitudinally oriented *dorsomedian lamella of the proximal endophallite region* (**lesrpl**), itself corresponding to the *ventromedian sulcus of the proximal endophallite region* (**lesrps**). The *distal endophallite region* (lesrd) is anterolaterad the *dorsal endophallite sulcus* (less); it is upcurved with the lateral margins downcurved distally.

The ***endophallus*** (**le**) is an anatomical complex, including: **(1)** The *proximal endophallic duct* (**ledp**), which extends distad the *endophallic sclerite* (les) and ends at the *gonopore* (=*primary gonopore*) (**lg**); **(2)** the *endophallic bladder* (**leb**), which is a large sack that fills the proximoventral space of the external genitalia from the cupula to the ventral gonopodal-volsellar-penial membrane; and **(3)** the *distal endophallic chamber* (**lec**), which is contained within the penis, forms the *distal endophallic duct* (**ledd**), and ends distally at the opening of the internal genitalia to the outside of the body, that is, the *phallotreme* (**lp**).

4 | DISCUSSION

4.1 | Discussion overview

In the present study, we have sampled and documented the anatomy of the male genitalia of *P. clavata* using multiple approaches, each of which provided a distinct but complementary layer of information. Based on our comparative results with other Hymenoptera (Section 3.1), we present a perspective on systematic morphology (Section 4.2), the overlap of our concepts with those of the HAO (Section 4.2.1), and empirically evaluate the 5-category system of serial homology proposed by DiFrisco et al. (2023). At the end of Section 4.2, in our discussion of paramorphs (Section 4.2.1.5), we propose a basic model of hierarchical homology for male (and female) insect genitalia, and in Section 4.2.2, we extend hierarchical-homological thinking to the developmental stages of insects. We then consider the value of muscles for the alignment of sclerites and homology inference in general (Section 4.3) and for the specific cases of the gonostylus (Section 4.3.1) and the cupula and volsella (Section 4.3.2). We correct some points in the literature (Section 4.3.3) then provide a brief perspective on harmonizing the alternative terminological systems that have been recently applied to the Hymenoptera (Section 4.4), before providing our study synopsis in the conclusion (Section 5).

4.2 | Systematic morphology

From our perspective, the delimitation and naming of anatomical entities is the practice of systematic morphology, while hypothesis testing for the causal history of anatomical change are evolutionary and developmental morphology. Anatomical systematization requires detailed observation and comparison across individuals to detect consistencies. The basis for these observations arises from our visual and tactile sensory modalities, augmented by available technologies for physical sampling and documentation, including micro-photography (broad spectrum visible light), CLSM (narrow spectrum visible light), μ-CT (X-rays), SEM (electrons). The hands themselves can be used when the anatomical structure or complex is sufficiently large, as in many vertebrates, or when the complex is modeled at sufficient scale, as we have performed via 3D-printing. By repeated observation, consistencies of presence or absence and properties such as shape, material variation, and mechanical function can be recognized as individual or iterated entities. These consistencies can be identified under a particulate model as fundamental units – characters (structures that may be present or absent) with states (attributes or conformations that may vary continuously) – which can be conceived of as anatomical entities or "phenotypic species," with their own history of evolution and individuation ("speciation") across phylogeny (Wagner, 2014).

4.2.1 | Formalizing anatomical-structural concepts

Here, we report a (nearly) complete set of concepts necessary to comprehend the three-dimensional structure of the male genitalia of *P. clavata*. These concepts are linked to the broader system of hymenopteran terminology via the HAO, for which we find that of the 182 non-muscular concepts required for *P. clavata*, 40 are formalized in the ontology. A number of the concepts newly provided herein are positional, recognizing proximal and distal portions of an entity, or defined margins, for example. Such classes are precluded from the HAO but are useful for landmarking and characterization of structural complexity and variation. Other concepts are new and composed via recognition of serial homology, such as the cupular apodeme (CA), while others are entirely new and without serial homology, such as those defined for the endophallic sclerite (=fibula ducti) (les). All concepts newly derived in the present study are marked with an asterisk in Section 3.1.1. In the following Sections (4.2.1.1–5), we consider all of our explicitly recognized concepts in light of the five-category system of DiFrisco et al. (2023) for "various

phenomena associated with serial homology," including attributes, structures, replicas, homomorphs, and paramorphs. Among the next steps beyond the present work would be to develop "ABox" and "TBox" (universal and assertional) statements and a semantic knowledge graph to link the anatomical concepts used here and their hierarchical homological classes for the purpose of processing complex data (Mabee et al., 2020; Vogt et al., 2022).

4.2.2 | Hierarchical homology: Classification

Attributes

(1) *Attributes* (**@**), or numerical and geometrical elements, such as size, count, overlap, and curvature. In the original classification of DiFrisco et al. (2023), basic geometrical elements were not included. However, we find that geometrical attributes (points, lines, areas, and volumes) are critical for the comparative definition of body parts and defined regions. We further found that each instance of an attribute that could be observed or mapped on the genitalia was positionally defined (**#**), suggesting that spatial information plays at least some role in the formation of these uniquely identifiable aspects of separable parts. The likely source of this spatial information that provides splits in the pathways for individuation would be hox genes, which have been mapped for the male and female genitalia of *Drosophila* (e.g., Estrada et al., 2003; see also Chen & Baker, 1997 and Sánchez & Guerrero, 2001 for genital disc compartmentalization and development along sex-specific pathways). As a consequence of hox patterning, the genital appendages have meaningful biological axes, including the lateromedial, the anteroposterior, and the proximodistal, for which apical identity is important. In other words, because the apex (as a point) or apical region of a structure is significant as it is positional defined, even if it is not an individual and separable part of a structure.

For our purposes, we recognized six geometrical subclasses of attributes after classifying the concepts (Section 3.1) that we used to structure our anatomical observations of *P. clavata* (Section 3.2). In retrospect, it is clear that defining the geometrical shape of separable (i.e., material) structures is important, as this allows for clear definitions using the following subclasses, which are only generally defined in the HAO.

(1: **-P**) Points, or positionally defined such as the apex of the distivolsella (=cuspis) (VPc, Figure 15) or of the apex of the apical penital process (BPpa, Figure 19). (2: **-M**) Margins, such as the anterior and posterior margins of sternum IX (S9Ma, S9Mp, Figure 8). The number of margins depends on the basic geometrical shape of an object, whether flat and unidirectional with one margin, such as the apical margin of a lamella, or flat with bidirectional differentiation of form, thus having two margins, and so on. By accounting for the basic geometry of a single structure, margins can be ontologically defined. Currently, for example, attributes are largely precluded from the HAO, which means that many uniquely identifiable margins, for example, cannot be defined and accounted for within that framework. (3: **-Am**) Areas or surfaces of material, such as the dorsal and ventral discs of sternum IX (S9Dd, S9dv, Figure 8). Material surfaces are delimitable and further divisible based on uniformity of curvature and margins, irrespective of the roundness or sharpness of these margins along their lengths. Subdivision of the surface of the lateral clasping appendage of hymenopteran genitalia, for example, may not be discretely defined, but may differ based on proximodistal patterning of the sensilla. The lateral clasping appendage surface is further defined by the proximal margin and apical point, regardless of their roundedness. (4: **-Ai**) Areas defined by but not including material (i.e., immaterial areas), such as the proximal and distal foramina of the cupula (CFa, CFp, Figure 11). (5: **-Vm**) Volumes of material that are regionally defined, such as the discs and posterior lamellae of sternum IX (S9D, S9U, Figure 8) and the cupula (CD, CL, Figure 11). The disc of the cupula is, for example, a ring that encompasses and immaterial volume (a lumen), while that of sternum IX is formed by distal evagination of the epidermis and is also defined by a lumen. The lamellae of these structures, in contrast, are solid and developed unidirectionally (distally), thus have a single distal margin and two surfaces (one outer, one inner [=the inflection]). (6: **-Vi**) Volumes that are defined by but not including material, such as the lumens of sternum IX and the cupula.

Additional, material subclasses of attributes could be defined, including: (7: **-C**) spectrum of reflectance (color), (8: **-S**) degree of sclerotization (-S°) and perhaps histological pattern (-S*) of a sclerite, and (9: **-R**) sharpness, roundness, or curvature. Considering that the topology of muscles is also a geometrical element, mapping the variation and inferring evolutionary patterns of muscle attachments is a form of geometrical proof, albeit difficult to convey (e.g., fig. 1 of Boudinot, 2018). Muscle attachments themselves are not strictly geometrical, however; see Section 4.3 below.

Structures

(2) *Structures* (**$**) are separable parts that are not individually specified; they are material, whereas *attributes* are immaterial. Given this definition by DiFrisco et al. (2023), we propose a refinement, given insect analogies to their examples of structures: (1) The spinous processes of the vertebral bones, (2) the zygomatic arch, and (3) peripheral vascular elements. In brief, we suggest that: (i) processes are homomorphs or candidate homomorphs because their position is defined (i.e., positionally indexed) and the material development of these parts must be coordinated by some means; (ii) arches and other "bridges" are not individual entities, but require some degree of coordination between constituent parts that is not due to mere chance, hence have identifiability as "specified composites" or *composite structures*; and (iii) peripheral vascular elements are stochastically realized yet are material and caused by developmental patterning, hence are *replicate structures* (i.e., iterations of a homomorphic character). All three of these suggested recategorizations of exemplar structures *sensu* DFL are distinct from immaterial/geometrical attributes.

(1) The transverse and spinous processes of vertebral bones are analogous to the apodemes of insects, such as those of sternum IX (S9A, Figures 8–10). In order for an apodeme to develop, a point of

material distal expansion needs to be spatially specified, which meets the criterion of positional indexing for the narrower "homomorph" and broader "paramorph" classes. Further, the anterolateral (S9Aal) and median (S9Aam) apodemes of sternum IX are discretely individuated with respect to their shape and other attributes, similar to the thumb versus digits 2–4, as well as the transverse and spinous processes, which are paired (transverse) or unpaired (spinous) and have distinct and complex form patterning. Perhaps the median and anterolateral apodemes of sternum IX (and the transverse and spinous processes) are paramorphs, or perhaps they have different developmental reaction norms. Evidence for paramorphy of these apodemes is provided by the lateromedial duplication of the median apodeme in various *Leptomyrmex* ants (e.g., fig. 2C,D of Barden et al., 2017), for example. In either case, paired or unpaired processes of insects and vertebrates are positionally indexed and traceable across phylogeny, and presumably require the integration of signals to realize during development, hence meet the definitional criteria of the homology class "homomorph." An additional example – that of the prosternum of *Paraponera* – is provided in Figure 27c.

(2) The zygomatic arch is analogous to the sternal bridges of the insect thorax (no clear examples are available from the presently sampled genitalia). The prosternal bridge (Figure 27c), for example, forms when the dorsal lamellae that develop on laterally paired invaginations of the insect prosternum (the profurcal arms) appear to "fuse" medially as cuticle is deposited, resulting in a single transverse bar that comprises two symmetrical parts. The bar itself is likely not a homomorph that develops from a single specified program but does appear to require some degree of coordination among epidermal cells during development, as once gained, occurrence and variation the prosternal bridge provides meaningful phylogenetic signal at various depths (Boudinot, unpubl. data). The zygomatic arch provides even more information, as the two parts that comprise this "bridge" are asymmetrical and are positionally indexed processes of individually identifiable bones. That is, the arch comprises the spatially defined, dissimilar appearing, and separable posterolateral (temporal) and anterolateral (zygomatic) processes of the zygomatic and temporal bones, respectively. At least some local coordination must be necessary for the arch to form completely. We posit that these arches or bridges be categorized as *composite structures*.

(3) The geometrical patterning of peripheral vascular elements of vertebrates (Figure 27b) and the cuticular sculpture of insects (Figure 27a) are similar in that their specific positions are stochastic rather than indexed. Hence, particular veins or cuticular ridges may be conceived of as *replicate structures*. Such patterned structures, however, display a spectrum of stochasticity, regional extent of expression, and orientation, such that some cuticular ridges that are part of a larger pattern of sculpture may be consistently identified. (See, e.g., the "dorsomedian costa" of the ant genus *Meranoplus* in figs. 23 and 24 of Boudinot & Fisher, 2013.) The complete set of replicate ridges or grooves that comprise a particular class of cuticular sculpture (e.g., Harris, 1979) can be considered a biological character that has variable states. *Vis à vis* the reasoning in Figure 27, we consider "replicate structures" and "(natural) replicates" to be synonymous.

Notably, the only *structure* (*sensu* DLW) that we recorded in our hierarchical label list for the male genitalia of *Paraponera*, is membrane (=conjunctiva, =corium, =arthrodial membrane), which we subdivide regionally for labeling purposes (e.g., GOp, Figure 18). Membrane in this usage is, however, almost a negative category, as it is defined here by spatial relationship to sclerite. As such, the abdominal-cupular membrane and all of the membrane distad the cupula are not individually specified, but are what is left over of the epidermis after sclerites are developed. Surely the total epidermis (sum of membrane) across an insect is homomorphic. We also observe that "inseparable parts" that are material (i.e., not strictly geometrical) are also individualized to some degree. For example, the black and red hues in insects are caused by material deposition from distinct biosynthetic pathways (Chapman, 2012), and there are specific, consistent, and positionally indexed curvatures of the epidermis and cuticle are recognizable in insects (*formative elements*, *sensu* Klass, 1997; see Section 4.2.1.4 below). Given this and points 1–3 above, we consider the homology class "structures" to be heterogeneous. We therefore encourage further reconsideration of "structures" and anticipate refinement of the five-class system of homology proposed by DLW.

Replicas (natural)

(3) *Replicas* (=), or repeated parts with the same identity but without positional indexing, such as individual hairs of the same shape and functional class (e.g., Altner & Prillinger, 1980) or individual cells of the same cell type. Although we observed several replicas across the genital complex of *P. clavata*, for example, cell patterning on the cupula (Figure 11) and various sensilla (Figure 14), we only formalized a subset of replica classes (see, e.g., Boudinot et al., 2021 for a more complete treatment of sensilla diversity). Notable natural replicas across the genitalia include the microtrichial field of the volsella (MV, Figure 14), the basivolsellar seta field (adjacent to VPb, Figure 14), the distivolsellar and lateropenital seta and microtrichia fields (Figure 18), the seta field of the gonostylus (across GS, Figure 14), the teeth of the valviceps (PBt, Figure 22), the various sensilla of the valviceps (Figure 22), and the testicular follicles. The distribution of fields of sensilla and cuticular modifications are spatially limited, hence provide information about the extent of signal for the development of these structures, which can be traced across phylogeny and can inform questions of regional epidermal identity. See Section 4.2.1.2 above for further considerations of replicas.

Homomorphs

(4) *Homomorphs* (**!**), or parts of the same identity, but with positional indexing, such as paired appendages, tarsomeres 2–4, simple flagellomeres, digits 2–5 of the hand, individual hairs or carinae in a specified and consistent position, or the shape and functional classes of hairs. To this we need to add *formative elements* (Klass, 1997), which are defined shapes that are positionally defined (i.e., indexed) and expressed through development via invagination, evagination, or folding, such as the complex shape of the endophallic sclerite (=fibula ducti). As for *structures sensu* DLW, the incorporation of *formative*

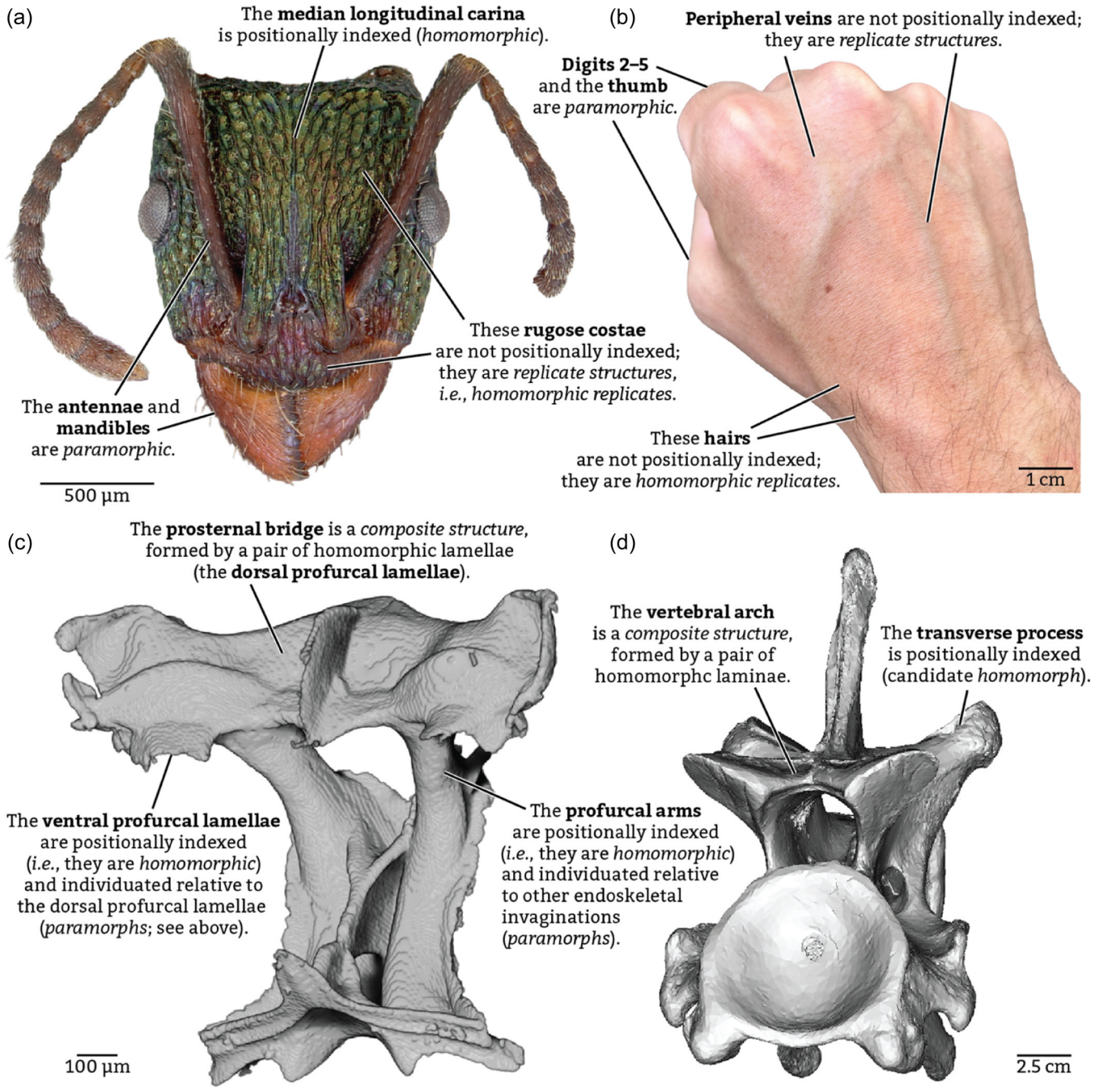

FIGURE 27 Some suggested refinements of the homology class *structure* of DiFrisco et al. (2023), as exemplified by the head of *Rhytidoponera metallica* (CASENT0172345) (a), a human hand (b), the prosternum of *Paraponera clavata* (SMFHYM0005630) (c), and the seventh cervical bone of *Giraffa camelopardalis* (d). **Views:** (a) Full-face; (b) anterodorsal oblique; (c and d) anterolateral oblique. The ant head in (a) was imaged by April Nobile and is available from AntWeb (2024), and the 3D model in (d) is from Müller et al. (2021) and rendered using 3D Slicer (Fedorov et al., 2012).

elements in a classification of homology requires further consideration, as some shapes are coincident from the action of other developmental mechanisms. The human chin, for example, continues to defy consistent classification despite having a defined location and measurable attributes (e.g., Meneganzin et al., 2024). Operationally, homomorphs or candidate homomorphs may be recognized by consistent location, shared geometrical patterning, and material composition. Without recourse to developmental experimentation to detect character identity mechanisms (ChIMs, DiFrisco et al., 2020), it appears that the special criterion for the recognition of developmental individuality, hence homomorphy, is the co-occurrence of serial homologs (paramorphic individuals) in the same body. Examples of such co-occurrence include the sympatry of two hair classes in the same local area of epidermis (e.g., ground and guard hairs of mammals

and the setae and pubescence of ants), or of similar yet distinct classes of cuticular outgrowths, such as the ventral and dorsal lamellae of the ant prosternum (Figure 27c) or the anterior and anterolateral apodemes of abdominal sternum IX in male ants (Figures 8–10). In other words, we propose *developmental sympatry* as an additional criterion of the recognition of homomorphs and paramorphs. Note that similarity ≠ identity, as identity of a biological character is provided by the signal integration mechanism (ChIM) during development, while similarity is due to the way that the identity is realized through coordinated material deposition.

Paramorphs

(5) *Paramorphs* (**%**), or parts that are distinct yet phylogenetically related, and with positional indexing, such as the thumb relative to digits 2–5, and developmentally differentiated sets of vertebrae and arthropod segments. We found that, for the specific purpose of classifying our concepts (Section 3.1.1), it was more useful to recognize homomorphs and to leave paramorphy implied, for which reason we relied on the paramorphy-neutral term "homomorph set." However, we recognize several candidate paramorph families when comparing elements across the genitalia. With indication of homomorph complexity (the "**!**" system), these include: **(1)** the anteromedian versus the anterolateral apodemes of sternum IX (!: S9aam, S9aal), as well as the penital apodeme (i.e., the valvura, !: PA); **(2)** the posterior or distal lamellae of sternum IX and the cupula (!: S9L, CL); **(3)** ridges of sternum IX, the cupula, and the gonocoxae (!: S9R, CR, GCr); **(4)** possibly similar shaping programs for the dorsal and ventral "notches" of the anterior cupular margin (!(?): CMand, CManv); **(5)** the cupular and gonocoxal apodemes (!: CA, GCa); **(6)** the paired, distal, digitate expansions of the volsella, that is, the distivolsella and lateropenite (!: VPc, VL), and possibly the proximomedial process of the lateropenite (!: VLp); **(7)** the setae (i.e., filiform hairs, !) and chaetae (i.e., peg-like traction hairs on the distal volsellar apices, !) that occ ur on the genitalia; **(8)** the dorsal and lateral carinae of the valviceps (!: PBkd, PBkl); **(9)** possibly the three portions of the ventral penisvalvar teeth that have differentiated orientation and size (!: PBt); **(10)** the gonopods and penis (**!!**: G, P); and ultimately **(11)** the genital appendages (**!!-!!!**) and those appendages of the thorax and head.

To propose those 11 putative paramorph sets, it is necessary to recognize some relatively higher degree of attribute similarity versus dissimilarity. Much of this hypothesis of serial homology is already coded into the language of entomology for sets of simple homomorphs (!), for example, the classes "apodeme" and "ridge." While there is some uncertainty for these, especially for the curves of the anterior cupular margin, the pattern of replication-with-differentiation is clear. The much more difficult question arises with respect to the relationships of complexes (**!!**: G, P) and supercomplexes (**!!–!!!**: appendages of the different tagma), as these deal with structures that have been so differentiated structurally and developmentally that their evolution from a shared ancestral developmental program can be overwhelmed. In effect, these putative paramorphs are subject to the Ship of Theseus problem: Gradual replacement over time, such that the form of the ship (=complex) is the same or at least recognizable but the physical material of the original ship that left port is gone. Are the structures of the abdomen that are used by male insects for copulation and by females for egg laying homologous to one another and to the appendages of the thorax and head? The hourglass or character identity mechanism (ChIM) model of DiFrisco et al. (2020) provides resolution to this issue: Although across phylogeny the outputs of development may be variable in attribute and form and the signaling inputs prone to drift and replacement, the resultant anatomical entity is homologous due to integration signal integration before developmental realization of the character. In other words, although the ships that left and arrived at port are made of different material, they are the same.

We argue that the problem of insect male genital homology is an issue of structural alignment due to the coupling of elaboration via the gain of lateropenites in Holometabola and the division ("fragmentation") or loss of musculated elements across the orders, the gradual change of structural form, and probably of phenotype-inducing genes. The paramorphy of male and female genitalia is largely uncontroversial (Estrada et al., 2003; Pavlicev et al., 2022), hence the similarity yet nonequivalence of elements indicates paramorphic expression of homomorph classes between the sexes, such as apodemes. In male insects, the elaboration of genitalia in terms of part count has reached several peaks, with the most extreme being Siphonaptera (e.g., Günther, 1961; Snodgrass, 1946), making the problem of recognizing interordinal homomorphy (i.e., homomorphy among insect orders) exceedingly difficult and a matter of structural alignment (see Boudinot, 2018, Section 4.3). Because of the controversies arising from the problem of individual part alignment (homomorphy inference), some have even proposed that the male genitalia of insects have been completely lost and regained at least once or obliterated due to "fusion" of genital anlagen during development (e.g., Snodgrass, 1935, 1957), resulting in what could be called a hypothesis of "absolute non-homology." Experimental developmental evidence, however, supports the basic observation that male (and female) insect genitalia are appendages of the abdomen (Estrada et al., 2003), albeit highly derived.

Below (Section 4.3), we re-present the case below with new considerations that the male (and female) genitalia of insects are derived from abdominal appendages, and that homomorphy of the proximal and distal segments of the male genital claspers (gonopods) is retained, despite the loss of boundary markers in many hymenopteran taxa. In effect, what is necessary for homology inference across the insect orders is developmental tree-thinking (e.g., Wagner, 2016), with morphogenetic ("ontological") trees representing the hierarchical homologies (homomorphy with paramorphy achieved via individuation) embedded within phylogeny. By adopting such a conceptual construction and explicitly incorporating phylogenetic and morphogenetic structure, it should be possible to ontologize problematic structural complexes, for example, where defining phenotypic elements are lost or variable across lineages.

The central issue addressed here is an example case for hierarchical homology (Figure 28): **(1)** The total paramorph set "appendages" would include the paramorph sets "head appendages," "thorax

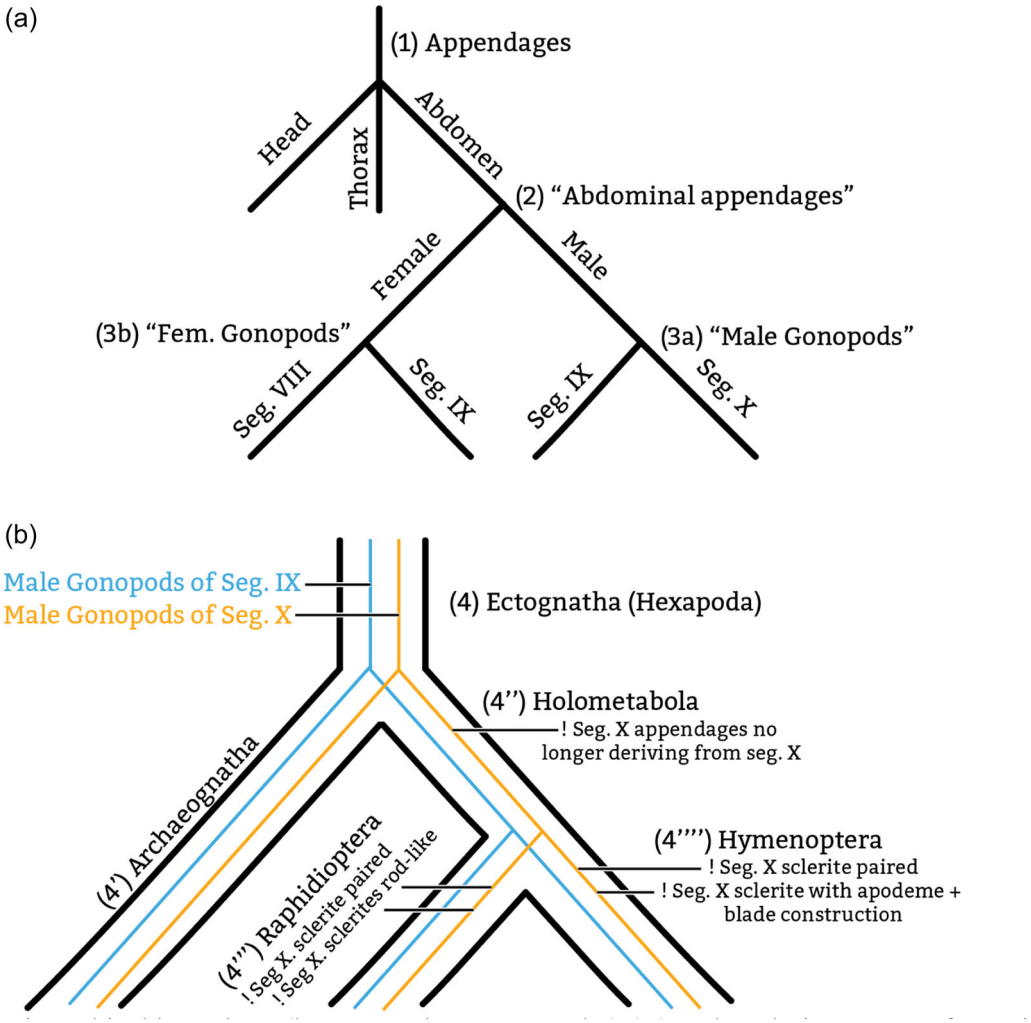

FIGURE 28 Hierarchical homology (homomorphy–paramorphy) (a) and evolutionary transformation of insect genital structures (b), with morphogenetic trees (character trees *sensu* DiFrisco et al., 2023) embedded in a phylogenetic tree, in analogy to gene trees and species trees. (a) General hierarchical homology, that is, fundamental developmental relationships. Each split represents a historical "parology event" (or individuation *sensu* Wagner); at this general level, it may also represent a spatial grouping of homomorphs or paramorphs, or a decision tree for the identification of structures. The tips of the tree represent individual homomorphs or sets of paramorphs and homomorphs in the case of appendages of the non-abdominal tagmata (head, thorax). (b) Specific hierarchical homology, that is, derivation of homomorphs across insect phylogeny. Splits of the black bounding tree represent ancient speciation events. The blue and orange morphogenetic trees represent individual homomorphs, in this case male genital appendages. Splits of the homomorphic trees do not represent parology events, but evolutionary-developmental derivations of specific elements of the homomorphs, with pairing of the Seg. X app being homoplastic and the form of the sclerite between Raphidioptera and Hymenoptera being autapomorphic (see Figure 30b,e,f). Additional genital transformations at the ordinal level are mapped by Boudinot (2018). By contrasting (a) and (b), it is clear that structural parology (a) and the evolution of homomorphs (b) are not identical; we maintain that it is necessary to consider morphology at both levels. Additionally, given that robust phylogenies are available at many levels across the insects, analytical emphasis should be on estimating transformations rather than the estimation of phylogeny itself, except in the case of fossils or taxa without sequence data.

appendages," "abdominal appendages"; **(2)** the paramorph set "abdominal appendages" would include (among others) the paramorph sets "male genitalia" and "female genitalia," each comprising two succeeding pairs of appendages; **(3) (a)** the paramorph set "male genitalia" would include the paramorph appendages "gonopods IX" and "penis," while **(b)** the homomorph set "female genitalia" would include the paramorph appendages "gonopods VIII" and "gonopods IX"; and **(4)** the homomorph set "male genitalia" could be anchored to specific orders or other nodes in the phylogeny, to address the specific differences in these supercomplexes with respect to development and structure. The transition from splits 1–3 to 4 is that of a general versus specific homology relationship, as the left fore-leg pretarsus of a mayfly (Ephemeroptera) is *not* the left fore-leg pretarsus of a bullet ant (Hymenoptera), but both are developmental instances of the inherited pretarsal program that is expressed in the left fore-leg compartment of the body. Likewise, we maintain that the penis is appendicular in evolutionary origin yet is substantially different in its instantiations across insect phylogeny (Boudinot, 2018).

4.2.3 | Hierarchical homology and life stages

Considering the developmental history of adult *Paraponera*, other Holometabola, and other Arthropoda, we are faced with another set of questions pertinent to the expression of stage-specific phenotypes: Are larvae homologous? Are the adult and larval stages paramorphic? What does the temporal seriality of homomorphs tell us?

The timing and extent of development are critical and variable across evolution. The epidermis of an individual is structurally continuous despite replacement over the lifespan; it is *continuant*. The setae developed on the surface in fields, without spatial indexing, are *replicants* (=*replicate*, *sensu* DLW). But what of the individual itself? Each individual body is a *duplicant* of the forebearers and ancestors, and each individual part or complex of parts are *subduplicants* if they are spatially indexed, that is, they are homomorphs expressed within the lifetime of the whole duplicant, and whole organism is an ultra- or hypercomplex complexes of homomorphs and paramorphs. Within the continuous lifetime of a duplicant individual insect, the epidermis is singular, but the cuticle is duplicated (i.e., homomorphically copied) across molts in all of its complexity.

The cuticle of a hemimetabolous insect is duplicated until the terminal form, with paramorphic copying of the genital appendage cuticle developing late in life, whereas the set of holometabolous larval cuticles are homomorphic and paramorphic in their (apparent) entirety with respect to the adult cuticle. In this way, the genital imaginal discs of holometabolan larvae are homologous and remain homomorphic during the lifetime until the developmental differentiation of the adult sex-specific paramorphic forms and elements. Changes in the timings of these developmental events are critical to digitize, map, and comparatively evaluate. Homomorphy and paramorphy of juvenile and terminal cuticles can be evaluated across the Arthropoda.

The systematic thinking of hierarchical homology clarifies many complicated problems of homology and makes anatomy and the totality of phenotype (the phenome) accessible to computation through graph theory ("trees") and reduction to anatomical particles (elements/characters and their set of variable states). The next step is to repeat the present study with a formalized (i.e., programmed) architecture of anatomical elements that are indexed by the refined five-category system of hierarchical homology, and used to parse input data from a selected set of taxa for complexity, eco-evo morphospace, and phylogenetic analysis.

4.2.4 | Summary

Across all 182 of the concepts that we formally recognized to characterize the genitalia of *P. clavata* (Section 3.1), 71 were non-set homomorphs and 94 were positionally indexed attributes. By considering the hierarchical organization of these homomorphs, we observe that the male genitalia of *Paraponera* – and insects more broadly – comprise a supercomplex, that is, a complex of anatomical complexes. We also observe that all geometrical attributes that are uniquely identifiable have definable, nonrandom variation are positionally indexed (Section 4.2.1.1), hence are a ontologizable and meaningful to individually conceive and delimit, even if they are dependent on development of a simple or complex homomorph. This points, furthermore, to the importance of defining the geometry of homomorphs, as this determines the quantity and class of geometrical attributes.

One difficulty we encountered in the empirical application of DiFrisco et al.'s (2023) serial homolog classification was separating "structures" (Section 4.2.1.2) from simple homomorphs (Section 4.2.1.4) and natural replicas (Section 4.2.1.3). We propose re-categorizing *structures sensu* DLW as (a) homomorphs or candidate homomorphs (e.g., apodemes and processes), (b) composite structures (e.g., arches and bridges), or (c) replicates, replicate homomorphs, or replicate structures. Membrane as treated in the present study fulfilled the definition of *structure sensu* DLW, as the set of genital membranes are what is left over after defining all of the recognizable homomorphs, although that does not exclude the possibility that certain membranous fields are also positively specified by gene expression during development. Moreover, we observe that formative elements (*sensu* Klass, 1997, i.e., positionally defined foldings or in- or evaginations of epidermis and cuticle) are consistent, definable, and have their own pattern of variation across phylogeny, indicating that they are indeed homomorphs, despite their simplicity (Section 4.2.1.4). To develop formative elements, moreover, require coordinated change – hence action – of cytoskeleton across a cellular field or differential rates of cell division, among other mechanisms, further indicating their individuality in the context of the ChIM model of DiFrisco et al. (2020).

We find that by explicitly categorizing our anatomical concepts following the hierarchical homology system of DLW, we both discover refinements that can be made to that system – such as the revision of the "structure" class and *developmental sympatry* as a key criterion for the recognition of homomorphs – as well as a means of ontologically accounting for positionally defined attributes, which would fill in the "preclusion zone" of the HAO (Section 4.2). The system of DLW further provides a logical solution to problems of homology across life stages (Section 4.2.2). Finally, reconsidering insect genitalia within the hierarchical homology framework clarifies fundamental homorphies and paramorphies (Figure 28), which we elaborate upon in the following section (Section 4.3).

4.3 | Muscle identity and epidermal history

Muscle identity is biologically meaningful and transformation series of muscle attachment across phylogeny provide information about the homology of epidermal areas, hence the identity of sclerites. The molecular and genetic mechanisms that specify muscle identity have been determined to some degree by experimental developmental studies of *Drosophila* (summarized in Sink, 2006b; therein, see especially Carmena & Baylies, 2006; Dutta & Raghavan, 2006; Sink, 2006a; and Volk, 2006, as well as Schweitzer et al., 2010 and

the more recent review of Schulman et al., 2015). Three key points can be taken from these studies: (1) Muscle identity is specified during embryogenesis, (2) epidermal attachment sites for muscle are specified by combinations of gene products, and (3) the consistency of muscle attachment across instars and is dependent on both muscle and epidermal identity.

(1) During embryogenesis, muscle progenitor cells of the mesoderm divide into daughter founder and precursor cells for the larva and adult, respectively. These larval founder and adult precursor cells contain the necessary information for the specification of larval and adult muscle identity, while the correct muscle size for each stage is achieved by fusion of myoblast cells, forming the syncytial myofibers or muscle strands.
(2) The free ends of the developing muscle bear myotubules, which sample the tendon precursor cells of the epidermis for particular combinations of genetic products, including *Stripe*, *Slit*, *Robo*, and *Derailed* (Volk, 2006, p. 107). In other words, the attachment site identity for muscles on the field of epidermal cells is specified by a combination of gene expression, which may be diffuse for broad attachments, such as muscle origins, or narrowly defined, as for the small attachment sites of muscle insertions. Changes in the extent and distribution of these and possibly other genes across the epidermis may provide the pathways across which muscles migrate, as observed in comparative study.
(3) Once a match has been found, the epidermal and muscle cells form an extracellular matrix, including linear arrays of microtubules (Volk, 2006, p. 110; for schematization, see fig. 1 of Bitsch & Bitsch, 2002), anchoring the muscle to designated tendon cells for action (see also Schweitzer et al., 2010 for comparison of *Drosophila* and vertebrate tendon). During molts between larval instars, the microtubule tendons are broken down during apolysis and replaced by muscles with the same precursor identity across the larval instars. These tendons are not always replaced; adult muscles comprise either remodeled or replaced larval muscles or entirely new, adult-specific muscles from precursor cells. When areas of the epidermis are deleted through genetic knockdown, such as for the homeobox gene *Wingless*, distal tendons cannot be made and the unpaired end of the muscle fiber will be left free floating in the body (e.g., Fabian et al., 2016).

Epidermal identity is of course not provided by muscle attachments alone. The inward (invagination) or outward (evagination) folding of the epidermis (formative elements *sensu* Klass, 1997) are the results of coordinated structuring of cytoskeleton across the epidermal field. (Invagination with muscle attachment produces "apodemes", which are not to be confused with tendons, which are extracellular structures, as outlined above.) It will be important to determine the timing of these folding events relative to muscular tendon formation. The joints and articulations of appendages are likewise highly specified and dynamically structured, taking on both a characteristic form and mechanical function (Mirth & Akam, 2002; Tajiri et al., 2010). The characteristic function of these joints is powered by developmentally specified musculature, which retain their identity information in spite of variation in the formative elements of the epidermis. This is especially important for structures that are complex in terms of the counts of parts, and complex in terms of shape variation, such as the male genitalia of the Hexapoda.

4.3.1 | Muscle identity: The case of the gonostylus

A recent study on skeletomuscular homologies and terminology for the Hymenoptera made a case for referring to the entire lateral clasping structures of the male genitalia as a "gonostyle." Because "gonostyle" is not to be confused with the gonostylus, we refer to the label of Dal Pos et al. (2023) as "gonostyle*." (*Note also*: "clasper" will be used here for the lateral appendages of the external genitalia in a neutral manner, as was done by, e.g., Michener, 1944a, 1944, so as to not unintentionally invoke the alternative theories of homology during discussion; see also Section 4.3.3 for some corrections.) The reasoning behind this case is the argument that, as various Hymenoptera lack clear physical distinction between the gonocoxa and gonostylus, one cannot recognize these parts and, effectively, that presence of the distinction does not imply homology (paraphrased from p. 26 therein). Because the authors make strong recommendations for the use of gonostyle* for the whole lateral appendage of hymenopteran male genitalia, it is necessary to consider the evidence for epidermal – hence sclerite – identity, as informed by the patterns of muscular attachment across the phylogeny of the insects (for a more comprehensive treatment, see Boudinot, 2018). We will ignore the resemblance point for this discussion as it was used as a criterion for term choice and not identity.

The groundplan for the genital skeletomusculature of the true insects, or Ectognatha, is reasonably approximated by the wingless orders Archaeognatha and Zygentoma, as the latter are sister to the Pterygota (e.g., Misof et al., 2014), thus these two groups form a grade. Each abdominal segment of these insects may comprise small sclerites called intersternites, a sternite, and a flattened appendage, the coxopod, which can bear one to two medially situated and eversible vesicles and one lateral ramus, the stylus (e.g., Klass & Matushkina, 2018). Each abdominal stylus may be controlled by one or two muscles, labeled either "60" by Bitsch (1973, 1974a, 1974b), "2" of Klass and Kristensen (2001), or "f" and "g" by Birket-Smith (1981), and each genital complex comprises the serially homologies appendages from two abdominal segments: VIII and IX for females, and IX and X for males. These appendages may be referred to as "gonopods," as they are limbs that together form the ovipositor complex of females, and the copulatory complex of males, even when simple. The abdominal coxae and styli of the ninth-segmental gonopods of males may be referred to as "gonocoxae" (GC) and "gonostyli" (GS) (Figures 29a and 30a) (see sec. 3.1 of Boudinot, 2018 for discussion of appendage segment alignments across the Pancrustacea, and sec. 3.1.4.1 for homologies of nongenital abdominal elements). (*Note also*: "Gonocoxite" is used in the present work interchangeably

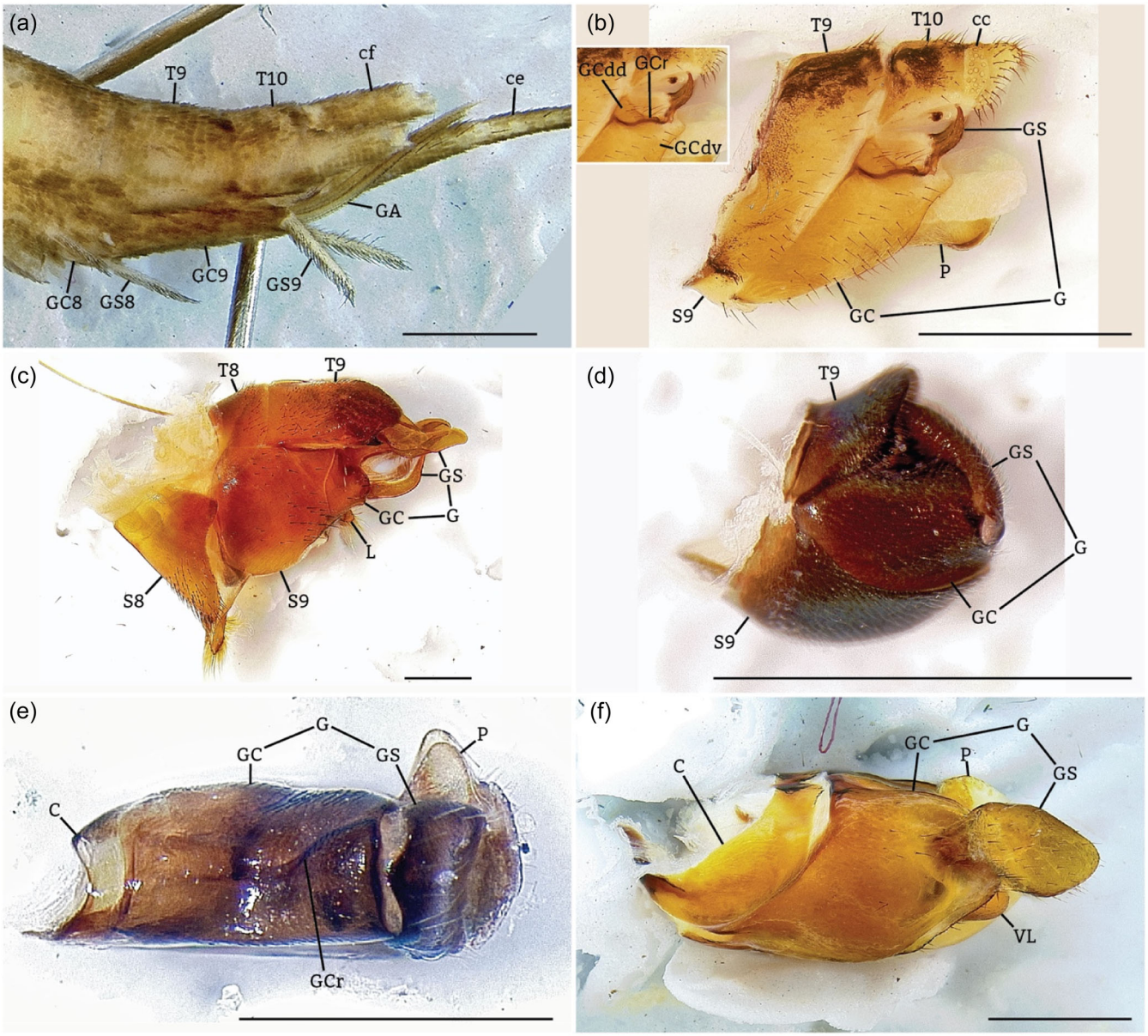

FIGURE 29 Outgroup comparisons in lateral view showing the basic homologies of the external genitalia, as determined by evaluation of skeletomuscular patterns (for details and extended reasoning, see Boudinot, 2018). Scale bars = 1.0 mm. **Sampled taxa:** (a) Archaeognatha female (*Machilis aurantiacus*). (b) Raphidioptera male (*Agulla* sp.); inset for (b) provides labels for gonocoxal structures that are reasonably homologous with *Xyela* and *Paraponera*. (c) Diptera male (*Tipula californica*). (d) Mecoptera male (*Boreus reductus*). (e) Hymenoptera "symphyta" male (*Xyela* sp.). (f) Hymenoptera "symphyta" male (*Cimbex rubidus*). **Abbreviations: C** = cupula; **ce** = cercus; **cf** = median caudal filament; **G** = gonopod; **GA** = gonapophysis; **GC** = gonocoxa; **GCdd** = dorsal (lateral) disc of the gonocoxa; **GCdv** = ventral (medial) disc of the gonocoxa; **GCr** = coxostylar ridge; **GS** = gonostylus; **L** = lateropenite, when not part of the volsellar complex; **P** = penite; **S#** = sternum; **T#** = tergum; **VL** = lateropenite, when part of the volsellar complex.

with "gonocoxa" but is used in a stringent sense here and in Boudinot, 2018 to indicate that the structure has undergone fragmentation.) The penis of true insects is a medially fused (or lateromedially undifferentiated) pair of gonopods, with extrinsic muscles attaching to the tenth tergum ("59" of Bitsch, "h10," "k10" of Birket-Smith) as evidenced by Archaeognatha. The penis is not a pair of gonapophyses of the ninth segment, as the ninth segmental gonapophyses are retained in the wingless groups and the topologically homologous rami of Remipedia, the possible sister group of Hexapoda, does not have tergal musculature (Hessler & Yager, 1998). The penis-gonopod complex are developmentally integrated in the Pterygota, and therein are no longer readily separable as distinct appendages of segments IX and X.

The gonocoxa–gonostylar organization and coxo-stylar musculature is retained in several orders of Holometabola, including Raphidioptera (Figures 29b and 30b), Diptera (Figures 29c and 30c), Mecoptera (Figures 29d and 30d), and Hymenoptera (Figures 29e,f and 30e,f). The gonostylus, as the ramus or distal element of the abdominal appendage, is

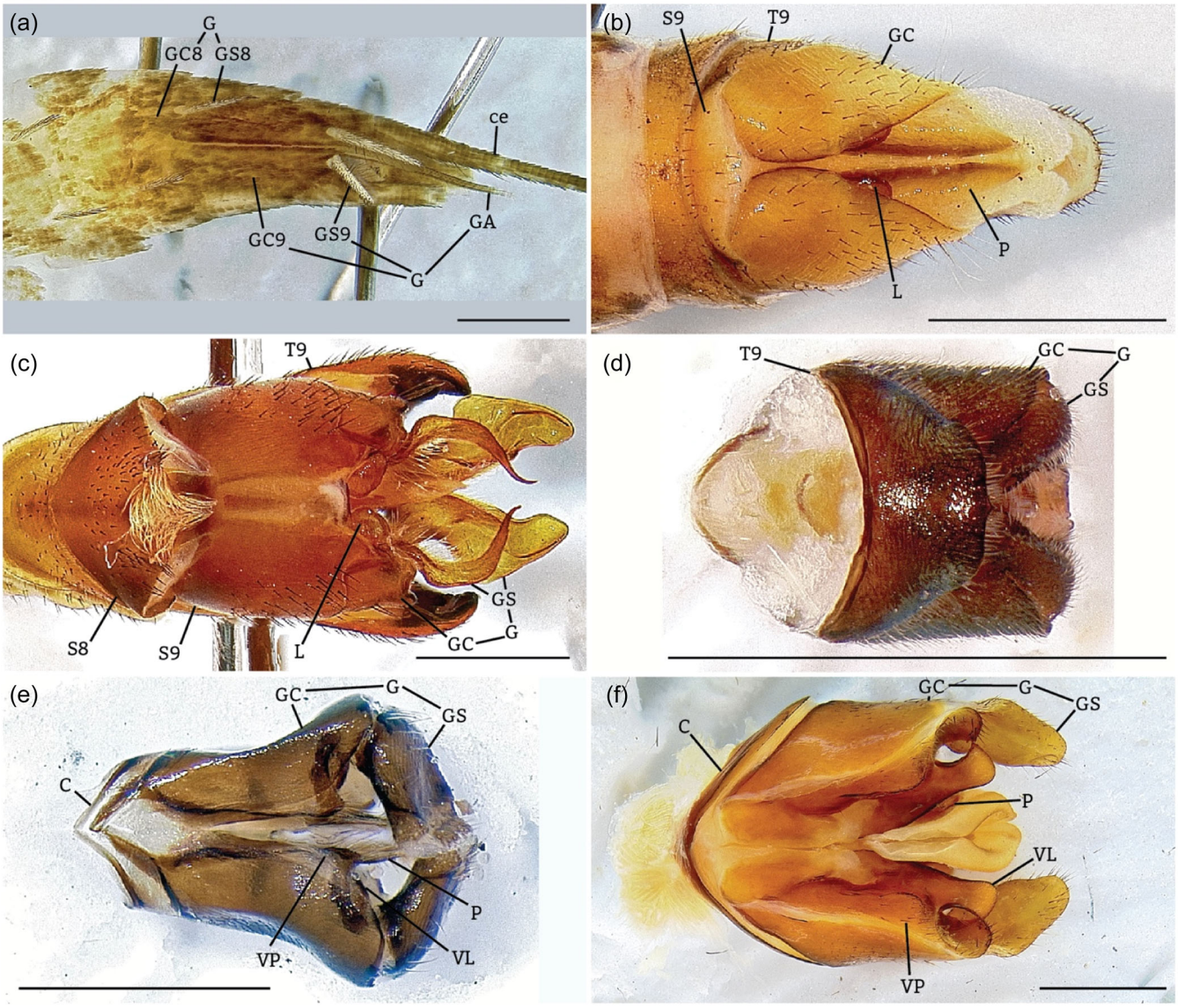

FIGURE 30 Outgroup comparisons in ventral view (except (d), which is in dorsal view) showing the basic homologies of the external genitalia, as determined by evaluation of skeletomuscular patterns (see Boudinot, 2018). Scale bars = 1.0 mm. **Taxa sampled:** (a) Archaeognatha female (*Machilis aurantiacus*). (b) Raphidioptera male (*Agulla* sp.). (c) Diptera male (*Tipula californica*). (d) Mecoptera male (*Boreus reductus*). (e) Hymenoptera "symphyta" male (*Xyela* sp.). (f) Hymenoptera "symphyta" male (*Cimbex rubidus*). **Abbreviations: C** = cupula; **ce** = cercus; **G** = gonopod; **GA** = gonapophysis; **GC** = gonocoxa; **GS** = gonostylus; **L** = lateropenite, when not part of the volsellar complex; **P** = penite; **S#** = sternum; **T#** = tergum; **VL** = lateropenite, when part of the volsellar complex; **VP** = parossiculus.

identified in Holometabola by a specific pair of muscles (*note*: the numbering of "stylar muscle #" here is arbitrary, the synonymies are not): **Stylar muscle #1** (**=IXAxab** of Boudinot, 2018; **=*u*** of Boulangé, 1924 and Schulmeister, 2001, 2003; **=9csm3** of Griebenow et al., 2023; **=ga-hra** of Dal Pos et al., 2023) and **stylar muscle #2** (**=IXAxad** of B'18; **=*t*, *w*** of B'24 and S'01, '03; **=9csm2** of G et al.'23; **=gs-gs**, **gs-hrd**, **gs-hrp** of DP et al. '23). This muscle-sclerite identity is retained even when the form of the gonostylar sclerite is grossly modified, as in the profound forking of the sampled *Tipula* (Figures 29c and 30d). Further, at least one of these two stylar muscles is retained in many Hymenoptera, regardless of whether a membrane is present between the proximal and distal elements of the clasper (Figures 29e and 30e vs. 29f and 30f). This contention is supported by the observation of these muscles across many groups of Hymenoptera and the ancestral state estimations of Schulmeister (2003) and Griebenow et al. (2023), which relied on different statistical frameworks and model assumptions.

When these proximal and distal elements both lack lateral membrane and musculature, they may still be recognizable due to their shapes in the topological position where the articulation was ancestrally, or in the occurrence of ventral or medial membrane, as in *Paraponera* (e.g., Figure 3b) and other ants (notably, many groups of ants have clearly recognizable gonocoxae and gonostyli, BEB pers. obs.). In other words, some signature of the ancestral proximal and distal identities of the epidermal cell populations is visible, whether

TABLE 2 Alignment of male genital musculature between the groundplan of the Holometabola, the groundplans of the Raphidioptera, Diptera, and Hymenoptera (as inferred by Boudinot, 2018), the system of Dal Pos et al. (2023) ("DP'23"), Griebenow et al., (2023) ("G'23"), *Paraponera* (this study), and Archaeognatha from Boudinot (2018, fig. 1A4).

Column: Maj. M. Group	I S9-C	II C-GC	III GC-GS	IV GC-VL(/V)	V GC-P	VI C-GS*	VII GS*-H	VIII GS*-V	IX GS*-P
Archaeognatha	Ca-7	Ca-5/B-4	E-11, 12	?[a]	+[b]	–	–	–	–
Holometabola Groundplan	s	tc	d/b	lm/lp	ppv/prv/ ppd/prd	–	–	–	–
Raphidioptera	+	+	+/+	+/+	–/+/+/+	–	–	–	–
Diptera	–	+	+/+	+/+	+/+/+/+	–	–	–	–
Hymenoptera	+	+	+/+	+/+	+/+/+/+	–	–	–	–
Hym: DP'23	+	–	–/–	–/–	–/–/–/–	+	+	+	+
Hym: G'23	+	+	+/+	+/+	+/+/+/+	–	–	–	–
Hym: *Paraponera*	+	+	–/–[c]	+/+	+/+/+/+	–	–	–	–

Note: Excluded from this alignment are penial intrinsic muscles as they were outside of the scope of Boudinot (2018), and the volsello-volsellar and penial-volsellar muscles as these are autapomorphic for Hymenoptera among Holometabola. The labels for the major muscle groups (top row) indicate sternum IX (S9), cupula (C), gonocoxa (GC), gonostylus (GS), gonostyle* (GS*), lateropenite (L) volsella (V), penis (P), and the "harpe" of Dal Pos et al. (2023) (H). Because the holometabolan outgroups do not have a volsella (=volsellar complex, i.e., parossiculus + [digitus = gonossiculus = lateropenite]), both lateropenite and volsella are indicated for the major muscle groups in column IV, that is, "VL(/V)." For the holometabolan groundplan muscle labels, the segment and tagma indicators ("IX" and "A") are left implied.

[a]See Section 4.3.2.

[b]The origins of the penial extrinsic muscles were inferred to have migrated from the sternum to the gonocoxae in the ancestor of the Holometabola by Boudinot (2018).

[c]The flexing ("clasping") function of the coxo-stylar muscles is replaced by the muscle ***o*** (=9clm4/gs-pss).

through curvature, medial membranes, or other phenotypic features. When there is no reliable distinction between proximal and distal elements, the lateral clasper (gonopod) does not automatically become the distal element (gonostylus), as this would require the penial (=aedeagal, e.g.) and lateropenial (=gonossicular, digital, e.g.) muscles to migrate wholesale out of the proximal (gonocoxal) epidermal field into the distal field. The unlikeliness of this homology interpretation is further demonstrated by alignment of the major muscle groups of the male genitalia across the Hymenoptera and relatively plesiomorphic representatives of Holometabola (Table 2). Certainly, when the proximal and distal elements of the clasper are not consistently demarcated, a term for referring to the whole clasper is warranted, but a gonostylus it is not and does not become. One choice could be "gonopod," or "gonopodites," as gonopods with both proximal and distal elements (gonocoxae and gonostyli) are recognizable and homologous across the Holometabola. There are other options, and lists of terminological synonyms are available.

In sum, the special (i.e., derived) case of indistinct gonocoxae and gonostyli should not be used to reject the theory of coxostylar, hence gonopodal identity. When abdominal styli are absent in Zygentoma, for example, the appendages are still recognizable due to the coxo-sternal distinction. If the phenotypic markers of the gonostyli are completely lost, as in some Hymenoptera, the gonocoxae (hence gonopods) would remain; their distal cell populations would be positional correspondents and could be spatially designated as the "apical region of the gonopod," for example. So as to avoid conflation with the gonostylus, we recommend that use of the term gonostyle* in the intended sense of Dal Pos et al. (2023) in future study should be clearly indicated. See Section 4.4 on the harmonious use of the alternative systems and best practices for clarity.

4.3.2 | Muscle identity: The volsellae and cupula

Two further structural elements of the male genital complex of Hymenoptera make homology inference more complicated, which we address here for the sake of providing a complete treatment: **(1)** The cupula and **(2)** the volsella.

(1) The cupula is a sclerite that forms a ring around the base of the gonopod-volsellar complex and penis. It is an autapomorphy of Hymenoptera and bears the attachments of two muscle sets. The extrinsic muscle set originate on sternum IX and are alignable with the sterno-coxal muscles of other Holometabola. It has been previously pointed out that the cupula (=gonobase, =basal ring) develops from the bases of the claspers (see, e.g., references in Michener, 1944a, 1944b). The other set of muscles originate in the cupula and attach to the bases of the claspers. These muscles pose a problem, as the gonopods of other holometabolan orders lack gonocoxal-intrinsic muscles. However, these other orders also often have tergal muscles that insert on the gonocoxae, which are absent in Hymenoptera. Therefore, the apparent gap in the muscular alignment – which could be due to loss of tergal muscles and gain of cupular-coxal muscle set – can be resolved

by inferring that the cupulo-coxal muscles are tergal in origin and gonocoxal in insertion, hence that the cupula has inherited gonocoxal identity (*vis à vis* the sterno-coxal muscles) and some degree of tergal identity (*vis à vis* the tergo-coxal/cupulo-coxal muscles). Note that the origin of these tergal muscles is on the developmentally differentiated postabdomen ("proctiger"), hence these muscles may also be conceived as "postabdominal-genital muscles". Hypothetical intermediate conditions are diagrammed in figs. 1G1 and G2 of Boudinot (2018).

(2) The volsella is an anatomical complex that comprises two sub-elements, the parossiculus, which is immediately mediad the ventromedial margin of the ninth-segmental clasper (gonopod), and the digitus/gonossiculus/lateropenite ("DGL" for the purpose of this discussion), which is a mobile element that is situated slightly mediad the apex of the parossiculus (see Schulmeister, 2001, for discussion of the history of volsellar terminology). The presence of the muscle-bearing DGL is an autapomorphy of the Holometabola with no clear analog among the Polyneoptera and Condylognatha, and it is a source of major confusion for works on male genital homologies, as it is an often-overlooked element of the holometabolan groundplan (L and VL in Figures 29c,f and 30b,c,e,f). With the exceptions of some highly to extremely derived groups, the DGL is a small and variably shaped sclerite that bears the insertion of one or more muscles, which themselves often attach at their origin within the proximal element of the clasper (gonocoxa). The parossiculus, on the other hand, is an autapomorphy of the Hymenoptera. In addition to being free or fused to the ventromedial gonocoxal margin (the sclerite of the parossiculus is continuous with the gonocoxa in *Paraponera*, e.g., Figures 5f, 14, and 19), the parossiculus bears the origin of a DGL muscle. As no holometabolan order has DGLs with intrinsic musculature, this muscular attachment to the parossiculus indicates that this sclerite is derived from the gonopod, that is, that the parossiculus is a gonopodal fragment.

With a broader phylogenetic scope, that is, outside of the extant Pterygota, there are three alternative hypotheses for the origin of the DGL that should be considered. The DGL is absent in all non-Holometabola and was inferred by Boudinot (2018) to *not* be homologous with the gonapophyses of segment IX, as gonapophyses are absent in Ephemeroptera, Odonata, Polyneoptera, Hemiptera, and Psocodea. The alternatives are that: (1) the gonapophyses (and their extrinsic muscles, see Bitsch, 1974a, 1974b) were lost independently in the ancestors of each of these groups and retained with strengthened growth in Holometabola (the "gonapophysis retention" hypothesis); (2) these were lost the ancestor of all Pterygota (or some combination of independent losses) and some genetic element was retained that re-expressed in the Holometabola (the "gonapophysis re-expression hypothesis"); or (3) these were lost and some lateral element of the penite or penites became separated in the ancestor of the Holometabola (the "lateropenite" hypothesis).

The case of the DGL is difficult, as the multiple losses mean that no solution is obviously more parsimonious (a scenario confronted for Coleoptera; Boudinot et al., 2023). Fossil evidence that became available after Boudinot (2018) went to press suggests that gonapophyses may have been retained among stem lineages of Odonata (the Odonatoptera), but that these were absent in Palaeodictyoptera, the long-beaked, three-winged insects that went extinct at the end of the Permian, and may be stem to Ephemeroptera, Odonata, or Polyneoptera (Prokop & Engel, 2019; Prokop et al., 2020; see also Simon et al., 2018). If gonapophyses were lost then regained due to cooption of some genetic system, or if they were retained uniquely in one lineage, should these be deep homologs, or mere plesiomorphies with variable expression or retention patterns? Regardless of the evolutionary pathway (hypotheses 1, 2, or 3), musculature suggests that the DGL may be homologous with gonapophyses IX or of fragments of the penite; the former does appear more parsimonious. Perhaps therein lies the key; does muscle attachment induce shape transformation of epidermis and its sclerotic cuticle? If so, then loss of the gonapophyseal muscle may also result in loss of this ramus. Phrased in another way, does communication between muscle and epidermis during muscular attachment inform shape? Is it more likely that epidermal cells fated to become part of the penis would subdivide into the DGL, or that the cells of the already fragmentation-prone gonopods would? Does the probable ancestral derivation of the penis from segment X play a role in this (in-)flexibility?

At present, it is not possible to make confident, discrete rejections of the alternative hypotheses for the origin of the DGL. It appears that the DGL–gonopod-IX relationship is stronger than the DGL–gonopod-X (=DGL-penis) relationship. More specifically, now that the at the scenario of multiple complex loss in Coleoptera is apparent, it is easier to consider the DGL as unexpected retentions or re-expressions of the gonapophyses. Because of this, it might be preferable to choose the more neutral term "parandrite" or "gonossiculus" over the Hymenoptera-specific "digitus" and the theory-laden "lateropenite," which was coined to be unique, hence have no conflating homonyms. "Gonossiculus" also has the advantage of (unintentionally) matching the "gono-" series of terms, that is, to remind one of the "gonapophysis" without invoking direct homology. Until more or decisive evidence becomes available, we apply "lateropenite" throughout the text and do not revise the system for the DGL here, for the purpose of consistency.

4.3.3 | Some corrections to the literature

It is necessary to address two of the claims that Dal Pos et al. (2023) made in their dismissal of the work of Boudinot (2018). We leave in peace other statements of the authors (e.g., the reasoning for rejecting the term paramere [p. 34] and the production of confusion [p. 3]), as we are all working together to understand these complex systems, and as we will continue to refine our understandings through conversation, presentation of evidence, and explicit reasoning.

(1) On p. 35, the authors remarked that "according to [Boudinot (2018)], the gonocoxa … is a fragment of the apical part of sternum IX [and] fragmented a second time, forming the parossiculus." This is

false. No element of the male genital complex of Hymenoptera was inferred by Boudinot (2018) as deriving from a fragment of the sternum (see, e.g., figs. 1F5, G1–3 and the "*Genital evolution*" section on pp. 581, 582 therein). The parossiculus was indeed inferred by Boudinot (2018) to be a fragment, but of the gonopod, with the gonopods homologous to the male genital appendages of segment IX (i.e., gonopods) of Holometabola and various other orders, not with the gonopods as homologous with a pair of fragments from sternum IX. **(2)** Also on p. 35, the authors further remarked that "Boudinot (2018) also homologized the harpe with the stylus, which he considered to have separated from the phallic apparatus (=aedeagus, see under Penisvalvae)." We did and continue to consider the terms "harpe" and "gonostylus" to be absolute synonyms representing the same homolog. However, an interpretation of this distal element of the archaeognathan gonopod or holometabolan "clasper" as derived from the penis is incompatible with the facts of anatomy as presented in Boudinot (2018) and in the present work (see, e.g., Figures 29 and 30).

To clarify the evolutionary scenario proposed by Boudinot (2018) and elaborated upon here, we rephrase this in brief (see also Sections 4.3.1 and 4.3.2). Sternum IX subtends and does not form a part the genital appendages (i.e., the external genitalia), but it does control genital pro- and retraction. The cupula is a sclerite derived from the proximal portions of the gonocoxae and may be a composite with a fragment of tergum IX due to the cupulo-coxal muscles, which are otherwise unexplainable without invoking total novelty. The gonopods are inherited from the most recent common ancestor (MRCA) of the Hexapoda and retain coxostylar identity, as indicated by the phenotypic markers of proximodistal differentiation, including the coxostylar ridge (when present), the coxostylar membrane (when present), differences in appendage thickness, and differences in setation, among others. The parossiculi are medial fragments of the gonopodites (*note*: we use "gonopods" more frequently in the text and speech for simplicity, as for "gonocoxites" and "gonocoxae"). The lateropenites are derived sclerites that are unique to the Holometabola and possibly derived from the sclerites of the penis (penites), and the penites are inherited and derived from the MRCA of the Ectognatha ("true insects").

4.4 | Muscular terminology: Harmonizing the systems

In addition to recognizing and refining the 5-category system of hierarchical homology of DLW, the homology inferences in the present study follow the criteria of Remane (1952). Namely that across individuals, (i) parts and subparts share "positional homology" (i.e., are positionally indexed *sensu* DLW); (ii) some "special quality," that is, complex parts share special mechanical and/or physiological properties, and/or special compositional qualities of their subparts; (iii) forms are linked through intermediates; and (iv) simple, corresponding structures are shared among closely related taxa. Fortunately, structural correspondences and positional indexing among the Hymenoptera have received abundant attention, such that most of the parts and subparts that have a broad phylogenetic occurrence have been documented to some degree and considered in some detail. Moreover, there are several resources available for term systems with explicit definitions and illustration. While there is conflict in the explicitly inferred or implied homologies of these systems, the strength of each may be considered in the context of their purposes, which does not detract from the value of any of these works.

The system of Boulangé (1924) as modified by Schulmeister (2001, 2003) provides an extremely valuable set of muscular and sclerite labels, as Schulmeister explicitly used this terminology in a homology-neutral manner relative to other orders. The system of Griebenow et al. (2023) forms an expansion of the topographical main-group system developed by Beutel and others from the glossary of von Kéler (1963) (e.g., Beutel et al., 2014, for the summary of head to thoracic muscular systems), recognizing serial homology of the pregenital abdomen (see Lieberman et al., 2022 for the abdomen and ovipositor apparatus). The system of Dal Pos et al. (2023) builds on the HAO (HAO Portal, 2024; Yoder et al., 2010), which is the chief resource for Hymenoptera, providing a comprehensive and structured set of terms, their synonyms from the depths of literature, hyperlinked definitions, and URIs for each concept. Finally, the system of Boudinot (2018) (and Griebenow et al., 2023, see especially p. 953) links the Hymenoptera to the remainder of the Holometabola and Hexapoda, based on skeletomusculature and explicit comparative and phylogenetic reasoning.

Above all, an important principle for all comparative work is to provide explicit reference (i.e., explanation and citation) for the source of concepts and definitions. This provides a critical basis for interpretability and the replicability of observation and reasoning. As outlined by Richter and Wirkner (2014), evolutionary morphological work proceeds in cycles and is, in part, a linguistic effort, ideally using homology-neutral descriptors (morphemes) for structures and their spatial relationships before explicit cladistic or phylogenetic inference of homology (e.g., in brief for via the treatment of the endophallic sclerite above, Section 3.2.7, and in more detail via Starck et al., 2022; Zahnle et al., 2020). Because homology-neutral terms are often topologically vague (see also discussion of Griebenow et al., 2023), or coined explicitly to avoid homonymy (e.g., Birket-Smith, 1981), they can be useful placeholders for consideration of possible homologies (e.g., "DGL" above) but are not always preferable as terms of choice alone. By indicating the homology neutral term or label alongside synonyms, as done here for musculature, it is possible to communicate to observers with different conceptual frameworks. In our case, we chose to use the Boulangé-Schulmeister label system as the authors of all of the recent works have familiarity with this but are otherwise speaking different languages. One further and effective means of linking conceptual and terminological frameworks is providing a table of terms, including synonymies, with explicit references to HAO URIs in the case of the Hymenoptera (Seltmann et al., 2012).

4.5 | Big phenotypic data: Phenomics and collectomics

To realize the broader objective of using big phenotypic (phenomic) data for the purposes of comparative and functional anatomy, developmental mapping, evolutionary analysis, and systematics, a workflow is necessary. Prior studies have significantly contributed to the problems of anatomical identity (homology) and the major patterns of structural variation of hymenopteran genitalia (e.g., Dal Pos et al., 2023; Griebenow et al., 2023; Mikó et al., 2013; Schulmeister, 2001, 2003). Here, we establish the foundation for the phenomic study of male ant genitalia, and for hymenopteran genitalia more broadly, by accounting for all of the individual parts and formative elements of *P. clavata* that were detectable given the sampling methods we applied. This work thus represents a reference phenome, substantiated by physical specimens, 3D models which are digitally manipulable and printable, and detailed 2D documentation. Limitations of this study and this approach include data image resolution (6.10 μm for the μ-CT data), manual effort, translating objects into numerical observations (data) for statistical analysis (i.e., the subjectiveness bottleneck), and the generation of sufficient replicate label sets for training an artificial intelligence. Nevertheless, our work will facilitate future detailed comparisons for the purpose of understanding evolutionary change, historical patterns of extinction, detection of sexual selection, and more, provided that the workflow can be replicated, and meaningful information captured.

5 | CONCLUSION

The male genitalia of insects are extreme in their complexity. This fact is easy to overlook. For example, there are 15 uniquely identifiable muscles in the groundplan of the male genitalia of ants (Boudinot, 2013), and more broadly, we see that despite her negligible size, an individual worker ant has a surprising quantity of skeletal parts (325) and muscles (316) when compared to humans (~206 and ~640, respectively) (Boudinot et al., in press). In the present study, we document the skeletomusculature and soft tissue anatomy of the male genitalia of an ant (*P. clavata*) in the greatest detail to date for Formicidae and Hymenoptera more broadly. In so doing, we discovered and documented several structural and formative elements of likely functional significance, such as the subdivision of the medial surface of the gonostylus and the complex shape of the endophallic sclerite (=fibula ducti). Using our detailed observations and broader comparison of skeletomuscular patterns across the Holometabola and with special reference to Archaeognatha, we also clarify the spatial and structural correspondences of male genitalic elements, providing a revised perspective on the likely homologies of the male genitalic complex across insects. From this, and especially in light of hierarchical homology (DiFrisco et al., 2023), we argue that the male and female genitalia are paramorphic, but that they are both homomorphic with abdominal appendages. Therefore, the penis-gonopod conceptual model fits the observations of male insect genitalic anatomy better than the phallic-periphallic model. We maintain that the latter model is more suited for tracking elaborations of the genitalia in cases of extreme derivation within the frame of abdominal appendage homology, but requires careful alignment of epidermal folds, which is informed by muscular topology. With *P. clavata* as a reference phenome, constructed by 3D modeling and accounting for all identifiable structural and formative elements via multimodal sampling, our work lays the foundation for the quantification of genital complexity between males and females across phylogeny, hence evaluation of relative patterns of sexual versus natural selection across the body, for example. The phenomic approach to biodiversity mapping and museum collection digitization will be fruitful, as it will form a bridge between extant and extinct taxa, providing insight into evolutionary patterns, contemporary adaptation, and the ecomorphological history of life on earth.

AUTHOR CONTRIBUTIONS

Brendon E. Boudinot: Conceptualization; methodology; data curation; investigation; visualization; writing—original; resources. **Thomas van de Kamp**: Methodology; data curation; writing—revision; resources. **Patricia Peters**: Methodology. **Katja Knöllinger**: Methodology; investigation; visualization; writing—revision.

ACKNOWLEDGMENTS

We thank: Jack Longino for the specimens; Ziv Lieberman for discussion, detailed comments on an early and later draft, and awakening us to our conflation of “gonostylus” and “gonostyle*”; Jill Oberski for sharing her Wild microscope and for repeatedly lending her ear for the writing; Ekin Tiliç and Marie-Louise Tritz (SMF Marine Invertebrates II) for SEM assistance; Henry Knauber and Torben Riehl (SMF Crustacea) for CLSM assistance; and Robin Kunz and Mónica Solórzano-Kraemer (SMF Paleozoology I) for microphotography assistance. We thank Tomáš Faragó (KIT) for tomographic reconstruction and Angelica Cecilia and Marcus Zuber (KIT) for the assistance at the beamline. We acknowledge the support of the Senckenberg Ocean Species Alliance (SOSA) for funding the Hitachi TM4000 plus SEM. We acknowledge the KIT Light Source for provision of instruments at their beamlines and we would like to thank the Institute for Beam Physics and Technology (IBPT) for the operation of the storage ring, the Karlsruhe Research Accelerator (KARA). We also thank Davide Dal Pos for positive and clarifying communication, and István Mikó for his radiance of thought and further discussion on the subjects of homology and ontology. We are grateful to our colleagues and collaborators. None of this work was produced with artificial intelligence.

CONFLICT OF INTEREST STATEMENT

The authors declare no conflict of interest.

DATA AVAILABILITY STATEMENT

The data that support the findings of this study are openly available in Zenodo at https://zenodo.org/.

ORCID

Brendon E. Boudinot http://orcid.org/0000-0002-4588-0430
Thomas van de Kamp http://orcid.org/0000-0001-7390-1318
Katja Knöllinger http://orcid.org/0009-0003-4490-4300

PEER REVIEW

The peer review history for this article is available at https://www.webofscience.com/api/gateway/wos/peer-review/10.1002/jmor.21757.

REFERENCES

Aibekova, L., Boudinot, B. E., Georg Beutel, R., Richter, A., Keller, R. A., Hita-Garcia, F., & Economo, E. P. (2022). The skeletomuscular system of the mesosoma of *Formica rufa* workers (Hymenoptera: Formicidae). *Insect Systematics and Diversity*, *6*(2), 2.

Aili, S. R., Touchard, A., Hayward, R., Robinson, S. D., Pineda, S. S., Lalagüe, H., Mrinalini, S., Vetter, I., Undheim, E. A. B., Kini, R. M., Escoubas, P., Padula, M. P., Myers, G. S. A., & Nicholson, G. M. (2020). An integrated proteomic and transcriptomic analysis reveals the venom complexity of the bullet ant *Paraponera clavata*. *Toxins*, *12*(5), 324.

Altner, H., & Prillinger, L. (1980). Ultrastructure of invertebrate chemo-, thermo-, and hygroreceptors and its functional significance. *International Review of Cytology*, *67*, 69–139.

Andrade, T. T., Gonçalves, W. G., Serrão, J. E., & Martins, L. C. B. (2019). Morphology of the mandibular gland of the ant *Paraponera clavata* (Hymenoptera: Paraponerinae). *Microscopy Research and Technique*, *82*(6), 941–948.

AntWeb. (2024). AntWeb v8.108. California Academy of Science. Retrieved July 18, 2024, from https://www.antweb.org/

Barden, P., Boudinot, B., & Lucky, A. (2017). Where fossils dare and males matter: Combined morphological and molecular analysis untangles the evolutionary history of the spider ant genus *Leptomyrmex mayr* (Hymenoptera: Dolichoderinae). *Invertebrate Systematics*, *31*(6), 765–780.

Baroni Urbani, C. (1994). The identity of the Dominican *Paraponera* (Amber Collection Stuttgart: Hymenoptera, Formicidae. V: Ponerinae, partim). *Stuttgarter Beiträge zur Naturkunde. Serie B (Geologie und Paläontologie)*, *197*, 1–9.

Beutel, R. G., Friedrich, F., Yang, X. K., & Ge, S. Q. (2014). *Insect morphology and phylogeny: A textbook for students of entomology*. Walter de Gruyter.

Billen, J., Khalife, A., Ito, F., Anh, N. D., & Esteves, F. A. (2021). The basitarsal sulcus gland, a novel exocrine structure in ants. *Arthropod Structure & Development*, *61*, 101041.

Birket-Smith, S. J. R. (1974). On the abdominal morphology of Thysanura (Archaeognatha and Thysanura s. str.). *Entomologica Scandinavica Supplement*, *6*, 5–67.

Birket-Smith, S. J. R. (1981). The male genitalia of Hymenoptera—A review based on morphology in Dorylidae (Formicoidea). *Entomologica Scandinavica*, *15*, 377–397.

Bitsch, C., & Bitsch, J. (2002). The endoskeletal structures in arthropods: Cytology, morphology and evolution. *Arthropod Structure & Development*, *30*, 159–177.

Bitsch, J. (1973). Morphologie abdominale des Machilides (Insecta Thysanura). I. Squelette et musculature des segments pregenitaux. *Annales des Sciences Naturelles, Zoologie et Biologie Animale*, *15*, 173–200.

Bitsch, J. (1974a). Morphologie abdominale des machilides (Thysanura). II. Squelette et musculature des segments genitaux femelles. *International Journal of Insect Morphology and Embryology*, *3*, 101–120.

Bitsch, J. (1974b). Morphologie abdominale des machilides (Thysanura). III. Squelette et musculature des segments genitaux mâles et des segments postgenitaux. *International Journal of Insect Morphology and Embryology*, *3*, 203–224.

Bolton, B. (2003). Synopsis and classification of Formicidae. *Memoirs of the American Entomological Institute*, *71*, 1–370.

Boudinot, B. (2013). The male genitalia of ants: Musculature, homology, and functional morphology (Hymenoptera, Aculeata, Formicidae). *Journal of Hymenoptera Research*, *30*, 29–49.

Boudinot, B. E. (2015). Contributions to the knowledge of Formicidae (Hymenoptera, Aculeata): A new diagnosis of the family, the first global male-based key to subfamilies, and a treatment of early branching lineages. *European Journal of Taxonomy*, *120*, 1–62.

Boudinot, B. E. (2018). A general theory of genital homologies for the Hexapoda (Pancrustacea) derived from skeletomuscular correspondences, with emphasis on the Endopterygota. *Arthropod Structure & Development*, *47*(6), 563–613.

Boudinot, B. E., Casadei-Ferreira, A., da Silva Probst, R., Lieberman, Z. E., & Richter, A. (in press). Ch. 18. Ecomorphology of ants. In O. Betz (Ed.), *The ecomorphology of insects*. Elsevier.

Boudinot, B. E., & Fisher, B. L. (2013). A taxonomic revision of the *Meranoplus* F. Smith of Madagascar (Hymenoptera: Formicidae: Myrmicinae) with keys to species and diagnosis of the males. *Zootaxa*, *3635*, 301–339.

Boudinot, B. E., Moosdorf, O. T. D., Beutel, R. G., & Richter, A. (2021). Anatomy and evolution of the head of *Dorylus helvolus* (Formicidae: Dorylinae): Patterns of sex-and caste-limited traits in the sausagefly and the driver ant. *Journal of Morphology*, *282*(11), 1616–1658.

Boudinot, B. E., Yan, E. V., Prokop, J., Luo, X. Z., & Beutel, R. G. (2023). Permian parallelisms: Reanalysis of †Tshekardocoleidae sheds light on the earliest evolution of the Coleoptera. *Systematic Entomology*, *48*(1), 69–96.

Boulangé, H. (1924). *Recherces sur lápparеil copulateur des Hyménopterès et spécialement des Chalastogastres* (Vol. 28). Facultés catholiques de Lille.

Breed, M. D. (2002). Allometry in the giant tropical ant, *Paraponera clavata*. *Insectes Sociaux*, *49*, 125–128.

Breed, M. D., & Bennett, B. (1985). Mass recruitment to nectar sources in *Paraponera clavata*: A field study. *Insectes Sociaux*, *32*, 198–208.

Breed, M. D., & Harrison, J. M. (1988). Worker size, ovary development and division of labor in the giant tropical ant, *Paraponera clavata* (Hymenoptera: Formicidae). *Journal of the Kansas Entomological Society*, *61*(3), 285–291.

Caetano, F. H., Camargo Mathias, M. I., & Overal, W. L. (1986). The digestive tract of *Dinoponera gigantea* and *Paraponera clavata* under anatomical and histological point of view (Formicidae, Ponerinae). *Naturalia (São José do Rio Preto)*, *11/12*, 125–134.

Carmena, A., & Baylies, M. (2006). Development of the larval somatic musculature. In H. Sink (Ed.), *Muscle development in Drosophila* (pp. 79–91). Eurekah.com and Springer Science + Business Media Inc.

Carpenter, F. M. (1933). A new *Boreus* from British Columbia (Mecoptera). *The Canadian Entomologist*, *65*(4), 94–95.

Cecilia, A., Rack, A., Douissard, P.-A., Martin, T., dos Santos Rolo, T., Vagovič, P., Hamann, E., van de Kamp, T., Riedel, A., Fiederle, M., & Baumbach, T. (2011). LPE grown LSO: Tb scintillator films for high-resolution X-ray imaging applications at synchrotron light sources. *Nuclear Instruments and Methods in Physics Research Section A: Accelerators, Spectrometers, Detectors and Associated Equipment*, *648*, S321–S323.

Chapman, R. F. (2012). *The insects: Structure and function* (5th ed). Cambridge University Press.

Chen, E. H., & Baker, B. S. (1997). Compartmental organization of the *Drosophila* genital imaginal discs. *Development*, *124*(1), 205–218.

Crampton, G. C. (1919). The genitalia and terminal abdominal structures of males, and the terminal structures of the larvae of

'chalastogastrous' Hymenoptera. *Proceedings of the Entomological Society of Washington*, *21*, 129–151.

Crampton, G. C. (1920). A comparison of the genitalia of male Hymenoptera, Mecoptera, Neuroptera, Diptera, Trichoptera, Lepidoptera, Homoptera, and Strepsiptera, with those of lower insects. *Psyche: A Journal of Entomology*, *27*(2–3), 34–45.

Cresson, E. T. (1880). Descriptions of new North American Hymenoptera in the collection of the American Entomological Society. *Transactions of the American Entomological Society*, *8*, 1–52.

Dal Pos, D., Mikó, I., Talamas, E. J., Vilhelmsen, L., & Sharanowski, B. J. (2023). A revised terminology for male genitalia in Hymenoptera (Insecta), with a special emphasis on Ichneumonoidea. *PeerJ*, *11*, e15874.

Daly, Jr. H. V. (1955). *A comparative survey of the sting of aculeate Hymenoptera* [Thesis: University of Kansas, p. 67 + 7 plates].

DiFrisco, J., Love, A. C., & Wagner, G. P. (2020). Character identity mechanisms: A conceptual model for comparative-mechanistic biology. *Biology & Philosophy*, *35*(4), 44.

DiFrisco, J., Love, A. C., & Wagner, G. P. (2023). The hierarchical basis of serial homology and evolutionary novelty. *Journal of Morphology*, *284*(1), e21531.

Doane, R. W. (1908). New North American *Pachyrhina*, with a table for determining the species. *Entomological News*, *19*, 173–179.

Douissard, P.-A., Cecilia, A., Rochet, X., Chapel, X., Martin, T., Kamp, T., Helfen, L., Baumbach, T., Luquot, L., Xiao, X., Meinhardt, J., & Rack, A. (2012). A versatile indirect detector design for hard X-ray microimaging. *Journal of Instrumentation*, *7*(09), P09016.

Dutta, D., & Raghavan, K. V. (2006). Metamorphosis and the formation of adult musculature. In H. Sink (Ed.), *Muscle development in Drosophila* (pp. 125–142). Eurekah.com and Springer Science + Business Media Inc.

Estrada, B., Casares, F., & Sánchez-Herrero, E. (2003). Development of the genitalia in *Drosophila melanogaster*. *Differentiation*, *71*(6), 299–310.

Evans, H. E. (1950). A taxonomic study of the Nearctic spider wasps belonging to the tribe Pompilini (Hymenoptera: Pompilidae) part I. *Transactions of the American Entomological Society*, *75*, 133–370.

Fabian, B., Schneeberg, K., & Beutel, R. G. (2016). Comparative thoracic anatomy of the wild type and wingless (wg1cn1) mutant of *Drosophila melanogaster* (Diptera). *Arthropod Structure & Development*, *45*(6), 611–636.

Fabricius, J. C. (1775). *Systema entomologiae, sistens insectorum classes, ordines, genera, species adiectis synonymis, locis, descriptionibus, observationibus* (p. 832). Flensburgi et Lipsiae [=Flensburg and Leipzig].

Faragó, T., Gasilov, S., Emslie, I., Zuber, M., Helfen, L., Vogelgesang, M., & Baumbach, T. (2022). Tofu: A fast, versatile and user-friendly image processing toolkit for computed tomography. *Journal of Synchrotron Radiation*, *1 29*(Pt 3), 916–927. https://doi.org/10.1107/S160057752200282X

Fedorov, A., Beichel, R., Kalpathy-Cramer, J., Finet, J., Fillion-Robin, J.-C., Pujol, S., Bauer, C., Jennings, D., Fennessy, F., Sonka, M., Buatti, J., Aylward, S., Miller, J. V., Pieper, S., & Kikinis, R. (2012). 3D slicer as an image computing platform for the quantitative imaging network. *Magnetic Resonance Imaging*, *30*(9), 1323–1341.

Fiorentino, G., Lattke, J., Troya, A., Sosiak, C., Dong, M., & Barden, P. (2023). Deep time extinction of largest insular ant predators and the first fossil *Neoponera* (Formicidae: Ponerinae) from Miocene age Dominican amber. *BMC Biology*, *21*(1), 26.

François, J. F., & Dallai, R. D. (1989). Anatomie et morphologie de l'appareil genital male des protoures (Apterygota). *Annales de la Societé Entomologique de France*, *255*, 121–133.

Griebenow, Z. H., Richter, A., van de Kamp, T., Economo, E. P., & Lieberman, Z. E. (2023). Comparative morphology of male genital skeletomusculature in the Leptanillinae (Hymenoptera: Formicidae), with a standardized muscular terminology for the male genitalia of Hymenoptera. *Arthropod Systematics and Phylogeny*, *81*, 945–1018.

Günther, K. K. (1961). Funktionell-anatomische Untersuchung des männlichen Kopulationsapparates der Flöhe unter besonderer Berücksichtigung seiner postembryonalen Entwicklung (Siphonaptera). *Deutsche Entomologische Zeitschrift*, *8*, 258–349.

Haendel, M. A., Balhoff, J. P., Bastian, F. B., Blackburn, D. C., Blake, J. A., Bradford, Y., Comte, A., Dahdul, W. M., Dececchi, T. A., Druzinsky, R. E., Hayamizu, T. F., Ibrahim, N., Lewis, S. E., Mabee, P. M., Niknejad, A., Robinson-Rechavi, M., Sereno, P. C., & Mungall, C. J. (2014). Unification of multi-species vertebrate anatomy ontologies for comparative biology in Uberon. *Journal of Biomedical Semantics*, *5*, 21.

HAO Portal. (2024). Hymenoptera anatomy ontology portal. Retrieved April 16, from, http://glossary.hymao.org/projects/32/public/ontology/

Harris, R. A. (1979). A glossary of surface sculpturing. *California Department of Food and Agriculture, Bureau of Entomology*, *28*, 1–31.

Harrison, J. M., & Breed, M. D. (1987). Temporal learning in the giant tropical ant, *Paraponera clavata*. *Physiological Entomology*, *12*(3), 317–320.

Hermann, Jr., H. R. (1967). *A comparative study of the hymenopterous poison apparatus* [Thesis, Louisiana State University, p. 103].

Hermann, Jr., H. R., & Blum, M. S. (1966). The morphology and histology of the hymenopterous poison apparatus. I. *Paraponera clavata* (Formicidae). *Annals of the Entomological Society of America*, *59*, 397–409.

Hermann, H. R., Blum, M. S., Wheeler, J. W., Overal, W. L., Schmidt, J. O., & Chao, J. T. (1984). Comparative anatomy and chemistry of the venom apparatus and mandibular glands in *Dinoponera grandis* (Guérin) and *Paraponera clavata* (F.) (Hymenoptera: Formicidae: Ponerinae). *Annals of the Entomological Society of America*, *77*, 272–279.

Hessler, R. R., & Yager, J. (1998). Skeletomusculature of trunk segments and their limbs in *Speleonectes tulumensis* (Remipedia). *Journal of Crustacean Biology*, *18*(1), 111–119.

Hölldobler, B., & Haskins, C. P. (1977). Sexual calling behavior in primitive ants. *Science*, *195*, 793–794.

Janzen, D. H., & Carroll, C. R. (1983). *Paraponera clavata* (Bala, Giant Tropical Ant). In D. H. Janzen (Ed.), *Costa Rican natural history* (pp. 752–753). University of Chicago Press.

Johnson, S. R., Rikli, H. G., Schmidt, J. O., & Evans, M. S. (2017). A reexamination of poneratoxin from the venom of the bullet ant *Paraponera clavata*. *Peptides*, *98*, 51–62.

von Keler, S. (1963). *Entomologisches Wörterbuch*. Akademie Verlag.

Keller, R. A. (2011). A phylogenetic analysis of ant morphology (Hymenoptera: Formicidae) with special reference to the poneromorph subfamilies. *Bulletin of the American Museum of Natural History*, *355*, 1–90.

Kempf, W. W. (1956). A morphological study on the male genitalia of *Paracryptocerus* (*P.*) *pusillus* (Hymenoptera: Formicidae). *Revista Brasileira de Entomologia*, *5*, 101–110.

Klass, K.-D. (1997). The external male genitalia and the phylogeny of Blattaria and Mantodea. *Bonner Zoologischer Monographien*, *42*, 1–341.

Klass, K., & Kristensen, N. P. (2001). The ground plan and affinities of hexapods: Recent progress and open problems. *Annales de la Societé Entomologique de France, (N.S.)*, *37*, 265–298.

Klass, K., & Matushkina, N. (2018). The exoskeleton of the male genitalic region in Archaeognatha, with hypotheses on the early evolution and the morphological interpretation of genitalia in insects. *Arthropod Systematics & Phylogeny*, *76*, 235–294.

Kugler, C. (1991). Stings of ants of the tribe Ectatommini (Formicidae: Ponerinae). *Insecta Mundi*, *5*, 153–166.

Lieberman, Z. E., Billen, J., van de Kamp, T., & Boudinot, B. E. (2022). The ant abdomen: The skeletomuscular and soft tissue anatomy of

Amblyopone australis workers (Hymenoptera: Formicidae). *Journal of Morphology*, *283*(6), 693–770.

Longino, J. T., & Hanson, P. (1995). Chapter 16. The ants (Formicidae). In P. Hanson, & I. Gauld (Eds.), *The Hymenoptera of Costa Rica* (pp. 587–620). Oxford University Press.

Mabee, P. M., Balhoff, J. P., Dahdul, W. M., Lapp, H., Mungall, C. J., & Vision, T. J. (2020). A logical model of homology for comparative biology. *Systematic Biology*, *69*(2), 345–362.

Martins, L. C. B., Serrão, J. E., Santos, H. P., & Araújo, V. A. (2022). Anatomy and histology of the metapleural gland in the giant tropical ant *Paraponera clavata* (Fabricius, 1775) (Formicidae: Paraponerinae). *Anais da Academia Brasileira de Ciências*, *94*, e20201368.

Mayr, G. (1886). Die Formiciden der Vereinigten Staaten von Nordamerika. *Verhandlungen der Kaiserlich-Königlichen Zoologisch-Botanischen Gesellschaft in Wien*, *36*, 419–464.

McKenna, K. Z., Wagner, G. P., & Cooper, K. L. (2021). A developmental perspective of homology and evolutionary novelty. *Current Topics in Developmental Biology*, *141*, 1–38.

Meneganzin, A., Ramsey, G., & DiFrisco, J. (2024). What is a trait? Lessons from the human chin. *Journal of Experimental Zoology Part B: Molecular and Developmental Evolution*, *342*(2), 65–75.

Michener, C. D. (1944a). A comparative study of the appendages of the eighth and ninth abdominal segments of insects. *Annals of the Entomological Society of America*, *37*(3), 336–351.

Michener, C. D. (1944b). Comparative external morphology, phylogeny, and a classification of the bees (Hymenoptera). *Bulletin of the American Museum of Natural History*, *82*, 6.

Mickoleit, G. (1973). über den ovipositor der neuropteroidea und coleoptera und seine phylogenetische bedeutung (Insecta, Holometabola). *Zeitschrift für Morphologie der Tiere*, *74*, 37–64.

Mikó, I., & Deans, A. R. (2013). What is fluorescing. *Hamuli*, *4*(2), 19–22.

Mikó, I., Masner, L., Johannes, E., Yoder, M. J., & Deans, A. R. (2013). Male terminalia of Ceraphronoidea: Morphological diversity in an otherwise monotonous taxon. *Insect Systematics & Evolution*, *44*(3–4), 261–347.

Mikó, I., Trietsch, C., Sandall, E. L., Yoder, M. J., Hines, H., & Deans, A. R. (2016). Malagasy *Conostigmus* (Hymenoptera: Ceraphronoidea) and the secret of scutes. *PeerJ*, *4*, e2682.

Mirth, C., & Akam, M. (2002). Joint development in the *Drosophila* leg: Cell movements and cell populations. *Developmental Biology*, *246*(2), 391–406.

Misof, B., Liu, S., Meusemann, K., Peters, R. S., Donath, A., Mayer, C., Frandsen, P. B., Ware, J., Flouri, T., Beutel, R. G., Niehuis, O., Petersen, M., Izquierdo-Carrasco, F., Wappler, T., Rust, J., Aberer, A. J., Aspöck, U., Aspöck, H., Bartel, D., … Zhou, X. (2014). Phylogenomics resolves the timing and pattern of insect evolution. *Science*, *346*(6210), 763–767.

Müller, M. A., Merten, L., Böhmer, C., & Nyakatura, J. A. (2021). 3D models related to the publication: Pushing the boundary? Testing the 'functional elongation hypothesis' of the giraffe's neck. *MorphoMuseuM*, *7*, e129.

Mungall, C. J., Torniai, C., Gkoutos, G. V., Lewis, S. E., & Haendel, M. A. (2012). Uberon, an integrative multi-species anatomy ontology. *Genome Biology*, *13*, R5.

Ogata, K. (1991). A generic synopsis of the Poneroid complex of the family Formicidae in Japan (Hymenoptera). Part II. Subfamily Myrmicinae. *Bulletin of the Institute of Tropical Agriculture Kyushu University*, *14*, 61–149.

Paganin, D., Mayo, S. C., Gureyev, T. E., Miller, P. R., & Wilkins, S. W. (2002). Simultaneous phase and amplitude extraction from a single defocused image of a homogeneous object. *Journal of Microscopy*, *206*, 33–40.

Pavlicev, M., Herdina, A. N., & Wagner, G. (2022). Female genital variation far exceeds that of male genitalia: A review of comparative anatomy of clitoris and the female lower reproductive tract in Theria. *Integrative and Comparative Biology*, *62*(3), 581–601.

Peeters, C. (2017). Independent colony foundation in *Paraponera clavata* (Hymenoptera, Formicidae): First workers lay trophic eggs to feed queen's larvae. *Sociobiology*, *64*(4), 417–422.

Piek, T., Duval, A., Hue, B., Karst, H., Lapied, B., Mantel, P., Nakajima, T., Pelhate, M., & Schmidt, J. O. (1991). Poneratoxin, a novel peptide neurotoxin from the venom of the ant, *Paraponera clavata*. *Comparative Biochemistry and Physiology Part C: Comparative Pharmacology*, *99*(3), 487–495.

Pohl, H. (2010). A scanning electron microscopy specimen holder for viewing different angles of a single specimen. *Microscopy Research and Technique*, *73*(12), 1073–1076.

Prokop, J., & Engel, M. S. (2019). Palaeodictyopterida. *Current Biology*, *29*, R306–R309.

Prokop, J., Pecharová, M., Sinitshenkova, N. D., & Klass, K.-D. (2020). Male postabdomen reveals ancestral traits of Megasecoptera among winged insects. *Arthropod Structure & Development*, *57*, 100944.

Qadri, M. A. H. (1940). On the development of the genitalia and their ducts of orthopteroid insects. *Transactions of the Royal Entomological Society of London*, *90*(6), 121–175.

Remane, A. (1952). *Die Grundlagen des natürlichen Systems, der vergleichenden Anatomie und der Phylogenetik*. Akademische Verlagsgesellschaft Geest und Portig.

Richter, A., Boudinot, B. E., Hita Garcia, F., Billen, J., Economo, E. P., & Beutel, R. G. (2023). Wonderfully weird: The head anatomy of the armadillo ant, *Tatuidris tatusia* (Hymenoptera: Formicidae: Agroecomyrmecinae), with evolutionary implications. *Myrmecological News*, *33*, 35–75.

Richter, A., Boudinot, B., Yamamoto, S., Katzke, J., & Beutel, R. G. (2022). The first reconstruction of the head anatomy of a Cretaceous insect, †*Gerontoformica gracilis* (Hymenoptera: Formicidae), and the early evolution of ants. *Insect Systematics and Diversity*, *6*(5), 4.

Richter, A., Garcia, F. H., Keller, R. A., Billen, J., Economo, E. P., & Beutel, R. G. (2020). Comparative analysis of worker head anatomy of *Formica* and *Brachyponera* (Hymenoptera: Formicidae). *Arthropod Systematics & Phylogeny*, *78*, 133–170.

Richter, A., Garcia, F. H., Keller, R. A., Billen, J., Katzke, J., Boudinot, B. E., & Beutel, R. G. (2021). The head anatomy of *Protanilla lini* (Hymenoptera: Formicidae: Leptanillinae), with a hypothesis of their mandibular movement. *Myrmecological News*, *31*, 85–114.

Richter, A., Keller, R. A., Rosumek, F. B., Economo, E. P., Hita Garcia, F., & Beutel, R. G. (2019). The cephalic anatomy of workers of the ant species *Wasmannia affinis* (Formicidae, Hymenoptera, Insecta) and its evolutionary implications. *Arthropod Structure & Development*, *49*, 26–49.

Richter, A., Schoeters, E., & Billen, J. (2021). Morphology and closing mechanism of the mandibular gland orifice in ants (Hymenoptera: Formicidae). *Journal of Morphology*, *282*, 1127–1140.

Richter, S., & Wirkner, C. S. (2014). A research program for evolutionary morphology. *Journal of Zoological Systematics and Evolutionary Research*, *52*(4), 338–350.

Romiguier, J., Borowiec, M. L., Weyna, A., Helleu, Q., Loire, E., La Mendola, C., Rabeling, C., Fisher, B. L., Ward, P. S., & Keller, L. (2022). Ant phylogenomics reveals a natural selection hotspot preceding the origin of complex eusociality. *Current Biology*, *32*(13), 2942–2947.e4.

Ross, H. H. (1945). Sawfly genitalia: Terminology and study techniques. *Entomological News (Philadelphia)*, *56*, 261–265.

Roux, J., & Robinson-Rechavi, M. (2010). An ontology to clarify homology-related concepts. *Trends in Genetics*, *26*(3), 99–102.

Sánchez, L., & Guerrero, I. (2001). The development of the *Drosophila* genital disc. *BioEssays*, *23*(8), 698–707.

dos Santos Rolo, T., Ershov, A., van de Kamp, T., & Baumbach, T. (2014). In vivo X-ray cine-tomography for tracking morphological dynamics. *Proceedings of the National Academy of Sciences*, *111*(11), 3921–3926.

Schindelin, J., Arganda-Carreras, I., Frise, E., Kaynig, V., Longair, M., Pietzsch, T., Preibisch, S., Rueden, C., Saalfeld, S., Schmid, B., Tinevez, J. Y., White, D. J., Hartenstein, V., Eliceiri, K., Tomancak, P., & Cardona, A. (2012). Fiji: An open-source platform for biological-image analysis. *Nature Methods*, *9*(7), 676–682.

Schmidt, J. O., Blum, M. S., & Overal, W. L. (1983). Hemolytic activities of stinging insect venoms. *Archives of Insect Biochemistry and Physiology*, *1*(2), 155–160.

Schoett, H. (1897). North American Apterygogonea. *Proceedings of the California Academy of Science, Series 2*, *6*, 169–196.

Schulman, V. K., Dobi, K. C., & Baylies, M. K. (2015). Morphogenesis of the somatic musculature in *Drosophila melanogaster*. *WIREs Developmental Biology*, *4*, 313–334. https://doi.org/10.1002/wdev.180

Schulmeister, S. (2001). Functional morphology of the male genitalia and copulation in lower Hymenoptera, with special emphasis on the Tenthredinoidea *s. str*. (Insecta, Hymenoptera, 'Symphyta'). *Acta Zoologica*, *82*(4), 331–349.

Schulmeister, S. (2003). Genitalia and terminal abdominal segments of male basal Hymenoptera (Insecta): Morphology and evolution. *Organisms Diversity & Evolution*, *3*(4), 253–279.

Schweitzer, R., Zelzer, E., & Volk, T. (2010). Connecting muscles to tendons: Tendons and musculoskeletal development in flies and vertebrates. *Development*, *137*(17), 2807–2817.

Seltmann, K., Yoder, M., Miko, I., Forshage, M., Bertone, M., Agosti, D., Austin, A., Balhoff, J., Borowiec, M., Brady, S., Broad, G., Brothers, D., Burks, R., Buffington, M., Campbell, H., Dew, K., Ernst, A., Fernandez-Triana, J., Gates, M., … Deans, A. (2012). A hymenopterists' guide to the Hymenoptera Anatomy Ontology: Utility, clarification, and future directions. *Journal of Hymenoptera Research*, *27*, 67–88.

Simon, S., Blanke, A., & Meusemann, K. (2018). Reanalyzing the Palaeoptera problem – The origin of insect flight remains obscure. *Arthropod Structure & Development*, *47*(4), 328–338.

Sink, H. (2006a). An introduction to muscle development in *Drosophila*. In H. Sink (Ed.), *Muscle development in Drosophila* (pp. 1–7). Eurekah.com and Springer Science + Business Media Inc.

Sink, H. (2006b). *Muscle development in Drosophila*. Eurekah.com and Springer Science + Business Media Inc.

Smith, E. L. (1970). Evolutionary morphology of the external insect genitalia. 2. Hymenoptera. *Annals of the Entomological Society of America*, *63*(1), 1–27.

Smith, E. L. (1972). Biosystematics and morphology of Symphyta—III External genitalia of *Euura* (Hymenoptera: Tenthredinidae): Sclerites, sensilla, musculature, development and oviposition behavior. *International Journal of Insect Morphology and Embryology*, *1*(4), 321–365.

Snodgrass, R. E. (1935). *The principles of insect morphology* (p. 667). McGraw-Hill.

Snodgrass, R. E. (1941). The male genitalia of Hymenoptera. *Smithsonian Miscellaneous Collections*, *99*, 1–86.

Snodgrass, R. E. (1946). The skeletal anatomy of fleas (Siphonaptera). *Smithsonian Miscellaneous Collections*, *104*, 1–78.

Snodgrass, R. E. (1957). A revised interpretation of the external reproductive organs of male insects. *Smithsonian Miscellaneous Collections*, *135*, 1–60.

Starck, J. M., Belojević, J., Brozio, J., & Mehnert, L. (2022). Comparative anatomy of the rostrosoma of Solifugae, Pseudoscorpiones and Acari. *Zoomorphology*, *141*(1), 57–80.

Tajiri, R., Misaki, K., Yonemura, S., & Hayashi, S. (2010). Dynamic shape changes of ECM-producing cells drive morphogenesis of ball-and-socket joints in the fly leg. *Development*, *137*(12), 2055–2063.

Tulloch, G. S. (1929). The proper use of the terms parapsides and parapsidal furrows. *Psyche: A Journal of Entomology*, *36*, 376–382.

Tulloch, G. S. (1935). Morphological studies of the thorax of the ant. *Entomologica Americana*, *15*, 93–130.

Tuxen, S. L. (1970a). Chapter 2. Collembola. In S. L. Tuxen (Ed.), *Taxonomist's glossary of genitalia in insects* (2nd ed., pp. 24–25). Munksgaard.

Tuxen, S. L. (1970b). Chapter 3. Diplura. In S. L. Tuxen (Ed.), *Taxonomist's glossary of genitalia in insects* (2nd ed., pp. 25–27). Munksgaard.

Urbani, C. B., Bolton, B., & Ward, P. S. (1992). The internal phylogeny of ants (Hymenoptera: Formicidae). *Systematic Entomology*, *17*, 301–329.

Vogelgesang, M., Farago, T., Morgeneyer, T. F., Helfen, L., dos Santos Rolo, T., Myagotin, A., & Baumbach, T. (2016). Real-time image-content-based beamline control for smart 4D X-ray imaging. *Journal of Synchrotron Radiation*, *23*, 1254–1263.

Vogt, L., Mikó, I., & Bartolomaeus, T. (2022). Anatomy and the type concept in biology show that ontologies must be adapted to the diagnostic needs of research. *Journal of Biomedical Semantics*, *13*(1), 18.

Volk, T. (2006). Muscle attachment sites: Where migrating muscles meet their match. In H. Sink (Ed.), *Muscle development in Drosophila* (pp. 104–112). Eurekah.com and Springer Science + Business Media Inc.

Wagner, G. P. (2014). *Homology, genes, and evolutionary innovation*. Princeton University Press.

Wagner, G. P. (2016). What is "homology thinking" and what is it for? *Journal of Experimental Zoology Part B: Molecular and Developmental Evolution*, *326*(1), 3–8.

Wheeler, G. C., & Wheeler, J. (1952). The ant larvae of the subfamily Ponerinae – Part I. *American Midland Naturalist*, *48*, 111–144.

Whiting, Jr., J. H., Black, H. L., & Jorgensen, J. D. (1989). A scanning electron microscopy study of the mouthparts of *Paraponera clavata* (Hymenoptera: Formicidae). *Pan-Pacific Entomologist*, *65*, 302–309.

Yoder, M. J., Mikó, I., Seltmann, K. C., Bertone, M. A., & Deans, A. R. (2010). A gross anatomy ontology for Hymenoptera. *PLoS One*, *5*(12), e15991.

Zahnle, X. J., Sierwald, P., Ware, S., & Bond, J. E. (2020). Genital morphology and the mechanics of copulation in the millipede genus *Pseudopolydesmus* (Diplopoda: Polydesmida: Polydesmidae). *Arthropod Structure & Development*, *54*, 100913.

How to cite this article: Boudinot, B. E., van de Kamp, T., Peters, P., & Knöllinger, K. (2024). Male genitalia, hierarchical homology, and the anatomy of the bullet ant (*Paraponera clavata*; Hymenoptera, Formicidae). *Journal of Morphology*, *285*, e21757. https://doi.org/10.1002/jmor.21757

APPENDIX

TABLE OF CONTENTS.